

Fall 1-31-1995

Analysis of plates and reinforced concrete columns by cubic b-spline function

Gang Wang
New Jersey Institute of Technology

Follow this and additional works at: <https://digitalcommons.njit.edu/dissertations>



Part of the [Civil Engineering Commons](#)

Recommended Citation

Wang, Gang, "Analysis of plates and reinforced concrete columns by cubic b-spline function" (1995).
Dissertations. 1125.
<https://digitalcommons.njit.edu/dissertations/1125>

This Dissertation is brought to you for free and open access by the Electronic Theses and Dissertations at Digital Commons @ NJIT. It has been accepted for inclusion in Dissertations by an authorized administrator of Digital Commons @ NJIT. For more information, please contact digitalcommons@njit.edu.

Copyright Warning & Restrictions

The copyright law of the United States (Title 17, United States Code) governs the making of photocopies or other reproductions of copyrighted material.

Under certain conditions specified in the law, libraries and archives are authorized to furnish a photocopy or other reproduction. One of these specified conditions is that the photocopy or reproduction is not to be “used for any purpose other than private study, scholarship, or research.” If a user makes a request for, or later uses, a photocopy or reproduction for purposes in excess of “fair use” that user may be liable for copyright infringement,

This institution reserves the right to refuse to accept a copying order if, in its judgment, fulfillment of the order would involve violation of copyright law.

Please Note: The author retains the copyright while the New Jersey Institute of Technology reserves the right to distribute this thesis or dissertation

Printing note: If you do not wish to print this page, then select “Pages from: first page # to: last page #” on the print dialog screen

The Van Houten library has removed some of the personal information and all signatures from the approval page and biographical sketches of theses and dissertations in order to protect the identity of NJIT graduates and faculty.

INFORMATION TO USERS

This manuscript has been reproduced from the microfilm master. UMI films the text directly from the original or copy submitted. Thus, some thesis and dissertation copies are in typewriter face, while others may be from any type of computer printer.

The quality of this reproduction is dependent upon the quality of the copy submitted. Broken or indistinct print, colored or poor quality illustrations and photographs, print bleedthrough, substandard margins, and improper alignment can adversely affect reproduction.

In the unlikely event that the author did not send UMI a complete manuscript and there are missing pages, these will be noted. Also, if unauthorized copyright material had to be removed, a note will indicate the deletion.

Oversize materials (e.g., maps, drawings, charts) are reproduced by sectioning the original, beginning at the upper left-hand corner and continuing from left to right in equal sections with small overlaps. Each original is also photographed in one exposure and is included in reduced form at the back of the book.

Photographs included in the original manuscript have been reproduced xerographically in this copy. Higher quality 6" x 9" black and white photographic prints are available for any photographs or illustrations appearing in this copy for an additional charge. Contact UMI directly to order.

UMI

A Bell & Howell Information Company
300 North Zeeb Road, Ann Arbor, MI 48106-1346 USA
313/761-4700 800/521-0600

UMI Number: 9525748

Copyright 1995 by
WANG, GANG
All rights reserved.

UMI Microform 9525748
Copyright 1995, by UMI Company. All rights reserved.

This microform edition is protected against unauthorized
copying under Title 17, United States Code.

UMI
300 North Zeeb Road
Ann Arbor, MI 48103

ABSTRACT

ANALYSIS OF PLATES AND REINFORCED CONCRETE COLUMNS BY CUBIC B-SPLINE FUNCTION

Gang Wang

Applying spline functions to numerical structural analysis has been more common in recent years. The recent increase use of spline functions is mainly due to their excellent characteristics, such as sectionalized continuity, linear combination, flexibility, and easy use for various boundary conditions. The whole deformed shape of some structures or substructures can be described with one displacement function constructed by a series of spline functions. By doing this, the mesh generation and the huge computer memory space are no longer needed because only one single superelement can be used in the whole process. The choice of spline functions as displacement functions has many advantages that have been demonstrated by several researchers for a limited range of structures. More extensive research on using spline functions in structural analysis hereafter can be expected. This research work represents an effort in that direction.

Based on cubic B-spline functions, this dissertation presents static and free vibration analysis of arbitrary quadrilateral flexural plates with various boundary conditions. Combination of cubic B-spline functions in two orthogonal directions constructs a superelement for the whole plate. The cubic B-spline displacement function has been formed to efficiently model the deflection shape and to yield more accurate results. A further step has been taken in the present research to apply the cubic B-spline function to a nonlinear problem. A numerical method is developed for the determination of complete load-deflection and

moment-curvature relationships for slender reinforced concrete columns with arbitrary cross sections under combined biaxial flexure and axial load. Improvement of computer time and accuracy has been demonstrated obviously due to the application of cubic B-spline function and introduction of p-multiplier in the numerical formulation.

Comparison of present analysis with analytical solutions, other numerical methods, and experimental results, appears to have a good agreement.

**ANALYSIS OF PLATES AND REINFORCED CONCRETE COLUMNS
BY CUBIC B-SPLINE FUNCTION**

by
Gang Wang

**A Dissertation
Submitted to the Faculty of
New Jersey Institute of Technology
in Partial Fulfillment of the Requirement for the Degree of
Doctor of Philosophy**

Department of Civil and Environmental Engineering

January 1995

Copyright © 1995 by Gang Wang
ALL RIGHTS RESERVED

APPROVAL PAGE

**Analysis of Plates and Reinforced Concrete Columns
by Cubic B-Spline Function**

Gang Wang

Dr. C. T. Thomas Hsu, Dissertation Advisor
Professor, Department of Civil and Environmental Engineering, NJIT

Dr. William Spillers, Committee Member
Professor and Chairman, Department of Civil and Environmental Engineering, NJIT

Dr. M. Ala Saadeghvaziri, Committee Member
Associate Professor, Department of Civil and Environmental Engineering, NJIT

Prof. Edward Dauenheimer, Committee Member
Professor and Associate Chairman, Department of Civil and Environmental Engineering,
NJIT

Dr. Rong Chen, Committee Member
Professor, Department of Mechanical Engineering, NJIT

BIOGRAPHICAL SKETCH

Author: Gang Wang

Degree: Doctor of Philosophy in Civil Engineering

Date: January 1995

Undergraduate and Graduate Education:

- Doctor of Philosophy in Civil Engineering
New Jersey Institute of Technology, Newark, NJ, 1995
- Master of Science in Computational Mechanics
Guangxi University, Nanning, P. R. China, 1986
- Bachelor of Science in Civil Engineering
Guangxi University, Nanning, P. R. China, 1982

Major: Structural Engineering

Professional Background:

- May 94 - Present, Structural Engineer, Lichtenstein Engineers, New York
Perform 3-dimensional modeling, seismic analysis, fatigue evaluation, and live load rating for different types of bridges; Develop computer software for the above engineering applications.
- 1989 - 1991, Visiting Scholar, NJIT, New Jersey
Conduct research on biaxially loaded reinforced concrete columns.
- 1986 - 1989, Instructor, Guangxi University, Nanning, P.R.China
Teach undergraduate courses; perform research on plate and shell structures, and fluid-structure interactions.

Publications:

Wang, G. and Hsu, C.T.T. (1994). Static and dynamic analysis of arbitrary quadrilateral flexural plates by B_3 -spline functions. *Int. J. Solids Struct.* 31(5), 657-667.

Wang, G. and Hsu, C.T.T. (1992). Complete biaxial load-deformation behavior of RC columns. *J. Struct. Engrg.* ASCE, 118(9), 2590-2609.

Wang, G. and Hsu, C.T.T. (1990). Complete load-deformation behavior of biaxially loaded RC columns. *Technical Report Structural series, No. 90-2*, Dept. of Civil and Environmental Engineering, New Jersey Institute of Technology, Newark, New Jersey.

Qin, R. and Wang, G. (1986). Spline subdomain method for thin arch dams (in Chinese). *Proc. of 2nd National Conf. on the Weighted Residual Method*. Hangzhou, P.R.China.

Qin, R. and Wang, G. (1986). Energy collocation method for arch dams (in Chinese). *Journal of Guangxi University*. 2(86), Nanning, P.R.China.

This dissertation is dedicated
to my wife, Yun Liu
to my son, Kevin Wang

ACKNOWLEDGMENT

The author wishes to express his sincere gratitude to his advisor, Dr. C.T. Thomas Hsu, for his guidance, friendship, and moral support throughout this research.

Special thanks to the other members of committee: Dr. William Spillers, Dr. M. Ala Saadeghvaziri, Prof. Edward Dauenheimer, and Dr. Rong Chen, for their careful review, productive comments, and helpful discussions.

The author is grateful to his fellow students, Wen Hu Tsao, Yuxiang Xing, Wei Wang, and Byong-Youl Bahn, who shared their valuable ideas and experience with the author.

A teaching assistantship awarded to the author from the New Jersey Institute of Technology throughout this research is also greatly acknowledged.

Finally the author would like to thank his family and friends for their continuous encouragement and best wishes, especially his wife, whose love, care, and support made this work possible.

TABLE OF CONTENTS

Chapter	Page
1. INTRODUCTION	1
2. LITERATURE REVIEW	3
2.1 Linear Structural Analysis by Spline Functions	3
2.2 Load-Deformation Behavior of Reinforced Concrete Columns Subjected to Axial Load and Biaxial Bending	5
3. B-SPLINE FUNCTION	8
3.1 Definition of B-spline Function.....	8
3.2 Features of B-spline Function.....	9
3.3 Elementary Applications of Cubic B-spline Function	13
3.3.1 One-Dimensional Deflection Function	14
3.3.2 Applications on Beams	16
4. STATIC AND DYNAMIC BEHAVIOR OF ARBITRARY QUADRILATERAL FLEXURAL PLATES	22
4.1 Originalities of Present Method	23
4.2 Geometrical Mapping.....	24
4.3 Displacement Function	25
4.4 Formulation of Present Analysis	28
4.5 Numerical Examples	29
5. NONLINEAR BEHAVIOR OF BIAXIALLY LOADED REINFORCED CONCRETE COLUMNS.....	38
5.1 Originalities of Present Numerical Analysis.....	38
5.2 Basic Assumptions and Constitutive Relations.....	39
5.3 Present Numerical Method	42
5.3.1 Section Stiffness Equation.....	42

TABLE OF CONTENTS
(Continued)

Chapter	Page
5.3.2 Member Stiffness Equation.....	45
5.3.3 Incremental Procedure and Flow Chart.....	49
5.3.4 Solver of Simultaneous Equations.....	50
5.3.5 Accuracy and Convergence.....	50
5.4 Comparison with Experimental Results	55
6. SUMMARY AND CONCLUSIONS.....	62
6.1 Conclusions for Plate Analysis	62
6.2 Conclusions for RC Column Analysis.....	63
APPENDIX A VALUES OF CUBIC B-SPLINE FUNCTION AND ITS FIRST AND SECOND DERIVATIVES.....	65
APPENDIX B DERIVATION OF EQUATION (3-8).....	66
APPENDIX C STRAIN UNDER TWO ARBITRARY CARTESIAN COORDINATE SYSTEMS.....	68
APPENDIX D MEMBER STIFFNESS MATRIX.....	70
APPENDIX E FLOW CHART	72
APPENDIX F FORTRAN STATEMENTS OF PRESENT SOLVER.....	73
APPENDIX G LOAD-DEFLECTION AND MOMENT-CURVATURE CURVES FOR NJIT COLUMN SPECIMENS	76
APPENDIX H MOMENT-CURVATURE CURVES FOR UNIVERSITY OF TEXAS AT AUSTIN COLUMN SPECIMENS.....	102
BIBLIOGRAPHY	115

LIST OF TABLES

Table	Page
3-1 Some Values of Ratio DOFB/DOFH	18
3-2 Maximum Deflections of Eccentrically Loaded Column.....	21
4-1 Correspondences between Boundary Conditions and Eliminating Terms	27
4-2 Relations between Corner Displacements, Rotations, Curvatures and Generalized Coordinates	27
4-3 Comparison of Central Deflections of Simply Supported and Clamped Square Plates under Uniformly Distributed and Central Concentrated Loads	31
4-4 Comparison of Central deflection and Bending Moments of Simply Supported Square Plates under Uniformly Distributed and Central Concentrated Loads	31
4-5 Central Deflections and Moments for Simply Supported Skew Plates under Uniformly Distributed Load.....	32
4-6 Central Deflections and Moments for Simply Clamped Skew Plates under Uniformly Distributed Load.....	33
4-7 Frequency Parameters of Simply Supported Rectangular Plate	34
4-8 Frequency Parameters of Simply Supported Trapezoidal Plate	34
4-9 Deflection and Moments at Midpoint for Irregular Quadrilateral Plate under Uniformly Distributed Load.....	36
5-1 Data of Reinforced Concrete Sections	51
5-2 Compressive Strength and Curvature of Square Section with Different Numbers of Elements	54
5-3 Compressive Strength and Curvature of L-Shaped Section with Different Numbers of Elements	54
5-4 Computational Results of Square Section Column with Different Number of Segments.....	55
5-5 Computational Results of L-Shaped Section Column with Different Number of Segments.....	55

LIST OF TABLES
(Continued)

Table	Page
5-6 Maximum Axial Load and Deflections for B Series Columns	58
5-7 Maximum Axial Load and Deflections for C Series Columns	58
A-1 Values of φ_3 , φ_3' , and φ_3'' at Spline Knots ($h_j \neq \text{constant}$)	65
A-2 Values of φ_3 , φ_3' , and φ_3'' at Spline Knots and Midpoints between Each Two Adjacent Knots ($h_j = h = \text{constant}$)	65

LIST OF FIGURES

Figure	Page
3-1 Cubic B-spline and Its First and Second Derivatives with Unequal Sections (C^2 everywhere)	10
3-2 Cubic B-spline and Its First and Second Derivatives with Equal Sections (C^2 everywhere)	11
3-3 Cubic B-spline and Its First Derivative (C^1 at knot $x_k=x_{k-1}$ and C^2 elsewhere)	12
3-4 Cubic B-spline (C^0 at knot $x_{k-1}=x_k=x_{k+1}$, C^2 elsewhere)	13
3-5 Basis of Cubic B-spline Expression	13
3-6 One-Dimensional Domain with $n+1$ Spline Knots	14
3-7 Cantilever Beam under n Concentrated Loads	16
3-8 Mild-Steel Cantilever Beam	19
3-9 Eccentrically Loaded Column	20
4-1 Geometrical Mapping	24
4-2 Skew Plate	32
4-3 Trapezoidal Plate	34
4-4 Nodal Patterns and Frequency Parameters for First Six Modes of Simply Supported Rectangular and Trapezoidal Plates	35
4-5 Irregular Quadrilateral Plate	35
4-6 Deflected Curves along Central Line AB	37
4-7 Deflected Curves along Central Line EF	37
5-1 Stress-Strain Curve of Confined and Unconfined Concretes	40
5-2 Cross Section with Confined and Unconfined Areas	41
5-3 Stress-Strain Curve of Steel	41
5-4 Arbitrary Column Cross Section	42
5-5 Deflected Curve for a Slender Biaxially Loaded Column	46

**LIST OF FIGURES
(Continued)**

Figure	Page
5-6 Reinforced Concrete Sections	51
5-7 Convergence of Compressive Strength for Square Cross Section	53
5-8 Convergence of Compressive Strength for L-Shaped Cross Section	53
5-9 Details of Specimens at University of Texas	61
C-1 Two Arbitrary Cartesian Coordinate Systems on a Cross Section.....	68
E-1 Flow Chart of Present Computational Process	72
G-1a Load-Deflection Curves in X-Direction for Specimen B2	76
G-1b Load-Deflection Curves in Y-Direction for Specimen B2	76
G-1c Moment-Curvature Curves about X-Axis for Specimen B2	77
G-1d Moment-Curvature Curves about Y-Axis for Specimen B2	77
G-2a Load-Deflection Curves in X-Direction for Specimen B3	78
G-2b Load-Deflection Curves in Y-Direction for Specimen B3	78
G-2c Moment-Curvature Curves about X-Axis for Specimen B3	79
G-2d Moment-Curvature Curves about Y-Axis for Specimen B3	79
G-3a Load-Deflection Curves in X-Direction for Specimen B4	80
G-3b Load-Deflection Curves in Y-Direction for Specimen B4	80
G-3c Moment-Curvature Curves about X-Axis for Specimen B4	81
G-3d Moment-Curvature Curves about Y-Axis for Specimen B4	81
G-4a Load-Deflection Curves in X-Direction for Specimen B5	82
G-4b Load-Deflection Curves in Y-Direction for Specimen B5	82
G-4c Moment-Curvature Curves about X-Axis for Specimen B5	83
G-4d Moment-Curvature Curves about Y-Axis for Specimen B5	83

LIST OF FIGURES
(Continued)

Figure	Page
G-5a Load-Deflection Curves in X-Direction for Specimen B6	84
G-5b Load-Deflection Curves in Y-Direction for Specimen B6	84
G-5c Moment-Curvature Curves about X-Axis for Specimen B6	85
G-5d Moment-Curvature Curves about Y-Axis for Specimen B6	85
G-6a Load-Deflection Curves in X-Direction for Specimen B7	86
G-6b Load-Deflection Curves in Y-Direction for Specimen B7	86
G-6c Moment-Curvature Curves about X-Axis for Specimen B7	87
G-6d Moment-Curvature Curves about Y-Axis for Specimen B7	87
G-7a Load-Deflection Curves in X-Direction for Specimen B8	88
G-7b Load-Deflection Curves in Y-Direction for Specimen B8	88
G-7c Moment-Curvature Curves about X-Axis for Specimen B8	89
G-7d Moment-Curvature Curves about Y-Axis for Specimen B8	89
G-8a Load-Deflection Curves in X-Direction for Specimen C1	90
G-8b Load-Deflection Curves in Y-Direction for Specimen C1	90
G-8c Moment-Curvature Curves about X-Axis for Specimen C1	91
G-8d Moment-Curvature Curves about Y-Axis for Specimen C1	91
G-9a Load-Deflection Curves in X-Direction for Specimen C2	92
G-9b Load-Deflection Curves in Y-Direction for Specimen C2	92
G-9c Moment-Curvature Curves about X-Axis for Specimen C2	93
G-9d Moment-Curvature Curves about Y-Axis for Specimen C2	93
G-10a Load-Deflection Curves in X-Direction for Specimen C3	94
G-10b Load-Deflection Curves in Y-Direction for Specimen C3	94
G-10c Moment-Curvature Curves about X-Axis for Specimen C3	95

**LIST OF FIGURES
(Continued)**

Figure	Page
G-10d Moment-Curvature Curves about Y-Axis for Specimen C3.....	95
G-11a Load-Deflection Curves in X-Direction for Specimen C4.....	96
G-11b Load-Deflection Curves in Y-Direction for Specimen C4.....	96
G-11c Moment-Curvature Curves about X-Axis for Specimen C4.....	97
G-11d Moment-Curvature Curves about Y-Axis for Specimen C4.....	97
G-12a Load-Deflection Curves in X-Direction for Specimen C5.....	98
G-12b Load-Deflection Curves in Y-Direction for Specimen C5.....	98
G-12c Moment-Curvature Curves about X-Axis for Specimen C5.....	99
G-12d Moment-Curvature Curves about Y-Axis for Specimen C5.....	99
G-13a Load-Deflection Curves in X-Direction for Specimen C6.....	100
G-13b Load-Deflection Curves in Y-Direction for Specimen C6.....	100
G-13c Moment-Curvature Curves about X-Axis for Specimen C6.....	101
G-13d Moment-Curvature Curves about Y-Axis for Specimen C6.....	101
H-1 Moment-Curvature Curves about Strong and Weak Axes for Specimen RC-1.....	102
H-2 Moment-Curvature Curves about Strong and Weak Axes for Specimen RC-2.....	102
H-3 <i>Moment-Curvature Curves about Strong and Weak Axes for Specimen RC-3.....</i>	103
H-4 Moment-Curvature Curves about Strong and Weak Axes for Specimen RC-4.....	103
H-5 Moment-Curvature Curves about Strong and Weak Axes for Specimen RC-5.....	104
H-6 Moment-Curvature Curves about Strong and Weak Axes for Specimen RC-6.....	104

**LIST OF FIGURES
(Continued)**

Figure		Page
H-7	Moment-Curvature Curves about Strong and Weak Axes for Specimen RC-7.....	105
H-8	Moment-Curvature Curves about Strong and Weak Axes for Specimen RC-8.....	105
H-9	Moment-Curvature Curves about Strong and Weak Axes for Specimen RC-9.....	106
H-10	Moment-Curvature Curves about Weak Axis for Specimen C-1....	107
H-11	Moment-Curvature Curves about Weak Axis for Specimen C-2....	107
H-12	Moment-Curvature Curves about Strong Axis for Specimen C-3...	108
H-13	Moment-Curvature Curves about Strong Axis for Specimen C-4...	108
H-14	Moment-Curvature Curves about Strong and Weak Axes for Specimen C-5	109
H-15	Moment-Curvature Curves about Strong and Weak Axes for Specimen C-6	109
H-16	Moment-Curvature Curves about Strong and Weak Axes for Specimen C-7	110
H-17	Moment-Curvature Curves about Strong and Weak Axes for Specimen C-8	110
H-18	Moment-Curvature Curves about Strong and Weak Axes for Specimen C-9	111
H-19	Moment-Curvature Curves about Strong and Weak Axes for Specimen C-10	111
H-20	Moment-Curvature Curves about Strong and Weak Axes for Specimen C-11	112
H-21	Moment-Curvature Curves about Strong and Weak Axes for Specimen C-12	112
H-22	Moment-Curvature Curves about Strong and Weak Axes for Specimen C-13	113

**LIST OF FIGURES
(Continued)**

Figure		Page
H-23	Moment-Curvature Curves about Strong Axis for Specimen C-14	113
H-24	Moment-Curvature Curves about Weak Axis for Specimen C-15..	114

LIST OF SYMBOLS

A_c	area of concrete portion on the cross section of column
A_s	area of steel portion on the cross section of column
C	displacement matrix of a plate or deformation matrix of column section
D	rigidity matrix of a plate
E	modulus of elasticity
e_x	eccentricity of axial force P along x-axis
e_y	eccentricity of axial force P along y-axis
f	load matrix of a plate
F	section force matrix of a column
f_c	stress on concrete portion of a section
f_s	stress on steel portion of a section
f_t	tensile strength of concrete
f'_c	compressive strength of unconfined concrete
f'_{cc}	compressive strength of confined concrete
G	stiffness matrix of a plate or column
h_j	spacing of spline knots
I_{xck}, I_{xcj}	moments of inertia of concrete element k and steel element j about the centroidal axis x_c on a column section
I_{yck}, I_{ycj}	moments of inertia of concrete element k and steel element j about the centroidal axis y_c on a column section
J	Jacobian matrix
K	section stiffness matrix of a column
M	mass matrix of a plate
M_x	bending moment about x-axis on the cross section of column
M_y	bending moment about y-axis on the cross section of column

LIST OF SYMBOLS
(Continued)

P	axial force on the cross section of column
N_i	shape function
p	multiplier to centroidal moment of inertia of each element in section stiffness matrix \mathbf{K} of a column
\mathbf{R}	force matrix of a column
t	thickness of plate
\mathbf{T}	transformation matrix
u	deflection along x-axis of a column
v	deflection along y-axis of a column
$w(x)$	displacement function of a beam
$w(x,y)$	displacement function of a plate
χ	plate curvature matrix
δ	displacement matrix of a column
ϵ_c	compressive strain of unconfined concrete corresponding to f'_c
ϵ_o	strain at the coordinate origin of a section
ϵ_t	tensile strain of concrete corresponding to f_t
ϵ_u	ultimate strain of unconfined concrete
ϵ_{cc}	compressive strain of confined concrete corresponding to f'_{cc}
ϵ_{cu}	ultimate strain of confined concrete
ϕ_x	curvature corresponding to bending moment M_x and with respect to x-axis
ϕ_y	curvature corresponding to bending moment M_y and with respect to y-axis
Φ_i, Ψ_j	B-spline functions by combining the cubic B-splines
$\varphi_3(s; k)$	cubic B-spline

LIST OF SYMBOLS
(Continued)

$\varphi_i(x)$	cubic B-spline when $k=i$
$\varphi_n(s; k)$	n-th degree B-spline
μ	Poisson's ratio
Π	total potential energy of a plate
ρ	mass density
ω	natural circular frequency

CHAPTER 1

INTRODUCTION

The finite element method (FEM) has been widely employed in structural analysis for last thirty years. The method has been proved to be an extremely powerful tool in solving various engineering problems, especially those involving complex geometries, arbitrary loads and rather general material properties. However, it has been found that FEM may be inefficient and uneconomic for certain types of structures. FEM becomes time consuming in preparing the appropriate element mesh, and requires huge memory space for computational purposes due to the large number of degrees of freedom involved. Some more efficient numerical methods, for certain types of problems, have been established, such as the finite strip method (FSM) and the boundary element method (BEM). Even though these methods can reduce the size of the problem, they are unable to overcome the drawbacks of FEM considerably. The reason is that FEM, FSM and BEM all belong to the classification of discretization method which requires mesh generation and element assembly.

In recent years, a new direction of research in numerical structural analysis has emerged. This is an application of spline functions to various engineering problems. Excellent characteristics from spline functions, such as sectionalized continuity, linear combination, flexibility, and easy satisfaction of boundary conditions, make it possible that the whole deformed shape of some structures or substructures can be described with one displacement function constructed by a series of spline functions. By doing this, the mesh generation and the huge computer memory space are no longer needed because only one single superelement is used in the whole process. The choice of spline functions

as displacement functions has many advantages that have been demonstrated by several researchers for a limited range of structures. It is expected that more extensive research is needed in applying spline functions to structural analysis. The proposed research represents an effort in that direction.

Most of the applications of spline functions are so far concentrated on plate and shell type structures having regular geometries. No literature can be found in using spline functions on nonlinear problems such as reinforced concrete structures. In the present research, a computationally efficient and highly accurate method based on the spline functions is proposed to solve the bending and free vibration problems of arbitrary quadrilateral Kirchhoff's plates with any combination of clamped, simply supported, free edge and corner point supported conditions. Furthermore, the first performance of spline functions in nonlinear structural analysis will be shown here by investigating the load-deformation behavior of slender reinforced concrete (RC) columns subjected to *biaxial flexure and axial compression*.

A numerical method with better computational efficiency, solution accuracy, and simplicity on plate and RC column analyses will be developed in this dissertation.

CHAPTER 2

LITERATURE REVIEW

The present research involves both linear analysis of plates and nonlinear analysis of reinforced concrete columns by using the spline functions for displacement interpolation. The spline functions, which have been used in engineering applications for twenty years, are an important tool for numerical analysis in structural engineering. Many authors have attempted to use spline functions for interpolation in a broad range of engineering problems, and more researchers are now working on the continuous development of spline function applications.

2.1 Linear Structural Analysis by Spline Functions

Spline function approximation was first introduced by Schoenberg (1946a, 1946b) for solving certain data fitting problems. In engineering applications, Spline functions were used by Raggett, Stone, and Wilson (1974) to solve the bending problem of a circular plate with varying thickness. Later, Mizusawa, Kajita, and Naruoka (1979, 1980) used B-spline functions of various orders as coordinate functions in the Rayleigh-Ritz method to solve problems concerning vibration and buckling of skew plate structures.

Applications of spline functions in structural analysis have attracted the efforts from many researchers since early 1980's. Due to excellent characteristics of spline functions in numerical analysis, these researchers replaced the conventional functions, such as polynomial functions and trigonometric functions, with spline functions for displacement interpolation. Qin (1982) presented the spline finite point method (SFPM) for the analysis of linear

elastic straight beams and flat rectangular plates. Based on the B-spline functions, the beam vibration functions and the variation principle, he displayed excellent analytical results on the rectangular plates. This method has been extended to study a variety of structures which included the static, dynamic, and stability problems (Qin, 1985). The conventional finite strip method was modified by Cheung, Fan, and Wu (1982) who then developed the spline finite strip method. In the spline finite strip method, the trigonometric functions for the interpolation of displacement used in the conventional finite strip method were replaced by cubic B-spline functions in the longitudinal direction. Several investigators have successfully solved various plate problems recently using the spline finite strip method (Li, Cheung, and Tham, 1986; Tham, Li, Cheung, and Chen, 1986). Shen and Wang (1987) investigated the vibration of flat shells and static behavior of cylindrical shells using the B-spline functions. Their illustrative examples demonstrated good agreement as compared with the exact results and other numerical results. Chen, Gutkowski, and Puckett (1990, 1991) used the spline compound strip method to analyze the stiffened plates under transverse loading and folded plates with intermediate supports. The convergence of the spline compound strip method was improved significantly in comparison to the conventional finite strip method, the compound strip method and the finite element method.

Various other authors have developed different spline finite elements for beams, plates, and shells, respectively. The element efficiency due to the choice of the spline functions has been demonstrated in their studies. In the spline finite elements for straight beams and rectangular plates presented by Leung and Au (1990), they introduced the physical coordinates into the formulation to overcome the drawbacks of the previous spline finite elements in which some spline parameters are located outside the elements. This improvement made the

assembly of elements and the imposition of boundary conditions much easier. These elements, however, can only be used for plates with rectangular shape and more computation time is needed to carry out the analysis due to the matrix transformation between the spline coordinates and the physical coordinates. Fan and Luah (1992) employed a set of B-spline shape functions for the displacement interpolation to develop a new spline finite element for plate bending. The element has nine nodes, in the shape of an arbitrary quadrilateral with biquadratic Lagrangian shape functions for geometric interpolation. For thin plate problems, they have concluded that elements based on Kirchhoff's theory are more efficient and reliable than their Mindlin-type counterparts. It has also been shown in their research that the use of B-spline functions generally yields an excellent result in two-dimensional structural analysis. However, a lot of input data due to the mesh generation has to be prepared carefully. Also, the exclusion of the twisting curvatures at corner nodes impairs the accuracy of the element in their method.

2.2 Load-Deformation Behavior of Reinforced Concrete Columns Subjected to Longitudinal Load and Biaxial Bending

Information on the load-deflection and moment-curvature relations of reinforced concrete columns under biaxial flexure and axial load is relatively scarce. Most existing methods for the analysis of cross sections under axial load and biaxial bending rely on the numerical integration of stress resultants on a small area of the standard cross section (Hsu and Mirza 1973; Hsu 1974; Chen and Shoraka 1975). Each small area is treated as a constant stress or linearly varying stress region. Recently, Rotter (1985) presented a numerical technique to provide an exact solution for sections with rectilinear boundaries that required less computational effort. Hsu (1985, 1987, 1989) also presented results of

experimental and analytical studies on the strength and deformation of biaxially loaded short and tied columns with L-, channel, T-shaped cross sections.

For the load and deformation behavior of slender reinforced concrete columns, Farah and Huggins (1969), Basu and Suryanarayana (1975), Mavichak and Furlong (1976), Furlong (1979), Al-Noury and Chen (1982), Poston et al. (1885a, 1985b), and Poston (1986) have either developed a numerical procedure or conducted experimental tests to determine the load-deformation curves for biaxially loaded columns with pinned-ended and restrained-ended conditions. At the beginning of the typical numerical analysis, a value of deflection at a particular point (usually the midspan about the minor axis) is assigned, and a trial set of load including axial force P and end moments M_x , M_y is assumed. Then the internal moments, including second-order effects at each division point, are calculated. The deformation (axial strains and curvatures) at each division point can be obtained through the moment-curvature calculation by the tangent stiffness approach or other similar approaches. Curvatures along the column are then integrated numerically to obtain deflections at all station points. If the calculated deflection at the particular station point does not agree with the initially assumed value, the trial set of loadings must be modified, and the procedure will be repeated until the difference is within an appropriate limit. During the iteration, the internal moments for each division point are calculated first by taking the deflection as zero and then by taking the calculated deflection as the new deflection for the subsequent iteration. This procedure is repeated for all station points until satisfactory agreements are achieved. After a solution is obtained corresponding to a particular value of assigned deflection at midspan, a new value is assigned and the whole procedure is repeated. Based on the above presented analysis and theory, in principle, a load-deflection curve including ascending and descending branches of the curve can be drawn, and

the strength of the column is the peak value of this curve. However, there had been no published literature to show how such a curve could be obtained numerically until the research work done by Wang and Hsu (1990, 1992). Different from other authors, Wang and Hsu (1990, 1992) used the secant modulus of elasticity and the finite difference approach to study the complete load-deformation behavior of biaxially loaded reinforced concrete columns. Deflections at the division points along the column are calculated through satisfaction of the section equilibrium equations at these points, and then the curvatures along the column are yielded by differentiating the deflections numerically. The load-deflection and moment-curvature curves from zero load until failure have been demonstrated in good agreement with the experimental results in their study. Tsao and Hsu (1993) also applied a similar procedure to analyze slender reinforced concrete columns with rectangular and L-shaped cross sections successfully. They developed a redivision formulation to investigate the column behavior after tremendous change of the midpoint curvature due to hinging behavior. Zak (1993) presented a modification of the secant modulus method on ultimate strength analysis of reinforced concrete sections under biaxial bending and longitudinal load. He proposed a version of the fictitious-domain method to allow essentially treatment of rectangular and nonrectangular sections in the same way and to make the presented approach easily programmable and readily adaptable to different sections.

CHAPTER 3

B-SPLINE FUNCTION

The definition, features, and elementary applications of B-spline function will be described in this chapter. Some descriptions relating B-spline function to numerical analysis and engineering applications are first proposed here.

3.1 Definition of B-spline Function

The B-spline function $\varphi_n(s; k)$ of n-th degree may be defined as

$$\varphi_n(s; k) = f_n(x_{i+1}, x_{i+2}, \dots, x_m) - f_n(x_i, x_{i+1}, \dots, x_{m-1}) \quad (3-1)$$

where

$$f_n(x_{i+1}, x_{i+2}, \dots, x_m) = \frac{f_n(x_{i+2}, \dots, x_m) - f_n(x_{i+1}, \dots, x_{m-1})}{x_m - x_{i+1}}$$

$$f_n(x) = (s-x)_+^n = \begin{cases} (s-x)^n, & s \geq x \\ 0, & s < x \end{cases}$$

$$i = k - \frac{n+1}{2}, \quad m = k + \frac{n+1}{2}$$

and x denotes a bi-infinite sequence of real numbers

$$\dots < x_i < x_{i+1} < \dots < x_{m-1} < x_m < \dots$$

when $n = 3$, $i = k-2$, and $m = k+2$, Eq. (3-1) becomes cubic B-spline function with unequal sections:

$$\varphi_3(s; k) = f_3(x_{k-1}, x_k, x_{k+1}, x_{k+2}) - f_3(x_{k-2}, x_{k-1}, x_k, x_{k+1}) \quad (3-2)$$

Expanding Eq. (3-2) gives

$$\varphi_3(s; k) = \begin{cases} 0, & s < x_{k-2} \\ A_1(s - x_{k-2})^3, & x_{k-2} \leq s < x_{k-1} \\ A_1(s - x_{k-2})^3 - B_1(s - x_{k-1})^3, & x_{k-1} \leq s < x_k \\ A_2(x_{k+2} - s)^3 - B_2(x_{k+1} - s)^3, & x_k \leq s < x_{k+1} \\ A_2(x_{k+2} - s)^3, & x_{k+1} \leq s < x_{k+2} \\ 0, & x_{k+2} \leq s \end{cases} \quad (3-3)$$

where

$$A_1 = \frac{1}{h_{k-1}(h_{k-1} + h_k)(h_{k-1} + h_k + h_{k+1})}, \quad B_1 = \frac{h_{k-1} + h_k + h_{k+1} + h_{k+2}}{h_{k-1}h_k(h_k + h_{k+1})(h_k + h_{k+1} + h_{k+2})}$$

$$A_2 = \frac{1}{h_{k+2}(h_{k+1} + h_{k+2})(h_k + h_{k+1} + h_{k+2})}, \quad B_2 = \frac{h_{k-1} + h_k + h_{k+1} + h_{k+2}}{h_{k+1}h_{k+2}(h_k + h_{k+1})(h_{k-1} + h_k + h_{k+1})}$$

and

$$h_j = x_j - x_{j-1}, \quad j = k-1, \dots, k+2$$

Letting all $h_j = h$ yields a cubic B-spline with equal sections:

$$\varphi_3(s; k) = \frac{1}{6h^3} \begin{cases} 0, & s < x_{k-2} \\ (s - x_{k-2})^3, & x_{k-2} \leq s < x_{k-1} \\ (s - x_{k-2})^3 - 4(s - x_{k-1})^3, & x_{k-1} \leq s < x_k \\ (x_{k+2} - s)^3 - 4(x_{k+1} - s)^3, & x_k \leq s < x_{k+1} \\ (x_{k+2} - s)^3, & x_{k+1} \leq s < x_{k+2} \\ 0, & x_{k+2} \leq s \end{cases} \quad (3-4)$$

Cubic B-spline function φ_3 and their first and second derivatives φ_3' and φ_3'' are shown in Figs. 3-1 and 3-2 with unequal and equal sections, and their values at spline knots are given in Appendix A.

3.2 Features of B-spline Function

B-spline function has the following main features that have been found useful in the numerical analysis:

1. B-spline is the smoothest interpolating function compared with other piecewise polynomial interpolating functions. For example, the cubic B-spline has C^2 continuity, whereas the cubic Lagrange and cubic Hermite have only C^0 and C^1 continuity, respectively.

2. B-spline function has non-zero values over a few mesh subintervals, thus the resulting matrix for the discretization equation is tightly banded. A cubic B-spline $\varphi_3(s; k)$ has non-zero values over four consecutive sections with the middle section knot $s = x_k$ (Figs. 3-1 and 3-2).

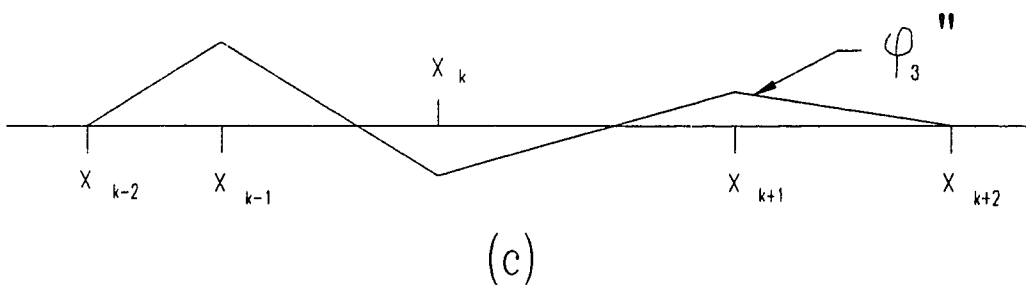
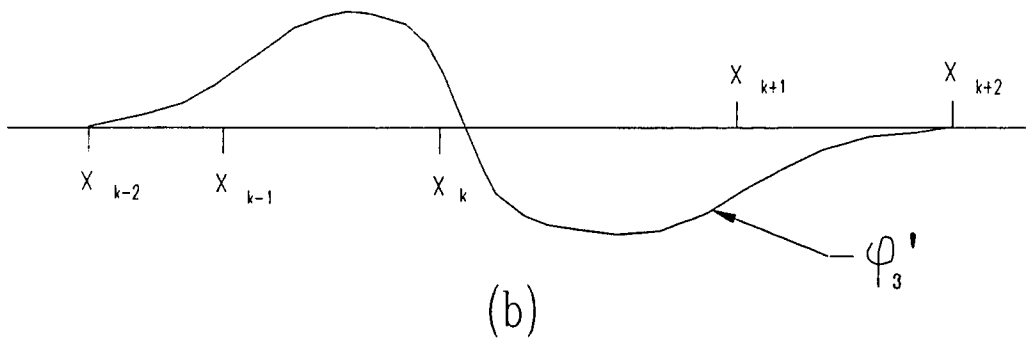
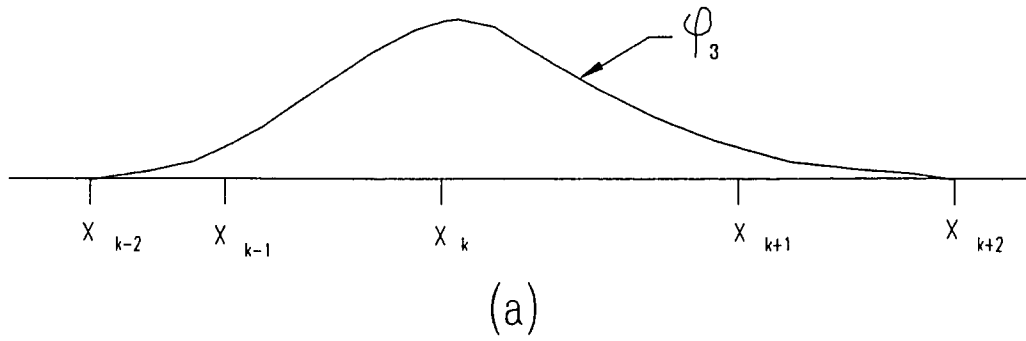


Fig. 3-1 Cubic B-spline and Its First and Second Derivatives with Unequal Sections (C^2 everywhere)

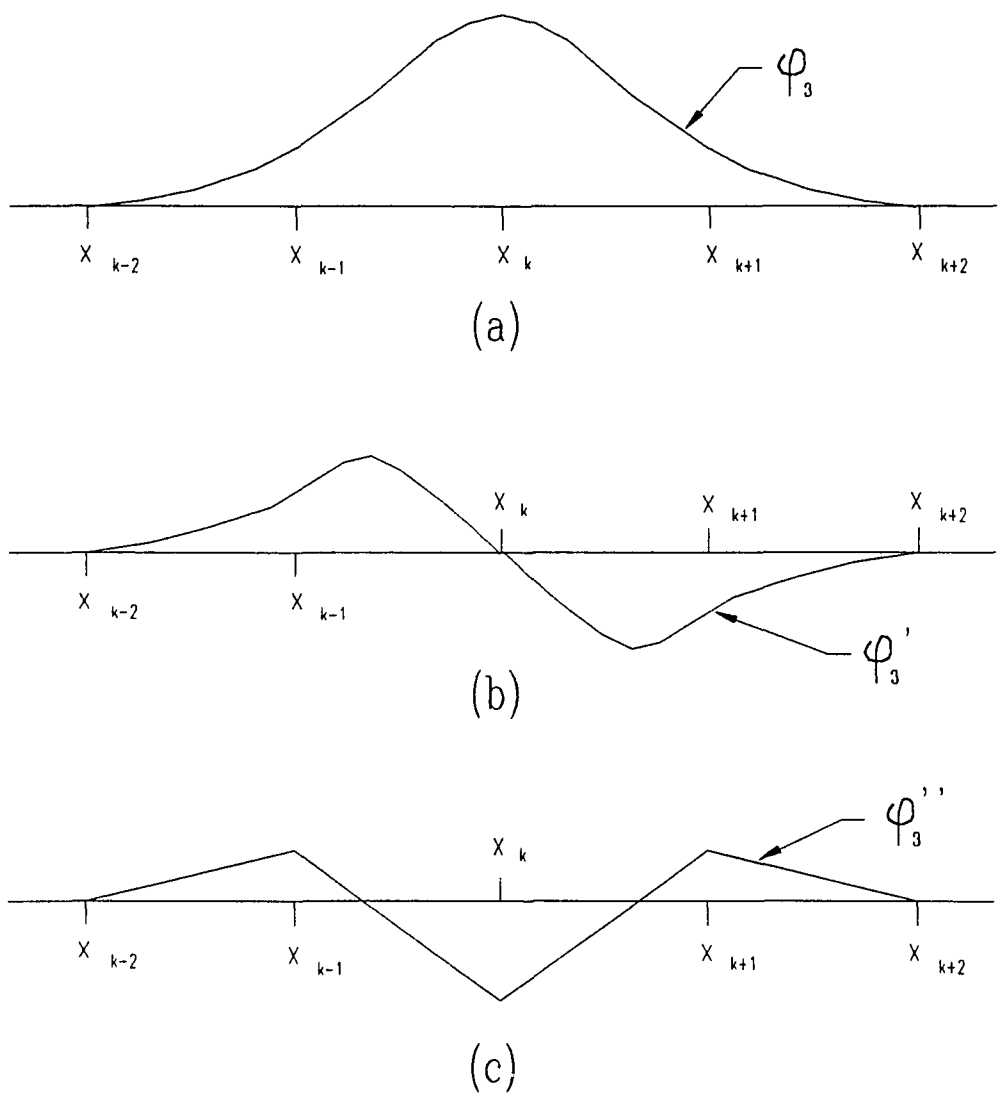


Fig. 3-2 Cubic B-spline and Its First and Second Derivatives with Equal Sections (C^2 everywhere)

3. Using B-spline function with unequal sections, one can locally modify mesh fineness in regions of high stress gradients to achieve a fast convergence. Besides, B-spline functions can be easily used to deal with the problems involving concentrated loadings, intermediate supports, abruptly changing properties and plastic hinges. The first, second, or third derivatives of displacement are discontinuous in those cases. The C^0 and C^1 continuities at spline knots in those cases can be attained by assuming $x_k = x_{k+1}$ and $x_{k-1} = x_k = x_{k+1}$, respectively (Figs. 3-3 and 3-4).

4. An arbitrary deflected curve or surface can be interpolated by the combination of a series of cubic B-splines, such as

$$w(x) = \sum_{i=-1}^{n+1} a_i \varphi_3(x; i) \quad , \quad w(x, y) = \sum_{i=-1}^{n+1} \sum_{j=-1}^{m+1} a_{ij} \varphi_3(x; i) \varphi_3(y; j) \quad (3-5)$$

where $w(x)$ or $w(x, y)$ = deflections of a curve or surface; a_i or a_{ij} = the unknown spline parameters; n and m = numbers of sections in x and y directions. The basis of cubic B-spline expression under a length L is plotted in Fig. 3-5 with the number of sections $n = 6$.

Cubic B-spline function will be used for the displacement interpolation in the proposed research. For simplicity, notation of cubic B-spline, $\varphi_3(x; i)$, will be replaced by $\varphi_i(x)$ hereafter in this dissertation.



**Fig. 3-3 Cubic B-spline and Its First Derivative
(C^1 at knot $x_k = x_{k+1}$ and C^2 elsewhere)**

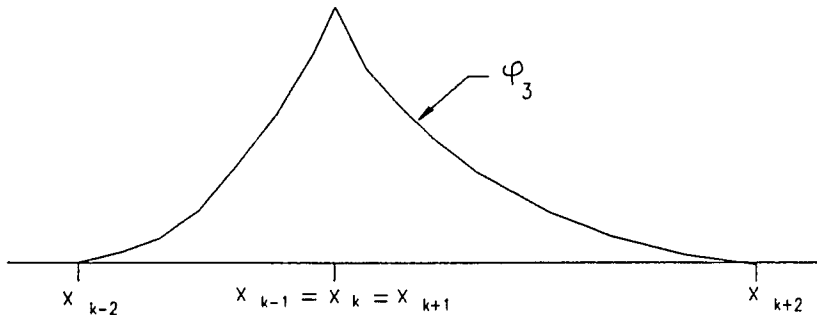


Fig. 3-4 Cubic B-spline
(C^0 at knot $x_{k-1} = x_k = x_{k+1}$, C^2 elsewhere)

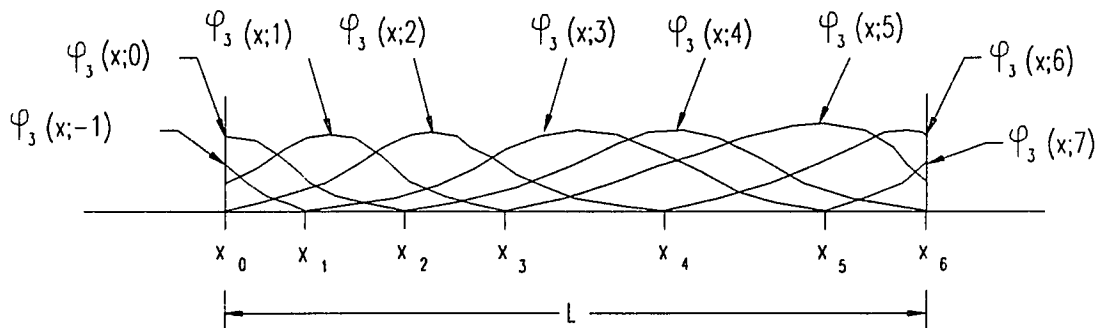


Fig. 3-5 Basis of Cubic B-spline Expression

3.3 Elementary Applications of Cubic B-spline Function

Prior to discussions on applications of cubic B-spline function to plates and RC columns, some elementary applications for beams are first introduced in the following. From these simple applications, some excellent characteristics of cubic B-spline function used in structural analysis can be demonstrated clearly.

3.3.1 One-dimensional Deflection Function

Displacement method is the most popular approach in the structural numerical analysis. Establishment of an efficient displacement field is thus important and essential in this approach.

Deflected shape of a one-dimensional problem, such as a beam, can be interpolated by the combination of a series of cubic B-splines. If $x_0, \dots, x_i, \dots, x_n$ are $n+1$ spline knots on the beam, and x_0 and x_n are at the left and right ends respectively (see Fig. 3-6), the deflection function of the beam can be expressed as

$$w(x) = \sum_{i=-1}^{n+1} \alpha_i \varphi_i(x) \quad (3-6)$$

where $w(x)$ = deflection function of the beam; α_i = generalized coordinates; and $\varphi_i(x)$ = cubic B-spline.

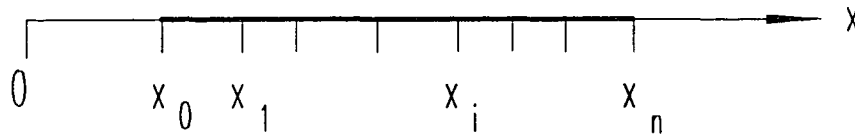


Fig. 3-6 One-Dimensional Domain with $n+1$ Spline Knots

Directly applying the above deflection function to the analysis involves extensive modifications of the generalized coordinates at or near the boundaries. In order to eliminate these modifications, the above deflection function can be reconstructed as follows:

$$w(x) = \sum_{i=-1}^{n+1} \alpha_i \phi_i(x) \quad (3-7)$$

in which α_i = modified generalized coordinates, and $\alpha_{-1} = w(x_0) = w_0$, $\alpha_0 = w'(x_0) = \mathcal{G}_0$, $\alpha_n = w(x_n) = w_n$, $\alpha_{n+1} = w'(x_n) = \mathcal{G}_n$, other $\alpha_i = \alpha_i$. Relating the

first and last two generalized coordinates to the deflections and rotations at the left and right ends of the beam respectively makes the imposition of boundary conditions much more convenient. During the computation, one does not need to consider the boundary conditions at all because the deflection equation has already satisfied all essential boundary conditions.

Expressions for $\phi_i(x)$ are (see Appendix B for further details)

$$\begin{aligned}
 \phi_{-1}(x) &= [\varphi_0'(x_0) \varphi_{-1}(x) - \varphi_{-1}'(x_0) \varphi_0(x)] / A_0 \\
 \phi_0(x) &= [\varphi_{-1}(x_0) \varphi_0(x) - \varphi_0(x_0) \varphi_{-1}(x)] / A_0 \\
 \phi_1(x) &= \{[(\varphi_0(x_0) \varphi_1'(x_0) - \varphi_1(x_0) \varphi_0'(x_0))] \varphi_{-1}(x) + \\
 &\quad [\varphi_1(x_0) \varphi_{-1}'(x_0) - \varphi_{-1}(x_0) \varphi_1'(x_0)] \varphi_0(x) + A_0 \varphi_1(x)\} / A_0 \\
 \phi_2(x) &= \varphi_2(x) \\
 &\dots \\
 \phi_{n-2}(x) &= \varphi_{n-2}(x) \\
 \phi_{n-1}(x) &= \{A_n \varphi_{n-1}(x) + [\varphi_{n-1}(x_n) \varphi_{n+1}'(x_n) - \varphi_{n+1}(x_n) \varphi_{n-1}'(x_n)] \varphi_n(x) + \\
 &\quad [\varphi_n(x_n) \varphi_{n-1}'(x_n) - \varphi_{n-1}(x_n) \varphi_n'(x_n)] \varphi_{n+1}(x)\} / A_n \\
 \phi_n(x) &= [\varphi_n'(x_n) \varphi_{n+1}(x) - \varphi_{n+1}'(x_n) \varphi_n(x)] / A_n \\
 \phi_{n+1}(x) &= [\varphi_{n+1}(x_n) \varphi_n(x) - \varphi_n(x_n) \varphi_{n+1}(x)] / A_n
 \end{aligned} \tag{3-8}$$

where

$$A_0 = \varphi_{-1}(x_0) \varphi_0'(x_0) - \varphi_0(x_0) \varphi_{-1}'(x_0)$$

$$A_n = \varphi_{n+1}(x_n) \varphi_n'(x_n) - \varphi_n(x_n) \varphi_{n+1}'(x_n)$$

If the spline knots x_0 to x_n are placed on the beam with equal intervals

$$h = x_{i+1} - x_i \quad (i = 0, 1, 2, \dots, n-1), \text{ Eq. (3-8) becomes}$$

$$\phi_{-1}(x) = 1.5 \varphi_0(x)$$

$$\phi_0(x) = 0.5 h \varphi_0(x) - 2 h \varphi_{-1}(x)$$

$$\phi_1(x) = \varphi_1(x) - 0.5 \varphi_0(x) + \varphi_{-1}(x)$$

$$\phi_2(x) = \varphi_2(x)$$

...

(3-9)

$$\phi_{n-2}(x) = \varphi_{n-2}(x)$$

$$\phi_{n-1}(x) = \varphi_{n-1}(x) - 0.5 \varphi_n(x) + \varphi_{n+1}(x)$$

$$\phi_n(x) = 1.5 \varphi_n(x)$$

$$\phi_{n+1}(x) = 2h \varphi_{n+1}(x) - 0.5h \varphi_n(x)$$

It is noted that Eq (3-7) can be used as a deflection function for the beams with different boundary conditions, various loadings, and arbitrary cross sections.

3.3.2 Applications on Beams

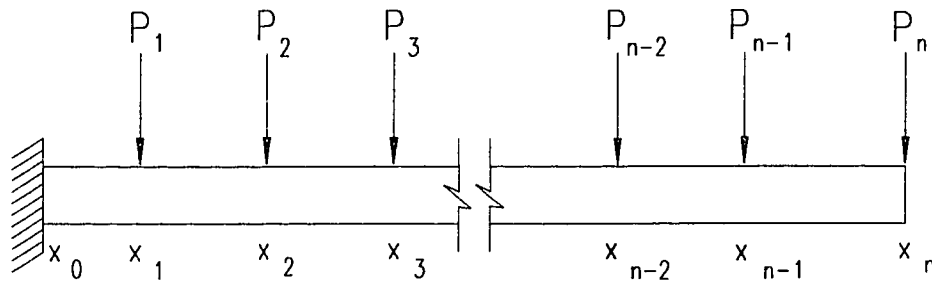


Fig. 3-7 Cantilever Beam under n Concentrated Loads

Fig. 3-7 shows a cantilever beam under n concentrated loads P_i ($i=1,2,\dots,n$) and with $n+1$ nodes at the fixed end and the application points of P 's. After introducing the boundary conditions at the fixed end, which are $w_0 = \alpha_{-1} = 0$ and $\vartheta_0 = \alpha_0 = 0$, the deflection function Eq. (3-7) becomes

$$w(x) = \sum_{i=1}^{n+1} \alpha_i \phi_i(x) \quad (3-10)$$

Eq. (3-10) can be used to exactly describe the deflection field of the beam. The deflection function in Eq. (3-10) contains $n+1$ degrees of freedom.

If a cubic Hermite polynomial is used to construct the deflection function, such as in a finite element formulation, the deflection field may be expressed as

$$w(x) = \begin{cases} N_{11}w_0 + N_{21}\vartheta_0 + N_{31}w_1 + N_{41}\vartheta_1 & (x_0 \leq x \leq x_1) \\ N_{12}w_1 + N_{22}\vartheta_1 + N_{32}w_2 + N_{42}\vartheta_2 & (x_1 \leq x \leq x_2) \\ \dots\dots\dots \\ N_{1i}w_{i-1} + N_{2i}\vartheta_{i-1} + N_{3i}w_i + N_{4i}\vartheta_i & (x_{i-1} \leq x \leq x_i) \\ \dots\dots\dots \\ N_{1n}w_{n-1} + N_{2n}\vartheta_{n-1} + N_{3n}w_n + N_{4n}\vartheta_n & (x_{n-1} \leq x \leq x_n) \end{cases} \quad (3-11)$$

where

$$\begin{aligned} N_{1i} &= 1 - [3(x - x_{i-1})^2 / h_i^2] + [2(x - x_{i-1})^3 / h_i^3] \\ N_{2i} &= (x - x_{i-1}) - [2(x - x_{i-1})^2 / h_i] + [(x - x_{i-1})^3 / h_i^2] \\ N_{3i} &= [3(x - x_{i-1})^2 / h_i^2] - [2(x - x_{i-1})^3 / h_i^3] \\ N_{4i} &= [-(x - x_{i-1})^2 / h_i] + [(x - x_{i-1})^3 / h_i^2] \\ h_i &= x_i - x_{i-1}, i = 1, 2, \dots, n \end{aligned} \quad (3-12)$$

With $w_0 = \vartheta_0 = 0$ and 2 DOF (w_i, ϑ_i) at each node, 2n DOF totally must be involved to yield an exact solution in the above deflection field by Hermitian interpolation.

From the above comparison, it can be seen that the deflection field constructed by the cubic B-splines contains less DOF than the deflection field constructed by a cubic Hermite polynomial to obtain results with the same accuracy. The ratio of DOF by the B-splines (DOFB) to DOF by a Hermite polynomial (DOFH) is $(n+1)/2n$ for the given case. Some values of the ratio are shown in Table 3-1. It is seen from the Table that the ratio DOFB/DOFH will approximately be 1/2 when $n > 20$. In other words, when compared with a Hermite interpolation with $n > 20$, only about half DOF will be needed if the B-splines are used for the deflection interpolation. Even though this conclusion is drawn from the given beam, it is applicable to general cases.

Table 3-1 Some Values of Ratio DOFB/DOFH

n	4	8	12	16	20	40
DOFB=n+1	5	9	13	17	21	41
DOFH=2n	8	16	24	32	40	80
DOFB/DOFH	1/1.60	1/1.78	1/1.85	1/1.88	1/1.90	1/1.95

Another advantage of using the B-splines over a Hermite polynomial can be shown from the comparison below. Displacement field of a whole domain can be interpolated by only one displacement function constructed from the B-splines (Eq. 3-10). Therefore, neither discretization of a domain nor an assembly of elements are needed. On the other hand, if using a Hermite polynomial to describe the displacement field (Eq. 3-11), the displacement function has different forms within different intervals $x_{i-1} \leq x \leq x_i$ ($i=1,2,\dots,n$), or different elements, so a lot of work has to be involved due to the domain discretization and element assembly.

Also, the displacement function by the B-splines can be used to analyze the problems with arbitrary cross sections, various loadings, different boundary conditions, and geometrical and material nonlinearities. They are demonstrated in the following two examples.

The first example is a 3-in wide mild-steel cantilever beam with dimensions shown in Fig. 3-8(a). Assume the beam has an ideal plastic material and $E = 30 \times 10^3 \text{ ksi}$, $\sigma_y = \pm 40 \text{ ksi}$.

The moment diagram is shown in Fig. 3-8(b). It is found that the largest stress in beam segment BC is $24.4 \text{ ksi} < \sigma_y$, which indicates the beam undergoes elastic behavior. An analogous calculation for the shallow section AB

gives a stress of 55 ksi, which is not possible as the material yields at 40 ksi. A check of the ultimate capacity for the 2-in deep section gives $M_{ult}=120$ k-in $>$ applied moment on segment AB = 110 k-in. This result shows that although the beam yields partially, it can carry the applied moment.

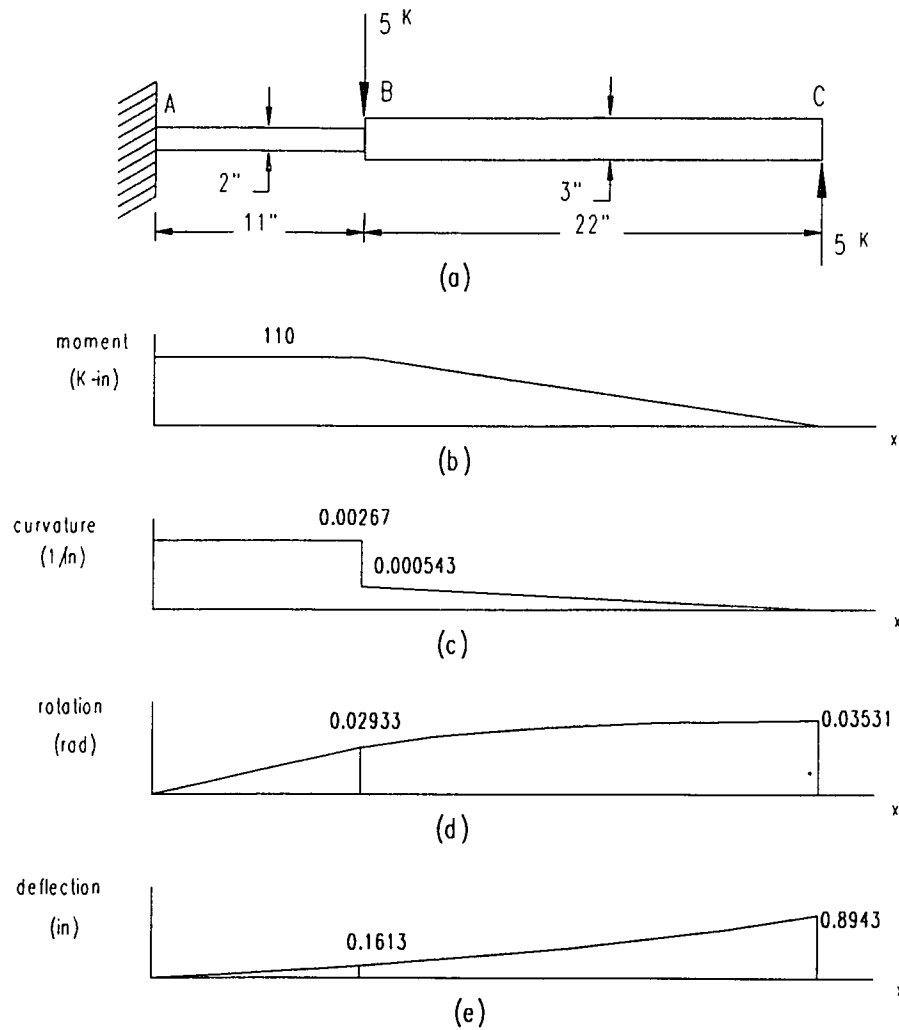


Fig 3-8 Mild-Steel Cantilever Beam

Using the B-spline function for deflection interpolation, one has

$$w(x) = \sum_{i=1}^4 \alpha_i \phi_i(x) \quad (3-13)$$

with $x_0 = 0$, $x_1 = x_2 = 11''$, and $x_3 = 33''$, where spline knots 1 and 2 both are at point B on the beam to reduce the order of continuity from C^2 to C^1 since the cross section of the beam changes abruptly at this point.

Applying the moment-curvature relation at four spline knots and solving the simultaneous equations yield

$$\alpha_1 = 0.05378 \quad \alpha_2 = 0.3764 \quad \alpha_3 = w_c = 0.8943 \quad \alpha_4 = \vartheta_c = 0.03531$$

Substitution of the above four parameters into Eq. (3-13) gives an exact deflection field of the whole beam. Data of curvature, rotation, and deflection are plotted in Fig. 3-8(c), (d), and (e), respectively.

The second example is an eccentrically loaded column with constant flexural rigidity EI , as shown in Fig. 3-9.

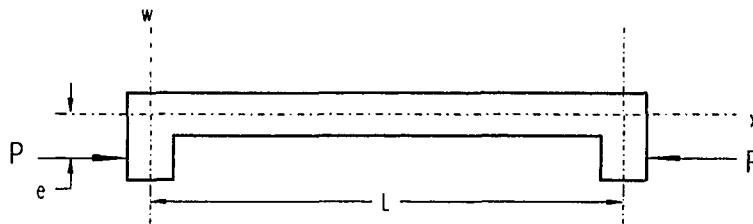


Fig. 3-9 Eccentrically Loaded Column

The exact equation of the elastic curve is

$$w(x) = e \left(\frac{1 - \cos \lambda L}{\sin \lambda L} \sin \lambda x + \cos \lambda x - 1 \right) \quad (3-14)$$

where $\lambda = \sqrt{P/(EI)}$. The maximum deflection occurs at $x = L/2$, which is found to be

$$w_{\max} = e \left(\sec \frac{\lambda L}{2} - 1 \right) \quad (3-15)$$

Due to the second order effect, deflection of an eccentrically loaded column can not be exactly expressed by a polynomial any more. Approximate solution will be given using the B-splines for deflection interpolation and this solution will converge to the exact result as more spline knots are placed on the column. Only half column is needed for analysis due to the symmetry. Considering $w(0) = 0$ and $\theta(\frac{L}{2}) = 0$, the deflection function from Eq. (3-7) becomes

$$w(x) = \sum_{i=0}^n \alpha_i \phi_i(x) \quad (3-16)$$

Assume the width of cross section = 3, height of cross section = 4, length of column $L = 100$, elastic modulus $E = 1000$, and eccentricity $e = 0.5$. The buckling load for this column is 15.79. Using Eq. (3-16), one can determine the elastic curve of the given column. Some maximum deflection values with certain eccentric loads are given in Table 3-2. Exact values are also shown in the same Table for a comparison. The maximum deflections by Eq. (3-16) are convergent to the exact solutions as numbers of segments increase. It is also noted from Table 3-2 that when the eccentrically applied load increases, the convergence of numerical solutions has been found to slow down. The reason may be due to a second order effect when the deflected curve of the column nears the buckling shape.

Table 3-2 Maximum Deflections of Eccentrically Loaded Column

Eccentric load	Maximum Deflections by Eq. (3-16)				Exact Solution
	n = 4	n = 8	n = 16	n = 32	
2	0.08961	0.08974	0.08977	0.08978	0.08978
6	0.3792	0.3815	0.3820	0.3822	0.3822
10	1.062	1.080	1.084	1.085	1.086
14	4.505	4.834	4.925	4.948	4.956

CHAPTER 4

STATIC AND DYNAMIC BEHAVIOR OF ARBITRARY QUADRILATERAL FLEXURAL PLATES

Arbitrarily shaped, elastic, thin plates are widely used in civil, marine, aeronautical, and mechanical engineering applications. Static and dynamic solutions to these plate problems are strongly dependent on the geometrical shape and boundary conditions. Exact solutions for plates are available only for certain shapes, boundaries, and loading conditions (Timoshenko and Woinowsky - Krieger, 1959). When the solutions for arbitrary shaped plates supported by complex boundary conditions are needed, a numerical method must therefore be used. Several numerical methods are usually adopted for the analysis, such as the finite element, finite difference, finite strip, and boundary element methods. The main problem with these methods is that they involve too many unknowns in order to obtain sufficiently accurate results. Extensive studies in search of more efficient approaches have been carried out on rectangular plates. Very little has been accomplished for static and dynamic analysis on plates with other geometrical shapes. This may be due to the difficulty in formulating a simple and adequate deflection function which can be used to describe the entire plate domain and at the same time it is able to satisfy the boundary conditions as well. A computationally efficient and highly accurate numerical approach using the cubic B-spline function is proposed herein to study both static and dynamic behavior of arbitrary quadrilateral flexural plates with any combination of clamped, simply supported, free edge support, and corner support conditions. More research work is needed in this area since such structural elements are commonly encountered in modern technology.

4.1 Originalities of Present Method

Using the B-spline function for displacement interpolation in structural analysis has been shown by many authors to have the advantages of higher accuracy and less degrees of freedom over other numerical methods, particularly for plate and shell type structures. In the present method, the efficient cubic B-spline functions are employed in two directions for displacement interpolation to study the static and dynamic behavior of thin arbitrary quadrilateral plates. Compared with other numerical methods of using spline functions for plate analysis, the present method may be found to be original in the following.

1. In the present method, the entire deformed shape of a plate can be described with only one displacement function constructed by a series of cubic B-spline functions. The mesh generation and large computer-memory space, drawbacks of the discretization methods, are no longer needed because only one single superelement is used in the whole process.

2. With the help of proper geometrical mapping, the present method can be used to analyze arbitrary quadrilateral plates. The plate geometries considered in the spline finite point method proposed by Qin (1982, 1985) and in the spline finite elements developed by Leung and Au (1990) were restricted to rectangular shape.

3. More flexibility of the displacement field in the present method can be obtained by applying the cubic B-spline functions in two directions. The displacement functions in the spline finite point method and in the spline finite strip method were constructed by B-spline functions in one direction and non-spline functions in another direction.

4. Due to the appropriate combination of cubic B-spline functions in the displacement field, the present method avoids the inverse computation resulting from the matrix transformation which occurs in the spline finite element method.

5. The necessary degrees of freedom to maintain the completeness of the displacement function, including the twisting curvatures at corner nodes, are all retained in the present method. In the spline finite elements developed by Fan and Luah (1992), the unavoidable approximate treatment of the twisting curvatures at corner nodes impairs the accuracy of the solutions.

4.2 Geometrical Mapping

An arbitrary quadrilateral plate in the x - y plane is shown in Fig. 4-1(a). It can be mapped into a 2×2 square region in the r - s plane as a basic plate (Fig. 4-1(b)). If the Cartesian coordinates x and y within the plate are defined by

$$x = \sum_{i=1}^4 N_i x_i, \quad y = \sum_{i=1}^4 N_i y_i \quad (4-1)$$

where x_i and y_i are the coordinates of node i in x - y plane, the shape functions N_i for mapping can be expressed as follows:

$$N_i = (1+r_0)(1+s_0)/4, \quad (i=1,2,3,4) \quad (4-2)$$

where $r_0 = r/r$ and $s_0 = s/s$; r_i and s_i = the coordinates of node i in r - s plane. For the higher order complex shape, the analysis procedure is straightforward so long as the appropriate mapping functions are selected.

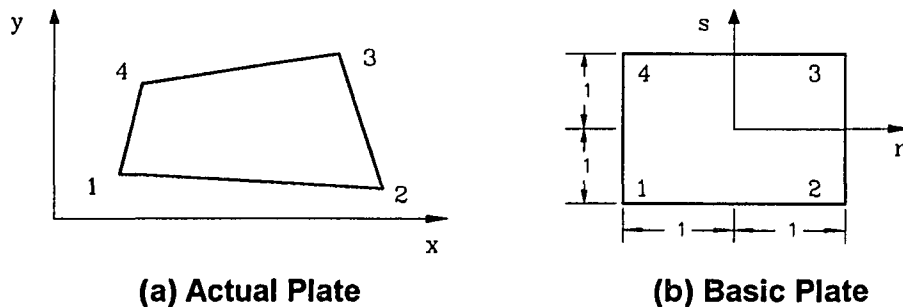


Fig. 4-1 Geometrical Mapping

By the chain rule of differentiation, the first and second derivatives of displacement w for the two coordinate systems are related as

$$\begin{Bmatrix} \frac{\partial w}{\partial x} \\ \frac{\partial w}{\partial y} \end{Bmatrix} = \mathbf{J}^{-1} \begin{Bmatrix} \frac{\partial w}{\partial r} \\ \frac{\partial w}{\partial s} \end{Bmatrix}, \quad \chi = \begin{Bmatrix} \frac{\partial^2 w}{\partial x^2} \\ \frac{\partial^2 w}{\partial y^2} \\ 2 \frac{\partial^2 w}{\partial x \partial y} \end{Bmatrix} = \mathbf{J}_2^{-1} (\mathbf{J}_1 \mathbf{J}^{-1}) \begin{Bmatrix} \frac{\partial w}{\partial r} \\ \frac{\partial w}{\partial s} \end{Bmatrix} = \begin{Bmatrix} \frac{\partial^2 w}{\partial r^2} \\ \frac{\partial^2 w}{\partial s^2} \\ \frac{\partial^2 w}{\partial r \partial s} \end{Bmatrix} \quad (4-3)$$

where

$$\mathbf{J} = \begin{bmatrix} \frac{\partial x}{\partial r} & \frac{\partial y}{\partial r} \\ \frac{\partial x}{\partial s} & \frac{\partial y}{\partial s} \end{bmatrix}, \quad \mathbf{J}_1 = \begin{bmatrix} \frac{\partial^2 x}{\partial r^2} & \frac{\partial^2 y}{\partial r^2} \\ \frac{\partial^2 x}{\partial s^2} & \frac{\partial^2 y}{\partial s^2} \\ \frac{\partial^2 x}{\partial r \partial s} & \frac{\partial^2 y}{\partial r \partial s} \end{bmatrix}, \quad \mathbf{J}_2 = \begin{bmatrix} \left(\frac{\partial x}{\partial r}\right)^2 & \left(\frac{\partial y}{\partial r}\right)^2 & \frac{\partial x}{\partial r} \frac{\partial y}{\partial r} \\ \left(\frac{\partial x}{\partial s}\right)^2 & \left(\frac{\partial y}{\partial s}\right)^2 & \frac{\partial x}{\partial s} \frac{\partial y}{\partial s} \\ \frac{\partial x}{\partial r} \frac{\partial x}{\partial s} & \frac{\partial y}{\partial r} \frac{\partial y}{\partial s} & \frac{1}{2} \left(\frac{\partial x}{\partial r} \frac{\partial y}{\partial s} + \frac{\partial x}{\partial s} \frac{\partial y}{\partial r} \right) \end{bmatrix} \quad (4-4)$$

\mathbf{J} and χ = the Jacobian matrix and the plate curvature matrix, respectively.

These above relations will be used in the later derivation of the present numerical analysis.

4.3 Displacement Function

Dividing the basic plate in r and s directions with n and m equal sections respectively, i.e.

$$-1 = r_0 < r_1 < r_2 < \dots < r_n = 1, \quad -1 = s_0 < s_1 < s_2 < \dots < s_m = 1$$

where

$$r_i = r_0 + i h_r, \quad h_r = 2/n \quad ; \quad s_j = s_0 + j h_s, \quad h_s = 2/m$$

generates a mesh with $(n+1)(m+1)$ spline finite knots on the plate.

The displacement function of the mid-surface is based on these spline finite knots and may be expressed as

$$w = \sum_{j=-1}^{M+1} \sum_{i=-1}^{N+1} c_{ij} \phi_i(r) \psi_j(s) = \mathbf{Q} \mathbf{C} \quad (4-5)$$

where

$$\mathbf{Q} = \Psi \otimes \Phi$$

$$\begin{aligned} \Phi &= [\phi_{-1} \quad \phi_0 \quad \phi_1 \quad \cdots \quad \phi_{n+1}] & \Psi &= [\psi_{-1} \quad \psi_0 \quad \psi_1 \quad \cdots \quad \psi_{m+1}] \\ \mathbf{C} &= [\mathbf{c}_{-1}^T \quad \mathbf{c}_0^T \quad \mathbf{c}_1^T \quad \cdots \quad \mathbf{c}_{m+1}^T]^T & \mathbf{c}_j^T &= [c_{-1j} \quad c_{0j} \quad c_{1j} \quad \cdots \quad c_{(n+1)j}] \end{aligned}$$

and $\Psi \otimes \Phi$ = the Kronecker product of the row matrices Ψ and Φ ; \mathbf{C} = the modified generalized spline coordinate column matrix with dimension $(n+3)(m+3)$; $\phi_i(r)$ and $\psi_j(s)$ have the same form as Eq. (3-9).

It can be found from Eq. (3-9) that

$$\begin{aligned} \phi_i(r_0) = \psi_j(s_0) = 0 \quad (i, j \neq -1) & \quad \phi_{-1}(r_0) = \psi_{-1}(s_0) = 1 \\ \phi_i'(r_0) = \psi_j'(s_0) = 0 \quad (i, j \neq 0) & \quad \phi_0'(r_0) = \psi_0'(s_0) = 1 \\ \phi_i(r_n) = \psi_j(s_m) = 0 \quad (i \neq n, j \neq m) & \quad \phi_n(r_n) = \psi_m(s_m) = 1 \\ \phi_i'(r_n) = \psi_j'(s_m) = 0 \quad (i \neq n+1, j \neq m+1) & \quad \phi_{n+1}'(r_n) = \psi_{m+1}'(s_m) = 1 \end{aligned} \quad (4-6)$$

where ϕ_i' and ψ_j' = the first derivatives of ϕ_i and ψ_j . Therefore, the treatment of the boundary conditions is easy due to the above features from the ingeniously combined displacement function Eq. (4-5). For example, eliminating ϕ_{-1} term represents a simply supported side between node 1 and 4 (Fig. 4-1(b)), and eliminating both ϕ_{-1} and ϕ_0 terms makes this side fixed. Based on Eq. (4-5), the corresponding displacement functions to the above two cases are

$$w(x) = \sum_{j=-1}^{m+1} \sum_{i=0}^{n+1} c_{ij} \phi_i(r) \psi_j(s) \quad \text{and} \quad w(x) = \sum_{j=-1}^{m+1} \sum_{i=1}^{n+1} c_{ij} \phi_i(r) \psi_j(s) \quad (4-7)$$

All correspondences between boundary conditions and eliminating terms from Eq. (4-5) are included in Table 4-1.

Table 4-1 Correspondences Between Boundary Conditions and Eliminating Terms

Side	Simply	Clamped	Sliding	Free
1 to 2	ψ_{-1}	ψ_{-1}, ψ_0	ψ_0	none
2 to 3	ϕ_n	ϕ_n, ϕ_{n+1}	ϕ_{n+1}	none
3 to 4	ψ_m	ψ_m, ψ_{m+1}	ψ_{m+1}	none
1 to 4	ϕ_{-1}	ϕ_{-1}, ϕ_0	ϕ_0	none

It is further noted that imposition of boundary conditions at corner nodes alone is also possible due to the relations shown in the following Table.

Table 4-2 Relations Between Corner Displacements, Rotations, Curvatures and Generalized Coordinates

Node	$w(r, s)$	$w_r'(r, s)$	$w_s'(r, s)$	$w_{rs}''(r, s)$
1 (r_0, s_0)	$c_{-1,-1}$	$c_{0,-1}$	$c_{-1,0}$	$c_{0,0}$
2 (r_n, s_0)	$c_{n,-1}$	$c_{n+1,-1}$	$c_{n,0}$	$c_{n+1,0}$
3 (r_n, s_m)	$c_{n,m}$	$c_{n+1,m}$	$c_{n,m+1}$	$c_{n+1,m+1}$
4 (r_0, s_m)	$c_{-1,m}$	$c_{0,m}$	$c_{-1,m+1}$	$c_{0,m+1}$

Numbers of side nodes in Table 4-1 and 4-2 refer to Fig. 4-1(b).

4.4 Formulation of Present Analysis

The total potential energy of a Kirchhoff's bending plate can be expressed as

$$\Pi = \frac{1}{2} \int_{-1}^1 \int_{-1}^1 (\chi^T \mathbf{D} \chi - 2q w) |J| dr ds = \frac{1}{2} \mathbf{C}^T \mathbf{G} \mathbf{C} - \mathbf{C}^T \mathbf{f} \quad (4-8)$$

Using the principle of minimum total potential energy, one obtains

$$\mathbf{G} \mathbf{C} = \mathbf{f} \quad (4-9)$$

where \mathbf{G} is the stiffness matrix

$$\mathbf{G} = \int_{-1}^1 \int_{-1}^1 \mathbf{B}^T \mathbf{D} \mathbf{B} |J| dr ds \quad (4-10)$$

$$\mathbf{B} = \mathbf{J}_2^{-1} (\mathbf{J}_1 \mathbf{J}^{-1} \left\{ \begin{array}{l} \Psi \otimes \Phi' \\ \Psi' \otimes \Phi \end{array} \right\} - \left\{ \begin{array}{l} \Psi \otimes \Phi'' \\ \Psi'' \otimes \Phi \end{array} \right\}) \quad (4-11)$$

For a plate of isotropic material, the rigidity matrix is

$$\mathbf{D} = \frac{E t^3}{12(1-\mu^2)} \begin{bmatrix} 1 & \mu & 0 \\ \mu & 1 & 0 \\ 0 & 0 & (1-\mu)/2 \end{bmatrix} \quad (4-12)$$

where E = Young's modulus; μ = Poisson's ratio; t = thickness of the plate.

The load matrix has the form

$$\mathbf{f} = \int_{-1}^1 \int_{-1}^1 \mathbf{Q}^T q |J| dr ds \quad (4-13)$$

where q = the intensity of applied load.

The functional of a thin plate for free vibration is

$$\Pi = \frac{\pi}{2\omega} \int_{-1}^1 \int_{-1}^1 (\chi^T \mathbf{D} \chi - \omega^2 \rho t w^2) |J| dr ds = \frac{\pi}{2\omega} \mathbf{C}^T (\mathbf{G} - \omega^2 \mathbf{M}) \mathbf{C} \quad (4-14)$$

According to the Hamilton's principle, one has

$$(\mathbf{G} - \omega^2 \mathbf{M}) \mathbf{C} = \mathbf{0} \quad (4-15)$$

where ω = the natural circular frequency.

The mass matrix

$$\mathbf{M} = \int_{-1}^1 \int_{-1}^1 \rho t \mathbf{Q}^T \mathbf{Q} |\mathbf{J}| dr ds \quad (4-16)$$

where ρ = the material mass density.

The integral functions of the stiffness, mass, and load matrices are quite complicated so that they have to be evaluated numerically. Simpson's integration formulation is applied in the present method. The values of functions ϕ_i and ψ_j and their first and second derivatives on the spline finite knots, which are needed in numerical integration and computation of displacements, rotations, and moments, are convenient to obtain.

4.5 Numerical Examples

Four plate examples with various shapes and boundary conditions are selected herein to demonstrate the efficiency and applicability of the present method. Excellent performance of the present method for this type of plate problems is achieved by comparing the results with analytical solutions and those of other numerical methods, such as the finite element method (FEM) and the spline finite strip method (SFSM). Some common symbols used in the Tables of results are defined as follows: q = the intensity of uniformly distributed load on the entire plate; P = the concentrated load at midpoint of the plate; $D = Et^3 / [12(1 - \mu^2)]$; and Poisson's ratio $\mu = 0.3$ for all test cases in this section.

Example 4-1: Bending of Square Plate

The investigation of square plates is fundamental in the analysis of plate problems. The results of a square plate using different methods are readily available in literature and the general characteristics of using different methods may be shown by comparisons of the obtained results. Both simply supported and clamped square plates under uniformly distributed and concentrated loads

are discussed in this example. Only a quarter of the plate is considered due to dual symmetry.

Table 4-3 gives the central deflections of square plates obtained by the present method as well as by FEM with a basic type of element — four-node nonconforming C^1 element with 12 degrees of freedom. Computed results from both the present method and the spline finite element method (SFEM) for a simply supported square plate under uniformly distributed load are shown in Table 4-4. Nine-node C^1 element in SFEM here has 21 degrees of freedom and has shown advantages over its counterparts in FEM through research carried out by Fan and Luah (1992). It should be noted, before a detailed observation on the compared results in Tables 4-3 and 4-4, that total number of unknowns without imposition of nodal restraints for FEM, SFEM, and the present method are $3nm+3(n+m)+3$, $2nm+2.5(n+m)+3$, and $nm+3(n+m)+9$ respectively under the same mesh $n \times m$ or the same number of nodes $(n+1)(m+1)$. With the imposition of nodal restraints, different methods may reduce a few and nearly the same number of unknowns for various boundary conditions. This indicates that the sequence of methods with fewer unknowns is the present method, SFEM, and FEM when they have equal number of nodes on the analyzed plate. By studying Tables 4-3 and 4-4, one can find that the accuracy and convergence of the present method are excellent and fewer number of nodes are needed than the other two methods to yield sufficiently accurate results. The degrees of freedom required using the present method are only about 30% and 50% when compared with the four-node element and nine-node spline element. It can be seen in Table 4-4 that the central deflection, the central bending moment and the corner twisting moment by the present method all converge rapidly, while the results by SFEM display a slower convergence caused mainly by the approximate elimination of the twisting curvatures at corner nodes.

Table 4-3 Comparison of Central Deflections of Simply Supported and Clamped Square Plates under Uniformly Distributed and Central Concentrated Loads

Number of Nodes	Simply Supported Plate				Clamped Plate			
	Uniform Load ^a		Point Load ^b		Uniform Load ^a		Point Load ^b	
	FEM	Present	FEM	Present	FEM	Present	FEM	Present
9	0.394	0.4064	1.23	1.143	0.140	0.1260	0.613	0.5419
25	0.403	0.4062	1.18	1.156	0.130	0.1265	0.580	0.5567
49	0.405	0.4062	1.17	1.158	0.128	0.1265	0.571	0.5592
81	0.406	0.4062	1.16	1.159	0.127	0.1265	0.567	0.5601
Exact	0.4062		1.16		0.1265		0.560	
multiplier ^a = $10^{-2}qa^4 / D$				multiplier ^b = $10^{-2}Pa^2 / D$				

Table 4-4 Comparison of Central Deflection and Bending Moments of Simply Supported Square Plates under Uniformly Distributed and Central Concentrated Loads

Number of Nodes	Central Deflection ^a		Bending Moment ^c at Center		Twisting Moment ^c at Corner	
	SFEM	Present	SFEM	Present	SFEM	Present
9	0.41189	0.40640	-	0.4867	-	0.3243
25	0.40675	0.40624	0.4911	0.4814	0.3554	0.3247
81	0.40627	0.40624	0.4824	0.4795	0.3390	0.3248
169	0.40624	0.40624	0.4804	0.4789	0.3330	0.3248
Exact	0.40624		0.4789		0.3248	
multiplier ^a = $10^{-2}qa^4 / D$			multiplier ^c = $10^{-1}qa^2$			

Example 2: Bending of Skew Plate

Two types of skew plates under uniformly distributed load q shown in Fig. 4-2 are analyzed in this example. They are simply supported (four simply supported edges) and simply clamped (two simply supported edges and two clamped edges). Central deflections and moments of the skew plates with different skew angles are used to compare with those by the spline finite strip method (SFSM) (Tham, Li, Cheung, and Chen, 1986). The total degrees of freedom without the imposition of boundary conditions by using SFSM for plate analysis are $2nm + 6n + 2m + 6$ under mesh $n \times m$, whereas $nm + 3(n + m) + 9$ is for the present method as mentioned above. Comparative results of two methods

shown in Tables 4-5 and 4-6 are found in a very good agreement for all different skew angle cases. It should be noted that the plate meshes generated to gain the results in Tables 4-5 and 4-6 are 17×11 by SFSM and 16×16 by the present method. The number of total parameters in the present method is about 70% of those in SFSM.

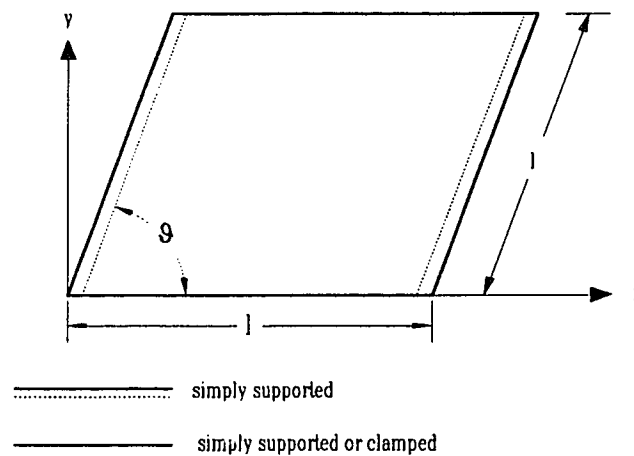


Fig. 4-2 Skew Plate

**Table 4-5 Central Deflections (w_c) and Moments (M_x, M_y)
for Simply Supported Skew Plates under Uniformly Distributed Load**

Skew Angle ϑ	α		β_x		β_y	
	SFSM	Present	SFEM	Present	SFEM	Present
90°	0.406	0.406	0.0479	0.0479	0.0479	0.0479
75°	0.376	0.376	0.0462	0.0462	0.0476	0.0476
60°	0.294	0.293	0.0409	0.0409	0.0463	0.0463
45°	0.179	0.177	0.0318	0.0315	0.0426	0.0424
30°	0.0705	0.0688	0.0190	0.0183	0.0339	0.0334

$w_c = \alpha q L^3 L_x / (100D)$, $M_x = \beta_x q L L_x$, $M_y = \beta_y q L L_x$, $L_x = L \sin \vartheta$, $t = 0.1L$.

**Table 4-6 Central Deflections (w_c) and Moments (M_x, M_y)
for Simply Clamped Skew Plates under Uniformly Distributed Load**

Skew Angle ϑ	α		β_x		β_y	
	SFSM	Present	SFEM	Present	SFEM	Present
90°	0.192	0.192	0.0244	0.0244	0.0333	0.0333
75°	0.176	0.176	0.0233	0.0234	0.0328	0.0329
60°	0.135	0.135	0.0203	0.0204	0.0310	0.0312
45°	0.0815	0.0814	0.0156	0.0157	0.0276	0.0278
30°	0.0327	0.0326	0.0098	0.0097	0.0216	0.0217

$w_c = \alpha q L^3 L_x / (100D)$, $M_x = \beta_x q L L_x$, $M_y = \beta_y q L L_x$, $L_x = L \sin \vartheta$, $t = 0.1L$.

Example 3: Flexural Free Vibration of Trapezoidal Plate

A simple supported trapezoidal plate is shown in Fig. 4-3 and it will become a rectangular plate when $b/a = 1.0$. The non-dimensionalized frequency parameters of the first six modes are given in Tables 4-7 and 4-8 for the rectangular and the trapezoidal plates respectively. An exact theoretical solution for the natural frequencies and normal modes of the simply supported trapezoidal plate is available only for the rectangular case, when $b/a = 1.0$ (Leissa, 1969). For the cases of $b/a \neq 1.0$, Chopra and Durvasula (1971) presented an approximate solution of the problem based on trigonometric series expansion with coefficients determined by the Galerkin method and their results are generally used as a reference. Exact results for the rectangular case and series solution for the trapezoidal case are included in Tables 4-7 and 4-8. Orris and Petyt (1973) used two type of high precision, conforming, plate bending elements, one a quadrilateral (16 DOF) and the other a triangular (12 DOF), to investigate the free vibration characteristics of the same plates. For comparison, their FEM results are also quoted in Tables 4-7 and 4-8, where the frequency parameters of FEM-1 and FEM-2 were computed by using 12 quadrilateral elements with 95 total DOF and 12 quadrilateral plus 2 triangular elements with 101 total DOF respectively on a half plate.

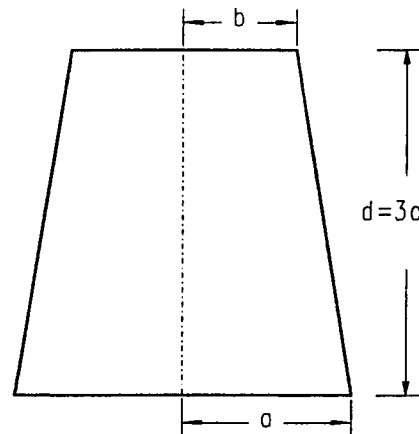


Fig. 4-3 Trapezoidal Plate

**Table 4-7 Frequency Parameters $\lambda = \omega(d^2 / \pi^2)(\rho t / D)^{1/2}$
of Simply Supported Rectangular Plate ($b/a = 1.0$)**

Mode	1	2	3	4	5	6
FEM-1	3.2505	6.253	10.029	11.279	13.033	18.070
Present	3.2502	6.252	10.014	11.277	13.018	18.047
Exact	3.25	6.25	10.0	11.25	13.0	18.0

**Table 4-8 Frequency Parameters $\lambda = \omega(d^2 / \pi^2)(\rho t / D)^{1/2}$
of Simply Supported Trapezoidal Plate ($b/a = 0.4$)**

Mode	1	2	3	4	5	6
FEM-1	5.3927	9.438	14.744	15.964	21.911	23.250
FEM-2	5.4616	9.463	14.753	16.146	21.968	23.267
Present	5.3906	9.431	14.727	15.936	21.909	23.205
Series	5.3896	9.424	14.685	15.911	21.700	23.146

The results obtained from the present method using 3×8 mesh with 66 total DOF are shown in the same tables along with the analytical solutions and better accuracy by fewer unknowns than the conforming quadrilateral and triangular elements can again be observed. The mode shapes and corresponding frequency parameters obtained from the first six modes for both rectangular and trapezoidal cases are exhibited in Fig. 4-4. They are similar to the nodal patterns presented by Chopra and Durvasula (1971), and Orris and Petyt (1973).

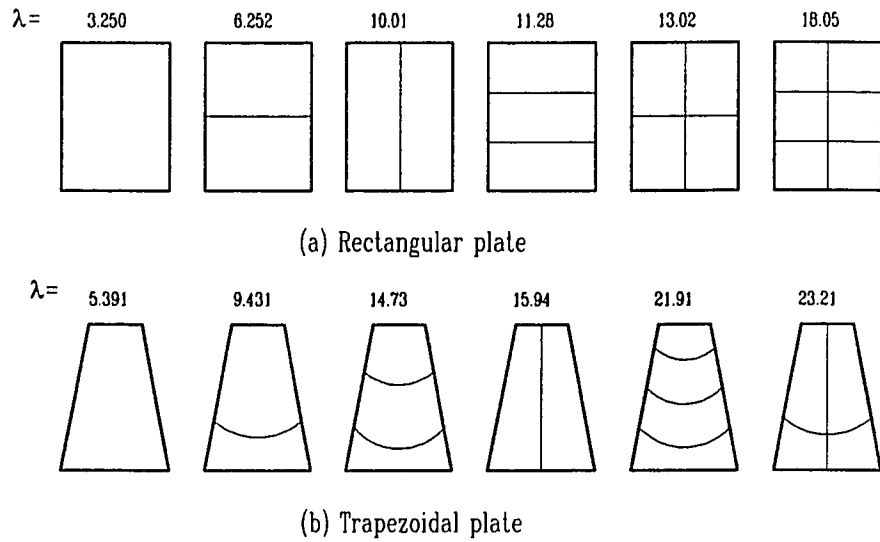


Fig 4-4 Nodal Patterns and Frequency Parameters for First Six Modes of Simply Supported Rectangular and Trapezoidal Plates

Example 4: Bending of Irregular Quadrilateral Plate

An irregular quadrilateral plate with the coordinates of four corner nodes 1, 2, 3, and 4 is shown in Fig. 4-5. The central lines AB and EF connect the midpoints at two opposite sides. Midpoint C of the plate is the intersection of the central lines AB and EF.

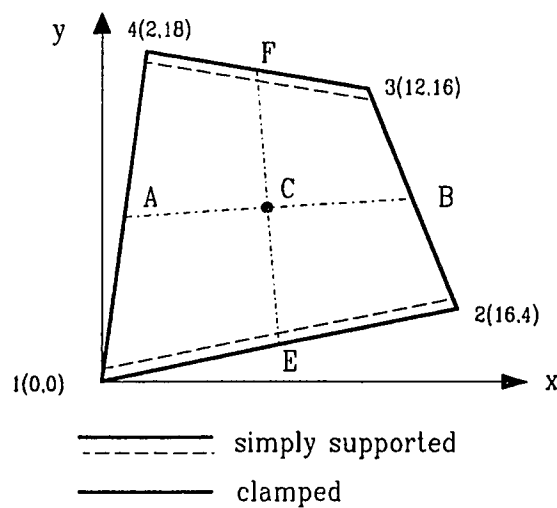


Fig. 4-5 Irregular Quadrilateral Plate

Bending analysis of this plate with two opposite sides simply supported and other two opposite sides clamped has been carried out. The results of deflection and moments at midpoint C for this plate under uniformly distributed load by the present method and FEM are shown in Table 4-9, and deflected curves along the central lines AB and EF under uniformly distributed load and a concentrated force at midpoint C by the present method are plotted in Figs 4-6 and 4-7. FEM results in Table 4-9 were obtained using structural analysis software GTSTRUDL. Plate element type is the bending plate hybrid quadrilateral element (BPHQ) which uses a quadratic interpolation for the stresses within the element. A cubic displacement expansion is used for the transverse displacement along the boundaries in BPHQ. Linear normal rotations are assumed on the boundaries. BPHQ is compatible and yields quite good results when compared with other types of plate elements.

Benefits of the present method were found from the results of this arbitrary quadrilateral plate. From the comparison of the deflections and twisting moments in Table 4-9, present method uses 143 DOF to give same accurate results as BPHQ with 705 DOF which is five times as much DOF as the present method. For bending moment results, difference of accuracy between two methods is reduced.

**Table 4-9 Deflection and Moments at Midpoint C
for Irregular Quadrilateral Plate under Uniformly Distributed Load
($q = 1, D = 1$)**

Mesh	DOF		Deflection		Bending Moment M_x		Bending Moment M_y		Twisting Moment M_{xy}	
	Pres.	FEM	Pres.	FEM	Pres.	FEM	Pres.	FEM	Pres.	FEM
8 x 8	63	161	58.88	58.78	6.082	6.002	3.717	3.649	0.215	0.218
12x12	143	385	58.92	58.89	6.010	5.973	3.705	3.675	0.209	0.211
16x16	255	705	59.93	58.92	5.984	5.963	3.700	3.683	0.207	0.209

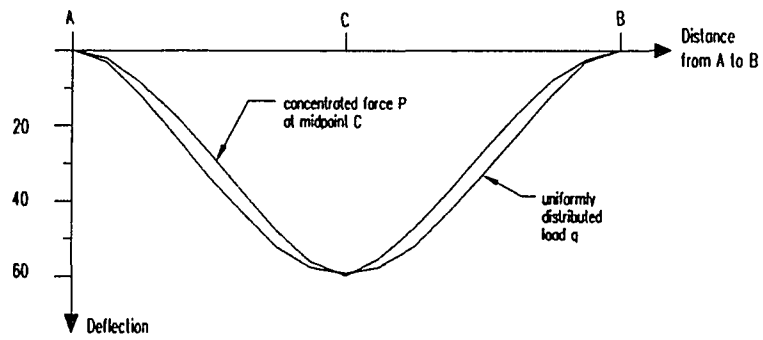


Fig 4-6 Deflected Curves along Central Line AB
($q = 1$, $P = 50$, $D = 1$, mesh 16×16 .)

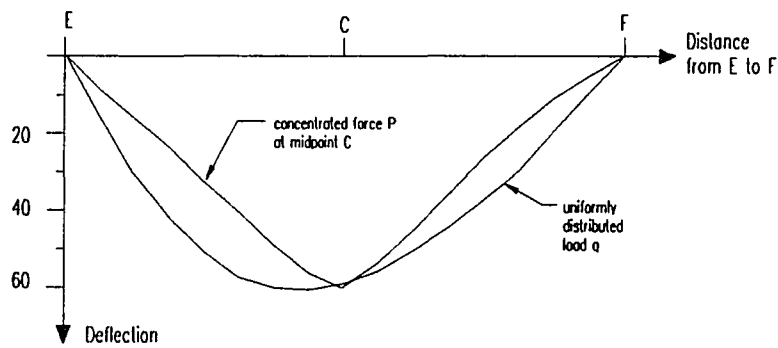


Fig. 4-7 Deflected Curves along Central Line EF
($q = 1$, $P = 50$, $D = 1$, mesh 16×16 .)

CHAPTER 5

NONLINEAR BEHAVIOR OF BIAXIALLY LOADED REINFORCED CONCRETE COLUMNS

A numerical analysis using the cubic B-spline functions for deflection interpolation has been developed in this chapter to determine the complete load-deflection and moment-curvature relationships, including ascending and descending behavior, for slender reinforced concrete (RC) columns. A multiplier p to the centroidal moment of inertia of each element is introduced in the section stiffness equation to give better results and to broaden the application of present method.

5.1 Originalities of Present Numerical Analysis

There are four originalities in the present numerical analysis as follows:

1. A B-spline function has been firstly employed to investigate into the nonlinear behavior of RC columns under biaxial bending and axial load in the present research.

2. Uniformly or linearly distributed stresses are usually assumed in a small element of the cross section to solve the problems of biaxially loaded columns. Numerical approaches under these assumptions must use a lot of elements on each cross section in order to obtain the sufficiently accurate results for general nonlinear problems. Too many elements used in analysis require more computer time. In the present method, a multiplier p is used for the section equilibrium equation based on a more logical consideration. As a result, fewer elements are needed to attain the accurate results.

3. For columns with nonrectangular sections, there is a need to use an additional formulation to solve the problems (Tsao and Hsu 1993, Zak 1993). The present method, however, can be used to analyze RC columns with arbitrary cross sections under a unified formulation.

4. The choice of B-spline function as a deflection function results in a tightly banded stiffness matrix. Based on the Gaussian elimination, an equation solver suitable for the simultaneous equations in the present approach is developed, so that the computations can be carried out more efficiently.

5.2 Basic Assumptions and Constitutive Relations

The present analysis is based on the following assumptions: (1) Plane sections remain plane during bending; (2) The stress-strain relations for the column materials are known; (3) No twisting occurs and the effects of axial and shear deformation are negligible; (4) Shrinkage and creep effects are neglected; (5) Perfect bond between steel and concrete elements; (6) The boundary conditions at two ends are known.

Both stress-strain relationships for unconfined and confined concretes are used here. The relationships for unconfined and confined concretes developed by Carreira and Chu (1985) and by Mander, Priestley and Park (1988), respectively, are used in this research. They are given below:

for nonconfined concrete

$$\frac{f}{f_c'} = \frac{\beta_c (\varepsilon / \varepsilon_c)}{\beta_c - 1 + (\varepsilon / \varepsilon_c)^{\beta_c}} \quad (5-1)$$

and for confined concrete

$$\frac{f}{f_{cc}'} = \frac{\beta_{cc} (\varepsilon / \varepsilon_{cc})}{\beta_{cc} - 1 + (\varepsilon / \varepsilon_{cc})^{\beta_{cc}}} \quad (5-2)$$

where

$$\beta_c = \frac{1}{1 - \frac{f_c'}{\varepsilon_c E_c}} \quad \beta_{cc} = \frac{1}{1 - \frac{f_{cc}'}{\varepsilon_{cc} E_c}}$$

$$\varepsilon_{cc} = \varepsilon_c \left[1 + 5 \left(\frac{f_{cc}'}{f_c'} - 1 \right) \right] \quad (5-3)$$

where $E_c = 5,000\sqrt{f_c'} \text{ Mpa} = 60,208\sqrt{f_c'} \text{ psi}$ is the initial tangent modulus of elasticity of the concrete.

Definition of above equations can be found from Fig. 5-1. Areas of confined and unconfined concrete are shown in Fig. 5-2 after consideration of average arch effect (Mander, Priestley and Park, 1988).

The stress-strain curve for the reinforcing steel including strain hardening has been idealized using piece-wise linear approximation as shown in Fig. 5-3. Both compressive and tensile branches of the curve consist of five straight segments.

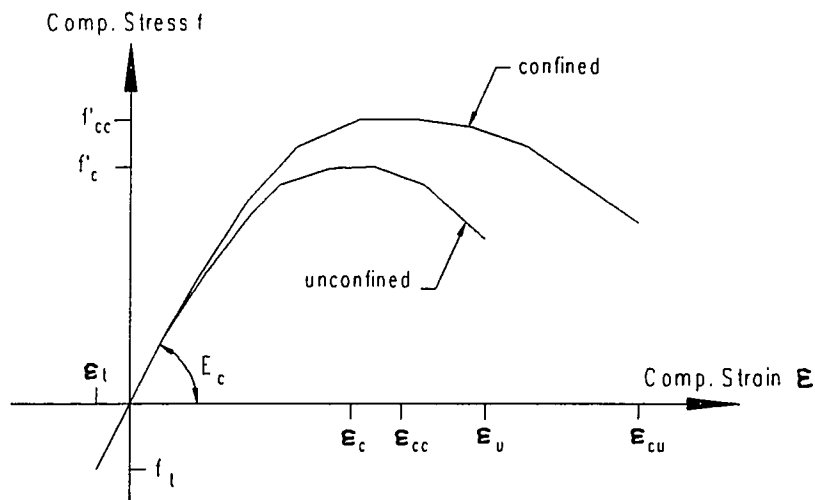


Fig. 5-1 Stress-Strain Curve of Confined and Unconfined Concretes

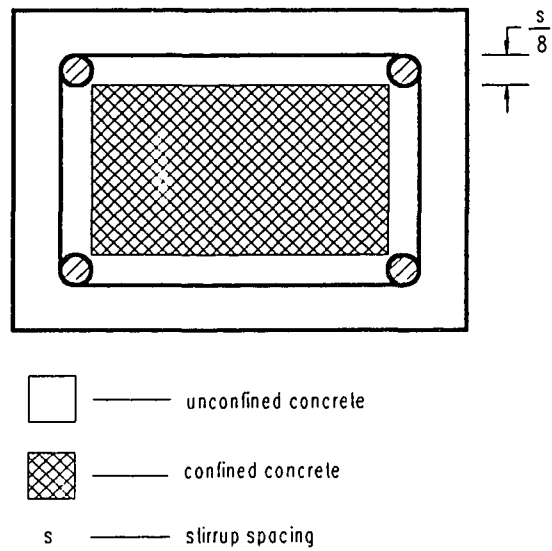


Fig. 5-2 Cross Section with Confined and Unconfined Areas

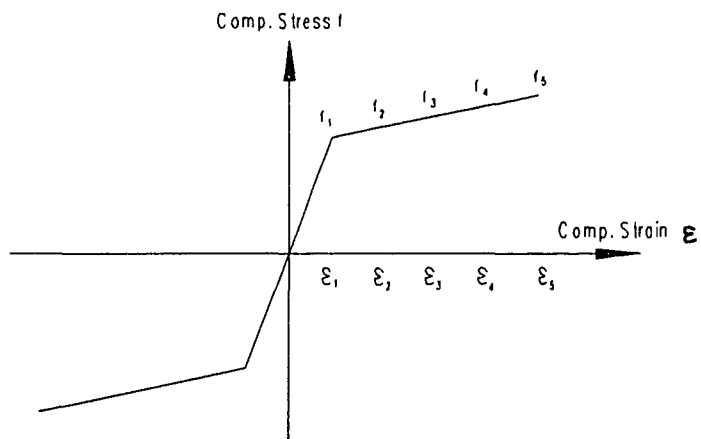


Fig. 5-3 Stress-Strain Curve of Steel

5.3 Present Numerical Method

Present analysis of RC slender columns is based on both section level and member level, and they are discussed below.

5.3.1. Section Stiffness Equation

There are three approaches to integrate section equilibrium equations. The first is based on the exact integration rules, and it is only used for some very simple cases. For general and practical RC slender columns, the second and third approximate integration approaches have to be adopted. In the second method, the section is divided into strips rotating parallel to the neutral axes in the solution process for equilibrium equations. This approach is rather cumbersome due to continuous determination of varying position of neutral axis. The third method is the simplest of all in that the section is divided into small elements and these elements are fixed in the whole solution process. The third method will be used and modified for the present work.

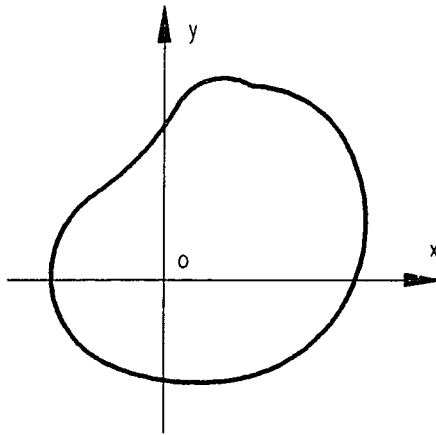


Fig. 5-4 Arbitrary Column Cross Section

On a column cross section with an arbitrary shape as shown in Fig. 5-4, the stress resultants P , M_x , and M_y with respect to Cartesian coordinate origin o may be expressed as follows according to section equilibrium equations:

$$\begin{aligned} P &= \int_A f \, dA = \int_{A_c} f_c \, dA_c + \int_{A_s} f_s \, dA_s \\ M_x &= \int_A f \, y \, dA = \int_{A_c} f_c \, y \, dA_c + \int_{A_s} f_s \, y \, dA_s \\ M_y &= \int_A f \, x \, dA = \int_{A_c} f_c \, x \, dA_c + \int_{A_s} f_s \, x \, dA_s \end{aligned} \quad (5-4)$$

where $A = A_c + A_s$ = the total area of the cross section; f = the normal stress at point (x, y) ; Subscripts c and s are corresponding to concrete and steel respectively; P and f are positive in compression and negative in tension. It is not necessary that x - and y -axes are principal axes. As a matter of the fact, no any limitation is attributed to the position of coordinate origin o and the orientation of Cartesian coordinate system under the plane assumption and small strain theory (see Appendix C for mathematical proof).

After dividing the cross section into small elements and integrating Eq. (5-4) element by element, Eq. (5-4) becomes

$$\begin{aligned} P &= \sum_i \int_{A_{ci}} f_{ci} \, dA_{ci} + \sum_j \int_{A_{sj}} f_{sj} \, dA_{sj} \\ M_x &= \sum_i \int_{A_{ci}} f_{ci} \, y \, dA_{ci} + \sum_j \int_{A_{sj}} f_{sj} \, y \, dA_{sj} \\ M_y &= \sum_i \int_{A_{ci}} f_{ci} \, x \, dA_{ci} + \sum_j \int_{A_{sj}} f_{sj} \, x \, dA_{sj} \end{aligned} \quad (5-5)$$

where subscripts i and j are corresponding to i th concrete element and j th steel element, respectively.

For convenience of generating element mesh on the cross section, the elements of concrete may be based on the total cross sectional area and then the concrete portion in steel area is subtracted. Hence, Eq. (5-5) is

$$\begin{aligned} P &= \sum_k \int_{A_{ck}} f_{ck} \, dA_{ck} + \sum_j \int_{A_{sj}} \Delta f_j \, dA_{sj} \\ M_x &= \sum_k \int_{A_{ck}} f_{ck} \, y \, dA_{ck} + \sum_j \int_{A_{sj}} \Delta f_j \, y \, dA_{sj} \end{aligned} \quad (5-6)$$

$$M_y = \sum_k \int_{A_{ck}} f_{ck} x dA_{ck} + \sum_j \int_{A_{sj}} \Delta f_j x dA_{sj}$$

where $\Delta f_j = f_{sj} - f_{cj}$; Subscript k is corresponding to k th concrete element based on the total cross sectional area. Letting the secant modulus of elasticity for the materials $E = f / \varepsilon$ and assuming constant E in each element, one has

$$\begin{aligned} P &= \sum_k E_{ck} \int_{A_{ck}} \varepsilon_{ck} dA_{ck} + \sum_j \Delta E_j \int_{A_{sj}} \varepsilon_{sj} dA_{sj} \\ M_x &= \sum_k E_{ck} \int_{A_{ck}} \varepsilon_{ck} y dA_{ck} + \sum_j \Delta E_j \int_{A_{sj}} \varepsilon_{sj} y dA_{sj} \\ M_y &= \sum_k E_{ck} \int_{A_{ck}} \varepsilon_{ck} x dA_{ck} + \sum_j \Delta E_j \int_{A_{sj}} \varepsilon_{sj} x dA_{sj} \end{aligned} \quad (5-7)$$

in which $\Delta E_j = E_{sj} - E_{cj}$.

Since plane sections remain plane during bending, the strain ε at any point (x, y) is given by

$$\varepsilon(x, y) = \varepsilon_o + \phi_x y + \phi_y x \quad (5-8)$$

where ε_o = strain at the coordinate origin o ; ϕ_x and ϕ_y = curvatures corresponding to M_x and M_y , the bending moments about the x - and y -axes, respectively.

Substituting Eq. (5-8) into Eq. (5-7) yields section stiffness equation in a matrix notation:

$$\mathbf{F} = \mathbf{K} \mathbf{C} \quad \text{or} \quad \begin{Bmatrix} P \\ M_x \\ M_y \end{Bmatrix} = \begin{bmatrix} k_{11} & k_{12} & k_{13} \\ k_{21} & k_{22} & k_{23} \\ k_{31} & k_{32} & k_{33} \end{bmatrix} \begin{Bmatrix} \varepsilon_o \\ \phi_x \\ \phi_y \end{Bmatrix} \quad (5-9)$$

where

$$\begin{aligned} k_{11} &= \sum_k E_{ck} A_{ck} + \sum_j \Delta E_j A_{sj} \\ k_{12} &= \sum_k E_{ck} y_k A_{ck} + \sum_j \Delta E_j y_j A_{sj} = k_{21} \\ k_{13} &= \sum_k E_{ck} x_k A_{ck} + \sum_j \Delta E_j x_j A_{sj} = k_{31} \\ k_{22} &= \sum_k E_{ck} (y_k^2 A_{ck} + p I_{xxk}) + \sum_j \Delta E_j (y_j^2 A_{sj} + p I_{xxj}) \\ k_{23} &= \sum_k E_{ck} x_k y_k A_{ck} + \sum_j \Delta E_j x_j y_j A_{sj} = k_{32} \end{aligned} \quad (5-10)$$

$$k_{33} = \sum_k E_{ck} (x_k^2 A_{ck} + p I_{yck}) + \sum_j \Delta E_j (x_j^2 A_{sj} + p I_{ycj})$$

where x_k, y_k and x_j, y_j = the centroidal coordinates of concrete element k and steel element j , respectively; I_{xck}, I_{xcj} and I_{yck}, I_{ycj} = the moments of inertia of concrete element k and steel element j about the centroidal axes x_c and y_c , respectively; p = multiplier to centroidal moment of inertia of each element.

The multiplier p of zero and a unit in Eq. (5-10) represents a uniform stress or linear stress distribution across each element. Both uniform or linear stress concept has been adopted by several researchers. These approximate approaches require many small elements in each cross section and are unable to give exact solutions for linear elastic and perfectly plastic columns problems, respectively. Introduction of the multiplier p into the present formulation generates a more logical and accurate approach. $p = 0$ represents perfectly plastic case and $p = 1$ represents linear elastic case. Thus, $0 < p < 1$ may be rationally used to represent a general nonlinear case. The present method can be used to obtain an exact solution for the linear elastic as well as perfectly plastic problems. For general nonlinear problems, it yields results with higher accuracy, using fewer elements in the cross section when compared with uniform stress or linear stress method. Another important feature is that the present method allows similar implementation of analysis for any arbitrary cross sections. Comparisons of computational results between the present method, uniform stress method, and linear stress method, are shown in 5.3.5.

5.3.2 Member Stiffness Equation

Deflected curve for a slender column under combined biaxial flexure and axial compression is shown in Fig. 5-5. The column is divided into n segments with arbitrary intervals, and the deflections in the x and y directions at division points

between these segments are denoted by $u_0, u_1, \dots, u_i, \dots, u_n$ and $v_0, v_1, \dots, v_i, \dots, v_n$ respectively. After consideration of the second order effect at division point i , Eq. (5-9) becomes

$$\mathbf{F}_i = \mathbf{K}_i \mathbf{C}_i \quad (5-11)$$

where

$$\begin{aligned} \mathbf{F}_i &= [P \quad M_{x0} + Pv_i \quad M_{y0} + Pu_i]^T = P[1 \quad e_y + v_i \quad e_x + u_i]^T \\ \mathbf{C}_i &= [\varepsilon_0 \quad \phi_x \quad \phi_y]_i^T = [\varepsilon_0 \quad -v'' \quad -u'']_i^T \end{aligned} \quad (5-12)$$

in which $M_{x0} = Pe_y$ and $M_{y0} = Pe_x$ are the end moments about the x- and y-axes at the initial division point 0; u'' and v'' are the second derivatives of deflections u and v along the longitudinal direction of the column; Expressions for \mathbf{K}_i are the same as the ones in Eq. (5-9) and (5-10) as long as the computations are based on the section property of division point i .

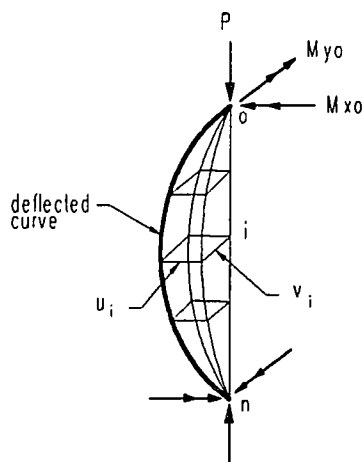


Fig. 5-5 Deflected Curve for a Slender Biaxially Loaded Column

Cubic B-spline functions are used to describe the displacement fields u and v as follows:

$$u = \sum_{k=1}^{n+1} a_k \phi_k(z) \quad v = \sum_{k=1}^{n+1} b_k \phi_k(z) \quad (5-13)$$

which are the same as Eq. (3-7).

Since cubic B-spline has non-zero values only over four consecutive sections, or on three consecutive spline knots, and $\phi_k(z)$ are combined from the cubic B-splines (see Eq. (3-8) and (3-9)), one can have

$$\begin{aligned} u_i &= a_{i-2} \phi_{i-2}(z_i) + a_{i-1} \phi_{i-1}(z_i) + a_i \phi_i(z_i) + a_{i+1} \phi_{i+1}(z_i) + a_{i+2} \phi_{i+2}(z_i) \\ v_i &= b_{i-2} \phi_{i-2}(z_i) + b_{i-1} \phi_{i-1}(z_i) + b_i \phi_i(z_i) + b_{i+1} \phi_{i+1}(z_i) + b_{i+2} \phi_{i+2}(z_i) \end{aligned} \quad (5-14)$$

where $\phi_{i-2}(z_i) = 0$ when $i \neq 1$; $\phi_{i+2}(z_i) = 0$ when $i \neq n-1$.

Similarly, the second derivatives of u and v , or the curvatures ϕ_y and ϕ_x , can be found to be

$$\begin{aligned} u''_i &= a_{i-2} \phi''_{i-2}(z_i) + a_{i-1} \phi''_{i-1}(z_i) + a_i \phi''_i(z_i) + a_{i+1} \phi''_{i+1}(z_i) + a_{i+2} \phi''_{i+2}(z_i) \\ v''_i &= b_{i-2} \phi''_{i-2}(z_i) + b_{i-1} \phi''_{i-1}(z_i) + b_i \phi''_i(z_i) + b_{i+1} \phi''_{i+1}(z_i) + b_{i+2} \phi''_{i+2}(z_i) \end{aligned} \quad (5-15)$$

where $\phi''_{i-2}(z_i) = 0$ when $i \neq 1$; $\phi''_{i+2}(z_i) = 0$ when $i \neq n-1$.

Substituting Eq. (5-15) into Eq. (5-11) yields

$$F_i = \sum_{k=i-2}^{i+2} g_{i,k} \delta_k \quad (5-16)$$

where

$$\begin{aligned} \delta_k &= [\varepsilon_k \quad b_k \quad a_k]^T \\ g_{i,k} &= - \begin{bmatrix} \beta(k_{11})_i & (k_{12})_i \phi''_k(z_i) & (k_{13})_i \phi''_k(z_i) \\ \beta(k_{21})_i & (k_{22})_i \phi''_k(z_i) & (k_{23})_i \phi''_k(z_i) \\ \beta(k_{31})_i & (k_{23})_i \phi''_k(z_i) & (k_{33})_i \phi''_k(z_i) \end{bmatrix} \end{aligned} \quad (5-17)$$

in which $\beta = 0$ when $i \neq k$ and $\beta = -1$ when $i = k$; $g_{i,i-2} = 0$ when $i \neq 1$ and $g_{i,i+2} = 0$ when $i \neq n-1$.

Summing all equations at different division points ($i = 0, 1, \dots, n$) from Eq. (5-16), the following member stiffness equation can be achieved:

$$G \delta = R \quad (5-18)$$

where

$$\delta = [\delta_{-1}^T \quad \delta_0^T \quad \dots \quad \delta_{n+1}^T]^T_{3(n+3) \times 1}$$

$$\mathbf{R} = \begin{bmatrix} \mathbf{F}_0^T & \mathbf{F}_1^T & \cdots & \mathbf{F}_n^T \end{bmatrix}_{3(n+1) \times 1}^T \quad (5-19)$$

\mathbf{G} = see Eq. (D-1) in Appendix D

There are no difficulties to impose boundary conditions using Eq. (5-18) due to the following relationships of the deflections and rotations at two ends,

$$\begin{aligned} a_{-1} = u_0 & & a_0 = u'_0 & & a_n = u_n & & a_{n+1} = u'_n \\ b_{-1} = v_0 & & b_0 = v'_0 & & b_n = v_n & & b_{n+1} = v'_n \end{aligned} \quad (5-20)$$

The above relationships also make it easy to use the deflection increment to control the iterative solution procedure of Eq. (5-18).

If the column is pinned-ended and the loads are symmetrically applied on the column, only half of the column needs to be considered. Dividing this half column into n segments, one has the following boundary conditions:

$$a_{-1} = u_0 = 0 \quad a_{n+1} = u'_n = 0 \quad b_{-1} = v_0 = 0 \quad b_{n+1} = v'_n = 0 \quad (5-21)$$

Introducing these boundary conditions into Eq. (5-18) gives

$$\begin{aligned} \delta &= \begin{bmatrix} \delta_0^T & \delta_1^T & \cdots & \delta_n^T \end{bmatrix}_{3(n+1) \times 1}^T \\ \mathbf{R} &= \begin{bmatrix} \mathbf{F}_0^T & \mathbf{F}_1^T & \cdots & \mathbf{F}_n^T \end{bmatrix}_{3(n+1) \times 1}^T \end{aligned} \quad (5-22)$$

\mathbf{G} = see Eq. (D-2) in Appendix D

The experimental specimens that are used for comparisons of results in 5.4 have the same conditions as above.

Solving the member stiffness Eq. (5-18), one can determine the complete load-deflection and moment-curvature relationships for slender RC columns under combined biaxial flexure and axial load. The numerical analysis developed here can be used for any end conditions and variable section geometries. With the increment of deflection, the analysis takes into account all stages of behavior up to and beyond maximum load and moment. The method is also applicable to cases in which the cross section of the column is made up of different materials, and the cross section varies along the length of the column.

5.3.3 Incremental Procedure and Flow Chart

In member stiffness equation (5-18), matrices \mathbf{G} and \mathbf{R} are functions of displacement vector δ due to the second order effect of slender column and nonlinear constitutive relationships of the column materials. Incremental approach of secant modulus is used to solve the member stiffness equation. The reason to adopt secant-modulus approach instead of tangent-modulus one is based on the fact that the secant-modulus approach gives more stable computation process and avoids divergence due to the small tangent stiffness of section. In order to determine the entire curves of load-deflection and moment-curvature, displacement or deformation may be chosen as an incremental parameter. The whole incremental path consists of many steps corresponding to points in plotting the whole curves. In each step, an iterative process is repeatedly used until it reaches convergence, then go to next step. The iterative expression of eq. (5-18) is given by

$$\mathbf{G}_j \delta_{j+1} = \mathbf{R}_j \quad (5-23)$$

The convergence criterion for an iterative process is

$$|\delta_{j+1} - \delta_j| \leq 0.00001 |\delta_{j+1}| \quad (5-24)$$

The above criterion guarantees sufficient accuracy of the present computed solution.

The incremental procedure will be terminated when the strain at the point of extreme compressive bar reaches 0.005. This is based on the assumption that crushing of concrete at this moment is immediately followed by concrete spalling. Subsequently, buckling of the compression reinforcement occurs at region where the concrete has spalled.

The flow chart of the present computational process for RC slender columns is shown in Appendix E.

5.3.4 Solver of Simultaneous Equations

By selecting the cubic B-splines to construct the deflection function, the member stiffness matrix (see Eq. D-1 and D-2) has been found to be tightly banded. The original sparse stiffness matrix of size $3(n+1)$ by $3(n+1)$ is compacted into a rectangular matrix of size $3(n+1)$ by 9 (see Eq. D-3). For this storage format, a solver based on Gauss elimination is developed, and its Fortran coding is provided in Appendix E. This special solver avoids storage and processing of zero coefficients in the stiffness matrix. Consequently it lowers the requirement of computer memory and reduces the time of computation. Even though the solver for equations with banded matrix can be found in the literature, without modification it is not the most efficient approach for the present formulation. It is because the solver has to store and process some zero coefficients in the present stiffness matrix.

Unlike Tsao and Hsu (1993), the present formulation maintains the well structured matrix form. Also the efficient solver is developed here which does not need to interchange columns between the stiffness matrix and load vector for dividing the knowns and unknowns.

5.3.5 Accuracy and Convergence

Numerical solutions are approximate, thus their accuracy and convergence must be studied thoroughly. There are several possibilities that may cause computational errors. Some of them affect the results very little and may be ignored. But some of them significantly affect the results and must be taken into account in modeling. Modeling error refers to the difference between a physical system and its mathematical model. Based on the assumptions given in 5.2, the present slender RC column model is established. Previous studies from many researchers have shown that the errors due to these assumptions are minor and

can be ignored. Discretization on the cross section and along the column are the major sources of computational errors, which is discussed in the following.

Errors can arise from the idealization of the cross section into element in which the stress distribution pattern is approximately assumed. This error can be reduced by increasing the number of elements in the cross section. How this may affect the final results and how many elements should be used for different sections are investigated from the analysis based on the two different reinforced concrete sections shown in Fig. 5-6. They are square and L-shaped cross sections, respectively. Basic required data are listed in Table 5-1.

Table 5-1 Data of Reinforced Concrete Sections

Cross Section	f_c' (ksi)	f_t (ksi)	f_y (ksi)	Bar	e_x (in.)	e_y (in.)
Square	4	0.5	60	8 #14	6	6
L-shaped	4	0.5	60	12 #9	16	20

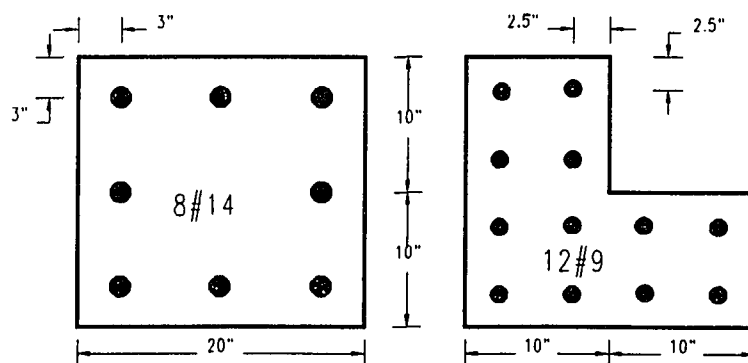


Fig. 5-6 Reinforced Concrete Sections

Computational results of compressive strength and corresponding curvatures under different numbers of elements by the present method (using $p = 0.2$ in Eq. 5-10), uniform stress method (USM) and linear stress method (LSM) are given in Tables 5-2 and 5-3, respectively. Figs. 5-7 and 5-8 show the values and convergence of these results. It can be seen that the present method can give more accurate results with fewer elements than other two methods. If taking the result by 408 elements of square cross section as most accurate one for comparison, the present method needs only 17 elements to yield a result with a error smaller than 0.1 percent. To achieve the same accurate result, the uniform stress method needs 44 elements and the linear stress method 108 elements. Similar conclusions can be drawn from the results of L-shaped cross section. In order to obtain sufficiently accurate results, numbers of elements required by uniform stress method and by linear stress method are more than 2 times and 10 times of that by the present method respectively. It is also noted that from Figs. 5-7 and 5-8 the results from all three methods converge to the same solution as increasing the number of elements. However, linear stress method seems to give a upper-bound solution, while uniform stress method yields a lower-bound solution. The present method generates a nearly horizontal line to which the other two methods converge.

Analysis of a slender column involves second order effect, so that the column has to be discreted into segments for analysis. Accuracy can be improved as more segments are used to model the column. Two pin-ended slender columns discussed here have different lengths and cross sections. One with square cross section is 40 ft long and another with L-shaped cross section is 30 ft long. Sizes and properties of these sections are the same as those shown in Fig. 5-6 and Table 5-1. Only half of the column is analyzed here due to its symmetry. The square and L-shaped cross sections are divided into 72

elements and 60 elements, respectively. Compressive strength, corresponding deflections and maximum moments, corresponding curvatures are computed by the present method using different numbers of segments and the computational results are shown in Table 5-4 and 5-5. Sufficiently accurate results can be obtained by 8 segments or above for both slender columns.

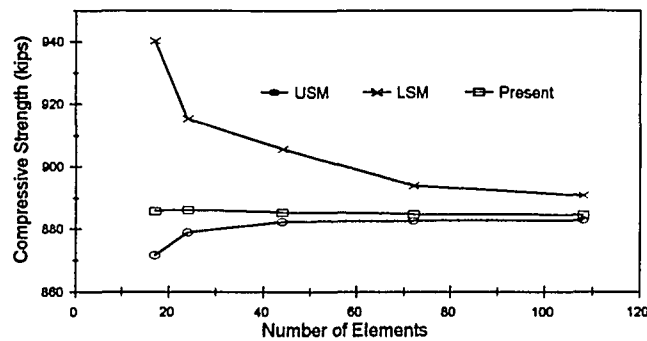


Fig. 5-7 Convergence of Compressive Strength for Square Cross Section

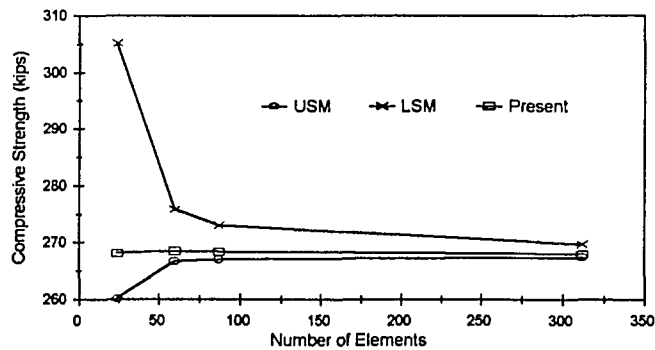


Fig. 5-8 Convergence of Compressive Strength for L-shaped Cross Section

**Table 5-2 Compressive Strength and Curvature of Square Section
with Different Numbers of Elements**

No. of elements	uniform stress method		linear stress method		present method	
	Pmax (kips)	$\phi_x = \phi_y$ (10^{-3} in/in)	Pmax (kips)	$\phi_x = \phi_y$ (10^{-3} in/in)	Pmax (kips)	$\phi_x = \phi_y$ (10^{-3} in/in)
12	833.7	0.22	1014	0.22	872.7	0.22
17	871.6	0.22	940.4	0.22	885.8	0.22
24	879.0	0.22	915.4	0.22	886.2	0.22
44	882.4	0.22	905.7	0.22	885.4	0.22
72	882.7	0.22	894.0	0.22	884.8	0.22
108	882.9	0.22	890.8	0.22	884.5	0.22
408	883.5	0.22	887.4	0.22	884.3	0.22

**Table 5-3 Compressive Strength and Curvature of L-Shaped Section
with Different Numbers of Elements**

No. of elements	uniform stress method		linear stress method		present method	
	Pmax (kips)	ϕ_x / ϕ_y (10^{-3} in/in)	Pmax (kips)	ϕ_x / ϕ_y (10^{-3} in/in)	Pmax (kips)	ϕ_x / ϕ_y (10^{-3} in/in)
24	260.2	0.443/0.4	305.2	0.674/0.4	268.2	0.468/0.4
60	266.8	0.460/0.4	275.9	0.462/0.4	268.6	0.460/0.4
87	267.1	0.459/0.4	273.1	0.460/0.4	268.4	0.459/0.4
312	267.5	0.459/0.4	269.8	0.459/0.4	268.0	0.459/0.4

Table 5-4 Computational Results of Square Section Column with Different Numbers of Segments

No. of segments	P _{max} (kips)	d _v = d _u (in.)	Max. M _x = M _y (kip-in)	ϕ _x = ϕ _y (10 ⁻³ in/in)
4	502.6	4.0	5552	0.2661
8	501.5	4.0	5544	0.2637
16	501.4	4.0	5542	0.2634
20	501.3	4.0	5542	0.2632

Table 5-5 Computational Results of L-Shaped Section Column with Different Numbers of Segments

No. of segments	P _{max} (kips)	d _v (in.)	d _u (in.)	Max. M _x (kip-in)	ϕ _x (10 ⁻³ in/in)	Max. M _y (kip-in)	ϕ _y (10 ⁻³ in/in)
4	175.7	4.46	4.0	4352	0.3865	3571	0.4263
8	175.6	4.46	4.0	4351	0.4786	3572	0.4333
16	175.5	4.46	4.0	4351	0.4784	3572	0.4331
20	175.5	4.46	4.0	4351	0.4796	3572	0.4342

5.4 Comparison with Experimental Results

In the test program performed at New Jersey Institute of Technology (NJIT) by Tsao (1991), six square and eight L-shaped slender RC columns were constructed and tested to failure under combined biaxial loading and axial compression. Different eccentricities were used to examine the behavior of the slender columns. The entire experiments were carried out using MTS loading system. The longitudinal concrete strains were measured at midheight by pairs of mechanical strain gages with a 6-in. gage length. The deflection components

along the x- and y-axes were also measured at midheight using dial gages. The concrete properties and maximum compressive strength were determined using 3x6 in. cylinders. C series represents square slender columns and B series denotes L-shaped slender columns. Details of the test specimens, experimental method, and test results can be found in Tsao (1991).

It was found that both the ascending and descending branches of the experimental load-deflection and moment-curvature curves as shown in Appendix G were successfully attained using MTS loading system. In the present numerical analysis, the cross sections of square column specimens are divided into 32 unconfined concrete elements, 4 confined concrete elements, and 4 steel elements. A total of 40 elements are used for square cross section. The cross sections of L-shaped column specimens are divided into 20 unconfined concrete elements, 9 confined concrete elements, 8 steel elements. Totally 37 elements are used for each L-shaped cross section. Both types of columns have the total length of 48 inches. Only half length of columns divided into 8 segments longitudinally due to its symmetry is used for analysis. Based on the present numerical analysis, the theoretical load-deflection and moment-curvature curves shown in the same figures as the experimental curves in Appendix G are computed using deflection control. They are noted to be in satisfactory agreement through all loading stages from zero load up to failure. It should be noted that the theoretical computations of biaxial load-deflection and moment-curvature curves were terminated when the strain at the point of extreme compressive bar reaches 0.005 according to the assumption in 5.3.3.

Maximum axial loads and corresponding midheight deflections for each specimen are given in Table 5-6 and 5-7. Results from the tests by Tsao and Hsu (1994), numerical approach by Tsao and Hsu (1993), and present method are listed in the same Tables for comparison. Maximum axial loads obtained by

Tsao and Hsu yield results close to those obtained by present method. However, It should be noted that the former method used more elements for each cross section (68 elements for square section, 108 elements for L-shaped section) than those used by present method (40 elements for square section, 37 elements for L-shaped section). Both methods used the same number of 8 segments for half column longitudinally. When compared with the experimental deflection results, the present method yields a more accurate values generally. Improvement in deflection accuracy by present method results from the introduction of cubic B-spline displacement function and a more logical concrete stress-strain relationship for confined elements.

Another significant advantage using the present method is that the same numerical formulation can be applied to any arbitrary cross sections for all phases of behavior from zero load to failure. Based on the approach for a rectangular section, Zak (1993) introduced an indicator function for the geometry of nonrectangular sections to determine the ultimate strength of nonrectangular biaxially loaded columns. The approach developed by Tsao and Hsu (1993) had to transform the deflections between two coordinate systems for L-shaped cross section. They also proposed redivision along the column when tremendous change in curvature near the midheight of the column due to hinging behavior. However, all of the above additional treatments become unnecessary in the present approach.

Table 5-6 Maximum Axial load and Deflections for B Series Columns

Specimen Number	Test			Analysis			Analysis		
	Tsao and Hsu (1994)			Tsao and Hsu (1993)			Present Method		
	P_{max}	u	v	P_{max}	u	v	P_{max}	u	v
B2	10045	0.69	0.40	10500	0.48	0.37	9928	0.55	0.41
B3	12565	0.72	0.28	11890	0.55	0.31	11243	0.62	0.34
B4	9915	0.82	0.38	9416	0.54	0.31	9215	0.63	0.36
B5	27955	0.37	0.20	25781	0.35	0.18	25563	0.38	0.20
B6	15750	0.61	0.28	16718	0.44	0.25	16009	0.54	0.29
B7	15740	0.48	0.27	17365	0.41	0.26	16578	0.50	0.30
B8	10310	0.65	0.46	10055	0.55	0.35	9819	0.59	0.37

units: P_{max} (lbs), u & v (inches)

Table 5-7 Maximum Axial load and Deflections for C Series Columns

Specimen Number	Test			Analysis			Analysis		
	Tsao and Hsu (1994)			Tsao and Hsu (1993)			Present Method		
	P_{max}	u	v	P_{max}	u	v	P_{max}	u	v
C1	15210	0.24	0.68	14659	0.31	0.59	14839	0.32	0.62
C2	12565	0.47	0.49	14109	0.47	0.47	14023	0.44	0.44
C3	8810	0.52	0.56	10195	0.47	0.47	10068	0.49	0.49
C4	18640	0.38	0.40	16465	0.35	0.35	16296	0.41	0.41
C5	10495	0.38	0.64	10345	0.26	0.53	10233	0.30	0.60
C6	18300	0.30	0.55	16945	0.24	0.47	16841	0.28	0.54

units: P_{max} (lbs), u & v (inches)

A test program for rectangular and partial circular columns under biaxially eccentric thrust was carried out by Mavichak and Furlong (1976) at University of Texas. These specimens were slender enough to deform laterally during the application of load. Twenty-four columns of the same length with two different shapes were tested to failure. Nine specimens with rectangular cross section were designated as RC-1 through RC-9. Fifteen partial circular columns were named as C-1 through C-15. During the sequence of loading, thrust was maintained at one of three different load levels, $0.2P_0$, $0.35P_0$, or $0.5P_0$, while the eccentric loads were increased to produce failure. P_0 was the squash load capacity of the section. Each type of cross section for the column was tested with one of three nominal skew load angles, $22\text{-}1/2^\circ$, 45° , or $67\text{-}1/2^\circ$, and at one of the three axial load levels. Uniaxial bending tests were made on partial circular columns (specimen C-1 to C4, C14, and C15), but not on rectangular columns. Fig. 5-9 show the dimensions and reinforcement of both cross sections. Measurements of longitudinal strain using a 6-in. gage length and lateral displacement along the length of each loaded specimen were used for plotting the experimental moment-curvature curves and the determination of experimental deflection at the mid-height of the columns. More details of experimental method, test results, and test specimen can be found in Mavichak and Furlong (1976).

Biaxial moment-curvature relations were computed using present method by assuming the same constant thrust on the specimens as Mavichak and Furlong (1976). At the same time the eccentricity along the direction of skew load angle was increased. Moment-curvature curves from both experimental and present analysis results are shown in Appendix H. As can be seen, the present analysis gives good agreement between the observed and computed values from zero up to ultimate moment capacities of the column specimens. No

comparison was made after the peak moments because the descending branch of the moment-curvature curves was not attained in the experiments. The maximum experimental moments about the strong axis in specimens C-5, C-6, and C-7 were reported greater than the maximum moments about the weak axis by Mavichak and Furlong (1976) which were not consistent with the rational behavior of these biaxial specimens with 45° loading angles. The present analysis results show a more rational behavior.

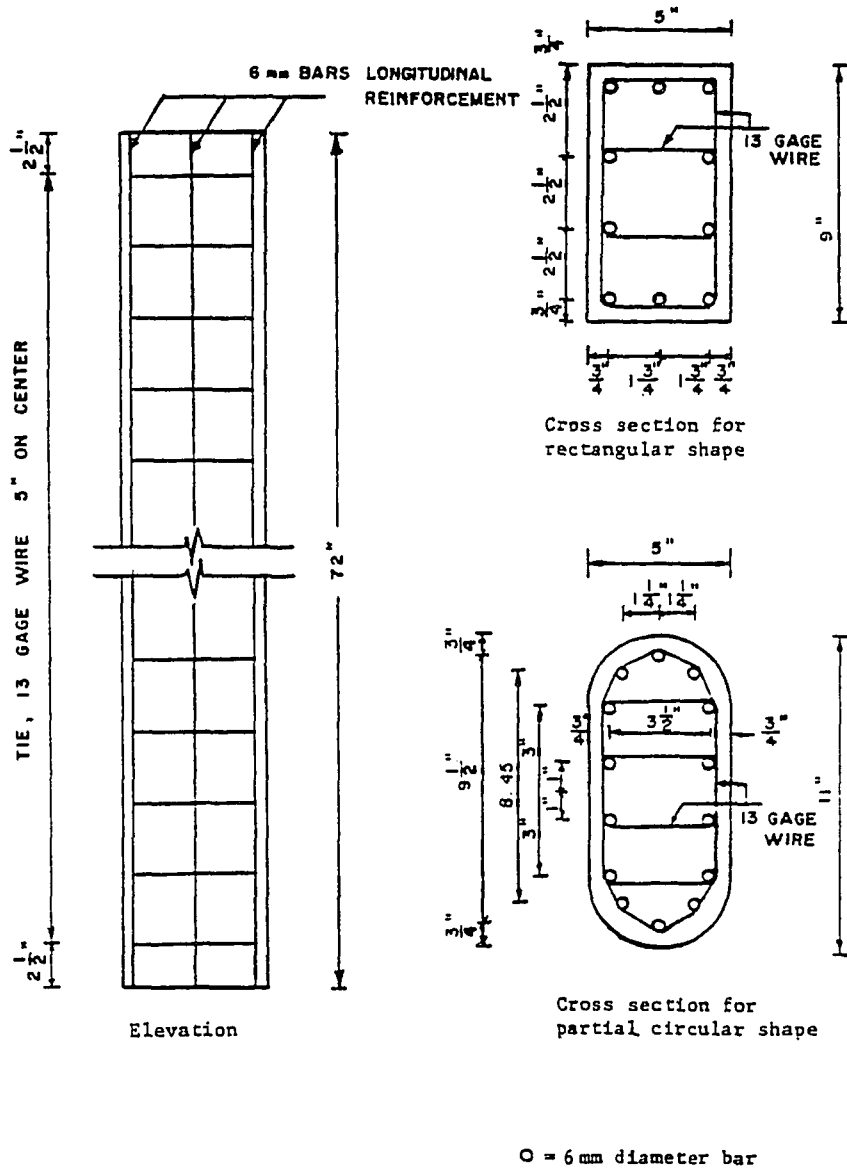


Fig. 5-9 Details of Specimens at University of Texas

CHAPTER 6

SUMMARY AND CONCLUSIONS

The purpose of this research is to develop a more efficient numerical method for flat plate and slender RC column analyses by using the cubic B-splines as displacement functions. The cubic B-spline function is a valuable tool for structural analysis in that it can be used to efficiently construct a displacement field for an entire structural element, such as a plate or a column. Compared with other discretization methods, the present method does not need mesh generation and element assembly, and yields more accurate results from a model with fewer degrees of freedom. Also, good agreement of results obtained from the present method and the RC column experiments has been demonstrated.

6.1 Conclusions for Plate Analysis

Cubic B-spline functions for interpolation of displacement in two directions are employed herein to analyze the arbitrary quadrilateral plate problems. From the theoretical considerations and the numerical examples, the present method can be summarized to achieve the following three advantages for this class of plate problems, as compared with other numerical methods.

1. By using the efficient and flexible cubic B-spline displacement function in a whole plate, the present method involves only one single superelement and does not require domain discretization and element assembly. More rapid convergence and better accuracy than those discretization methods have been demonstrated from the present method.

2. Under the mesh of $n \times m$ for an arbitrary quadrilateral plate, the present method with $(n+3)(m+3)$ parameters for the interpolation of displacement requires less degrees of freedom and yields more accurate results than other numerical methods, such as the conventional four-node element with $3(n+1)(m+1)$ parameters, the nine-node spline element with $2(n+1)(m+1) + (n+m+2)/2$ parameters, and the spline finite strip method with $2(n+1)(m+3)$ parameters.

3. Unlike other discretization method, the present method does not require mesh generation so that only minimal input data is needed. Also this method avoids the additional moment modifications which occur in discretization methods due to the different moment values at the sharing nodes.

6.2 Conclusions for RC Column Analysis

An analytical model using B-spline displacement function is presented to simulate the load-moment-curvature-deflection behavior of slender reinforced concrete (RC) columns subjected to biaxial bending and axial compression. With control of deflection increments and secant stiffness approach, the present method addresses complete relationships of load-deflection and moment-curvature of RC columns with arbitrary cross sections and boundary conditions.

Introduction of the p-multiplier enables the present method to give accurate results using fewer elements than other numerical methods. Good agreement was obtained between the experimental strengths and the analytical values calculated by the present computer program. The experimental curvature and deflection data obtained from the tests were noted to be in better agreement with the present analytical results through all load stages from zero load up to failure. The reason may be attributed to the applications of flexible B-spline

displacement function and the rational concrete stress-strain relationships for confined elements in the present analytical model.

APPENDIX A

VALUES OF CUBIC B-SPLINE FUNCTION AND ITS FIRST AND SECOND DERIVATIVES

Table A-1 Values of φ_3 , φ_3' , and φ_3'' at Spline Knots ($h_j \neq \text{constant}$)

Knot	$\varphi_3(x; k)$	$\varphi_3'(x; k)$	$\varphi_3''(x; k)$
x_{k-2}	0	0	0
x_{k-1}	$\frac{(h_{k-1})^2}{H_{k-1}^k H_{k-1}^{k+1}}$	$\frac{3h_{k-1}}{H_{k-1}^k H_{k-1}^{k+1}}$	$\frac{6}{H_{k-1}^k H_{k-1}^{k+1}}$
x_k	$\frac{2h_k h_{k+1} H_{k-1}^{k+2} + h_{k-1} h_{k+1} H_{k-1}^{k+2} + h_k h_{k+2} H_{k-1}^k}{H_{k-1}^{k+1} H_k^{k+1} H_k^{k+2}}$	$\frac{3(h_{k+1} H_{k+1}^{k+2} - h_k H_{k-1}^k)}{H_{k-1}^{k+1} H_k^{k+1} H_k^{k+2}}$	$\frac{-6(H_{k-1}^{k+2} + H_k^{k+1})}{H_{k-1}^{k+1} H_k^{k+1} H_k^{k+2}}$
x_{k+1}	$\frac{(h_{k+2})^2}{H_{k+1}^{k+2} H_k^{k+2}}$	$\frac{-3h_{k+2}}{H_{k+1}^{k+2} H_k^{k+2}}$	$\frac{6}{H_{k+1}^{k+2} H_k^{k+2}}$
x_{k+2}	0	0	0
Note: $H_{ii}^{i2} = \sum_{j=i}^{i2} h_j$			

**Table A-2 Values of φ_3 , φ_3' , and φ_3'' at Spline Knots and
Midpoints between Each Two Adjacent Knots ($h_j = h = \text{constant}$)**

Knot	x_{k-2}	$x_{k-1.5}$	x_{k-1}	$x_{k-0.5}$	x_k	$x_{k+0.5}$	x_{k+1}	$x_{k+1.5}$	x_{k+2}
$\varphi_3(x; k)$	0	1/48	1/6	23/48	2/3	23/48	1/6	1/48	0
$\varphi_3'(x; k)$	0	1/(8h)	1/(2h)	5/(8h)	0	-5/(8h)	-1/(2h)	-1/(8h)	0
$\varphi_3''(x; k)$	0	1/(2h ²)	1/h ²	-1/(2h ²)	-2/h ²	-1/(2h ²)	1/h ²	1/(2h ²)	0

APPENDIX B

DERIVATION OF EQUATION (3-8)

Eqs. (3-6) and (3-7) can be expressed in a matrix form as follows:

$$w(x) = \varphi \mathbf{a} \quad (\text{B-1})$$

and
$$w(x) = \Phi \alpha \quad (\text{B-2})$$

where

$$\begin{aligned} \varphi &= [\varphi_{-1}(x) \quad \varphi_0(x) \quad \cdots \quad \varphi_{n+1}(x)] & \Phi &= [\phi_{-1}(x) \quad \phi_0(x) \quad \cdots \quad \phi_{n+1}(x)] \\ \mathbf{a} &= [a_{-1} \quad a_0 \quad \cdots \quad a_{n+1}] & \alpha &= [\alpha_{-1} \quad \alpha_0 \quad \cdots \quad \alpha_{n+1}] \end{aligned}$$

According to Eq. (B-1) and the relations of $\alpha_{-1} = w(x_0)$, $\alpha_0 = w'(x_0)$, $\alpha_n = w(x_n)$, $\alpha_{n+1} = w'(x_n)$, and other $\alpha_i = a_i$, one has

$$\alpha = \mathbf{T} \mathbf{a} = \begin{bmatrix} \mathbf{T}_0 & \mathbf{0} & \mathbf{0} \\ \mathbf{0} & \mathbf{I} & \mathbf{0} \\ \mathbf{0} & \mathbf{0} & \mathbf{T}_n \end{bmatrix} \mathbf{a} \quad (\text{B-3})$$

where
$$\mathbf{T}_0 = \begin{bmatrix} \varphi_{-1} & \varphi_0 & \varphi_1 \\ \varphi_{-1}' & \varphi_0' & \varphi_1' \\ 0 & 0 & 1 \end{bmatrix}_{x=x_0} \quad \mathbf{T}_n = \begin{bmatrix} 1 & 0 & 0 \\ \varphi_{n-1} & \varphi_n & \varphi_{n+1} \\ \varphi_{n-1}' & \varphi_n' & \varphi_{n+1}' \end{bmatrix}_{x=x_n}$$

\mathbf{I} = unit matrix with (n-3) by (n-3) dimension.

Inversion of Eq. (B-3) gives

$$\mathbf{a} = \mathbf{T}^{-1} \alpha = \begin{bmatrix} \mathbf{T}_0^{-1} & \mathbf{0} & \mathbf{0} \\ \mathbf{0} & \mathbf{I} & \mathbf{0} \\ \mathbf{0} & \mathbf{0} & \mathbf{T}_n^{-1} \end{bmatrix} \alpha \quad (\text{B-4})$$

in which \mathbf{T}_0^{-1} and \mathbf{T}_n^{-1} = inverse matrices of \mathbf{T}_0 and \mathbf{T}_n .

Substituting Eq. (B-4) into (B-1) yields

$$w(x) = \varphi \mathbf{T}^{-1} \alpha \quad (\text{B-5})$$

By comparing Eq. (B-5) with (B-2), one has

$$\Phi = \varphi \mathbf{T}^{-1} \quad (\text{B-6})$$

which is a matrix form of Eq. (3-8).

APPENDIX C

STRAIN UNDER TWO ARBITRARY CARTESIAN COORDINATE SYSTEMS

Fig. C-1 shows two arbitrary cartesian coordinate systems on a cross section which is corresponding to a division point along the column. Points 0 and 1 are the origins of coordinate systems x_0y_0 and u_1v_1 respectively. System u_1v_1 is gained by translating the x_0y_0 system x_1 in x direction, y_1 in y direction and then rotating it θ counterclockwise. Point P is an arbitrary point on the cross section with coordinate (x_p, y_p) at system x_0y_0 and (u_p, v_p) at system u_1v_1 . Deflections at this division point under system x_0y_0 are denoted by d_x and d_y in x and y directions, and deflections under system u_1v_1 are expressed by d_u and d_v in u and v directions. According to the formula of coordinate transformation, one has

$$\begin{Bmatrix} x_p \\ y_p \end{Bmatrix} = \begin{Bmatrix} x_1 \\ y_1 \end{Bmatrix} + \begin{bmatrix} \cos \theta & -\sin \theta \\ \sin \theta & \cos \theta \end{bmatrix} \begin{Bmatrix} u_p \\ v_p \end{Bmatrix} = \begin{Bmatrix} x_1 \\ y_1 \end{Bmatrix} + \mathbf{T} \begin{Bmatrix} u_p \\ v_p \end{Bmatrix} \quad (\text{C-1})$$

$$\begin{Bmatrix} d_x \\ d_y \end{Bmatrix} = \mathbf{T} \begin{Bmatrix} d_u \\ d_v \end{Bmatrix} \quad (\text{C-2})$$

where

$$\mathbf{T} = \begin{bmatrix} \cos \theta & -\sin \theta \\ \sin \theta & \cos \theta \end{bmatrix} \quad \mathbf{T}^T = \mathbf{T}^{-1} \quad \mathbf{T}^T \mathbf{T} = \mathbf{I} \text{ (unit matrix)} \quad (\text{C-3})$$

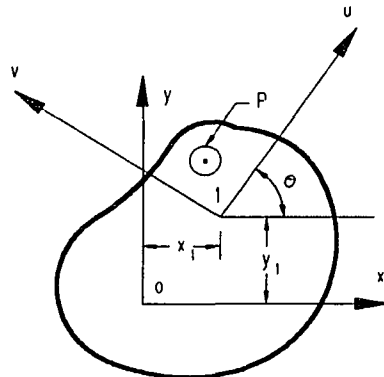


Fig. C-1 Two Arbitrary Cartesian Coordinate Systems on a Cross Section

The strain at point P is not varying with the different coordinate systems under plane section assumption. In other words, the strain at point P under system x0y

$$\varepsilon_{x_0y}^P = \varepsilon_0 + \phi_x y_p + \phi_y x_p = \varepsilon_0 + [\phi_y \quad \phi_x] \begin{Bmatrix} x_p \\ y_p \end{Bmatrix} \quad (C-4)$$

must equal the strain at the same point P under system u1v, which is

$$\varepsilon_{u_1v}^P = \varepsilon_1 + \phi_u v_p + \phi_v u_p = \varepsilon_1 + [\phi_v \quad \phi_u] \begin{Bmatrix} u_p \\ v_p \end{Bmatrix} \quad (C-5)$$

where

$$\varepsilon_1 = \varepsilon_0 + \phi_x y_1 + \phi_y x_1 = \varepsilon_0 + [\phi_y \quad \phi_x] \begin{Bmatrix} x_1 \\ y_1 \end{Bmatrix} \quad (C-6)$$

In the above equations, ε_0 and ε_1 = strains at points 0 and 1; ϕ_x, ϕ_y and ϕ_u, ϕ_v = curvatures at this division point under x0y and u1v coordinate systems. These curvatures can be always numerically related to the deflections along the column by deflection interpolation if the deformation is small, that is

$$\begin{Bmatrix} \phi_y \\ \phi_x \end{Bmatrix} = \sum_i \beta_i \begin{Bmatrix} d_x \\ d_y \end{Bmatrix}_i \quad (C-7)$$

$$\begin{Bmatrix} \phi_v \\ \phi_u \end{Bmatrix} = \sum_i \beta_i \begin{Bmatrix} d_u \\ d_v \end{Bmatrix}_i \quad (C-8)$$

where β_i = the parameters depending on the types of interpolation functions.

Substituting Eq. (C-1) into Eq. (C-4) and noting Eq. (C-6) gives

$$\varepsilon_{x_0y}^P = \varepsilon_1 + [\phi_y \quad \phi_x] \mathbf{T} \begin{Bmatrix} u_p \\ v_p \end{Bmatrix} \quad (C-9)$$

By using Eq. (C-7), (C-2), (C-3) and (C-8) one by one, Eq. (C-9) will be

$$\varepsilon_{x_0y}^P = \varepsilon_1 + (\sum_i \beta_i [d_u \quad d_v]_i) \mathbf{T} \mathbf{T}^T \begin{Bmatrix} u_p \\ v_p \end{Bmatrix} = \varepsilon_1 + [\phi_v \quad \phi_u] \begin{Bmatrix} u_p \\ v_p \end{Bmatrix} \quad (C-10)$$

Comparing Eq. (C-10) with Eq. (C-5), one concludes

$$\varepsilon_{x_0y}^P = \varepsilon_{u_1v}^P \quad (C-11)$$

$$\mathbf{G} = \begin{bmatrix} g_{0,0} & g_{0,1} & \\ g_{1,0} & g_{1,1} & g_{1,2} \\ \vdots & \vdots & \vdots \\ g_{n-1,n-2} & g_{n-1,n-1} & g_{n-1,n} \\ & g_{n,n-1} & g_{n,n} \end{bmatrix}_{3(n+1) \times 9} \quad (\text{D-3})$$

Coefficients $g_{i,k}$ in \mathbf{G} of Eq. (D-1), (D-2) and (D-3) are referred to Eq. (5-17).

APPENDIX E

FLOW CHART

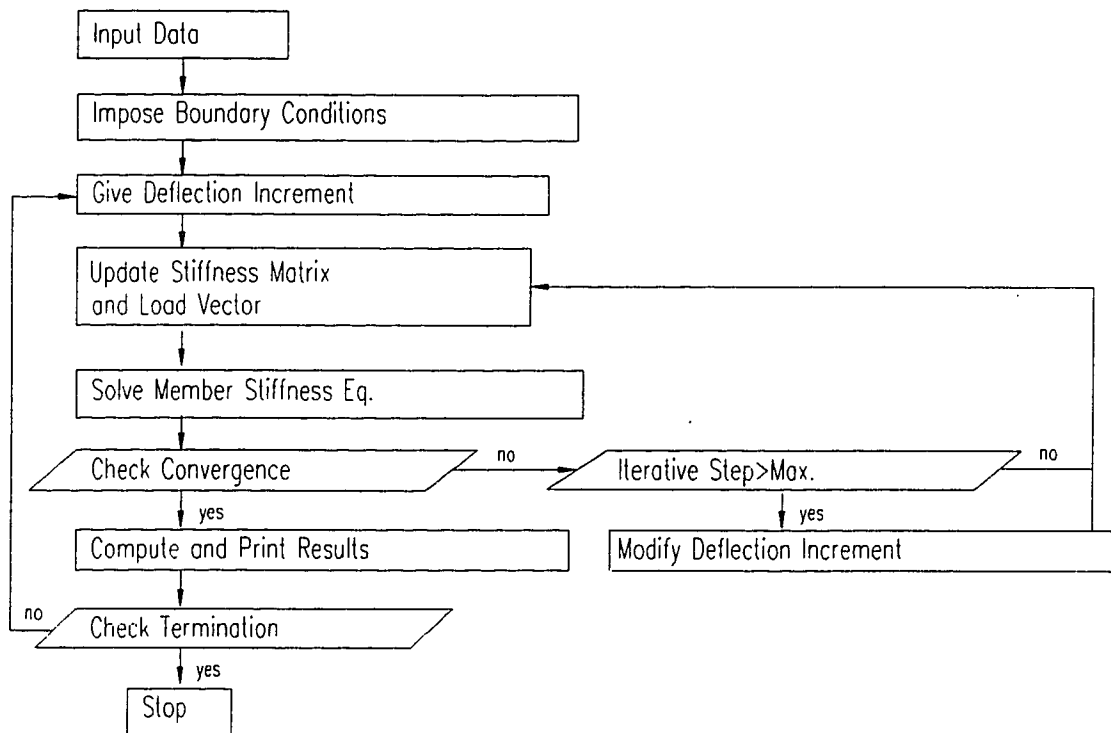


Fig. E-1 Flow Chart of Present Computational Process

APPENDIX F

FORTRAN STATEMENTS OF PRESENT SOLVER

The following subroutine is based on Gauss elimination and it is specially developed for solving the present member stiffness equation, where A = the compact stiffness matrix (see Eq. (D-3)) in the simultaneous equations $A \mathbf{x} = \mathbf{c}$; MB = an integer matrix to store the position of diagonal coefficients in original stiffness matrix; NON = number of spline nodes along the column; $NO3 = 3$ times NON .

```
      SUBROUTINE SOLVER(A,C,X,MB,NON,NO3)
      IMPLICIT DOUBLE PRECISION (A-H,O-Z)
      DIMENSION A(NO3,1),C(1),X(1),MB(1)
C     Forward reduction phase.
      DO 20 K=2,3
      DO 10 I=K,3
      R=A(I,MB(K-1))/A(K-1,MB(K-1))
      C(I)=C(I)-R*C(K-1)
      DO 10 J=K,6
10     A(I,J)=A(I,J)-R*A(K-1,J)
      DO 15 I=4,6
      R=A(I,MB(K-1))/A(K-1,MB(K-1))
      C(I)=C(I)-R*C(K-1)
      DO 15 J=K,9
15     A(I,J)=A(I,J)-R*A(K-1,J)
20     CONTINUE
      DO 50 L=2,NON-2
      L3=L*3
      DO 50 K=L3-2,L3
      KL2=K-L3+2
      KL3=KL2+1
      KL5=KL3+2
      KL6=KL5+1
      DO 41 I=K,L3
      R=A(I,KL5)/A(K-1,MB(K-1))
      C(I)=C(I)-R*C(K-1)
      IF(K.EQ.L3-2.AND.K.NE.4) THEN
```

```

DO 42 J=4,6
42  A(I,J)=A(I,J)-R*A(K-1,J+3)
    GO TO 41
    END IF
    DO 40 J=KL6,9
40  A(I,J)=A(I,J)-R*A(K-1,J)
41  CONTINUE
    IF(K.EQ.L3-2) GO TO 50
    DO 31 I=L3+1,L3+3
    R=A(I,KL2)/A(K-1,MB(K-1))
    C(I)=C(I)-R*C(K-1)
    DO 30 J=KL3,6
30  A(I,J)=A(I,J)-R*A(K-1,J+3)
31  CONTINUE
50  CONTINUE
    DO 80 K=NO3-5,NO3
    KN8=K-NO3+8
    KN9=KN8+1
    DO 71 I=K,NO3
    R=A(I,KN8)/A(K-1,MB(K-1))
    C(I)=C(I)-R*C(K-1)
    IF(K.EQ.NO3-5) THEN
    DO 72 J=4,6
72  A(I,J)=A(I,J)-R*A(K-1,J+3)
    GO TO 71
    END IF
    DO 70 J=KN9,9
70  A(I,J)=A(I,J)-R*A(K-1,J)
71  CONTINUE
80  CONTINUE
C   Back substitution phase (results stored in X).
    X(NO3)=C(NO3)/A(NO3,MB(NO3))
    DO 130 K=NO3-1,NO3-2,-1
    KK=MB(K)-K
    X(K)=C(K)
    DO 120 J=K+1,NO3
120  X(K)=X(K)-A(K,J+KK)*X(J)
130  X(K)=X(K)/A(K,MB(K))
    DO 160 L=NON-1,1,-1
    L3=L*3
    DO 150 K=L3,L3-2,-1
    KK=MB(K)-K
    X(K)=C(K)
    DO 140 J=K+1,L3+3
140  X(K)=X(K)-A(K,J+KK)*X(J)

```

```
150 X(K)=X(K)/A(K,MB(K))
160 CONTINUE
    RETURN
    END
```

APPENDIX G

LOAD-DEFLECTION AND MOMENT-CURVATURE CURVES FOR NJIT COLUMN SPECIMENS

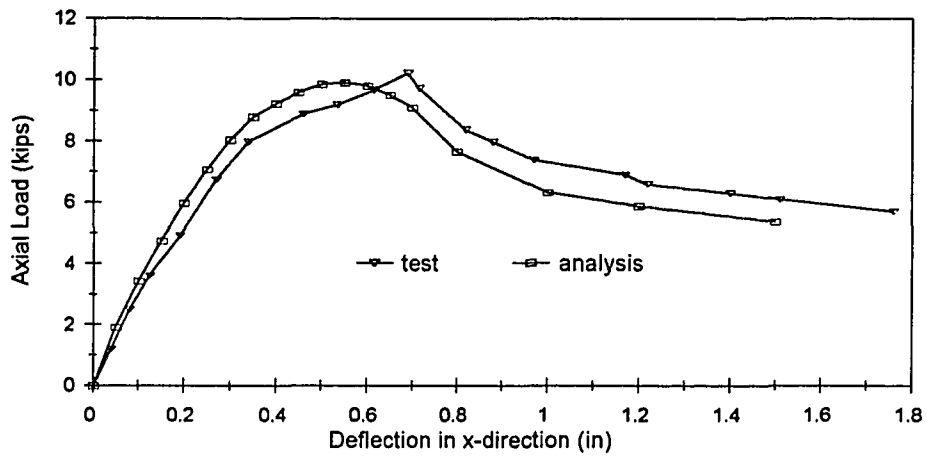


Fig. G-1a Load-Deflection Curves in X-Direction for Specimen B2

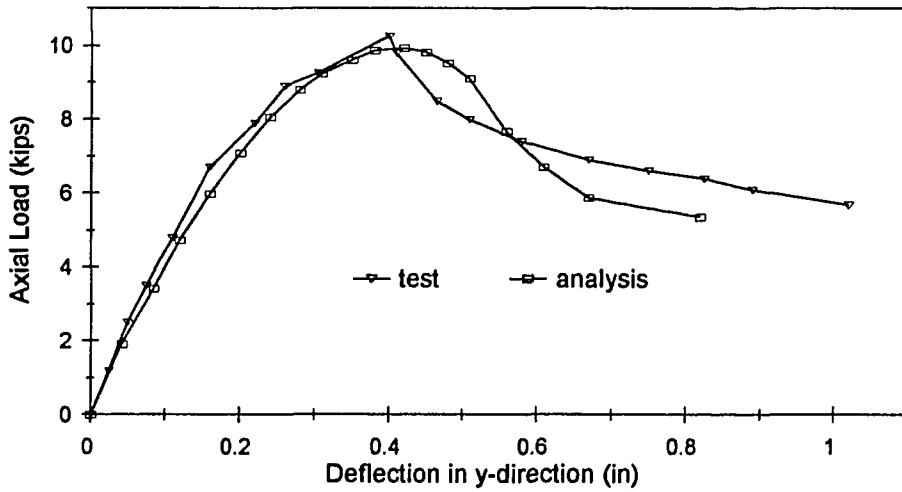


Fig. G-1b Load-Deflection Curves in Y-Direction for Specimen B2

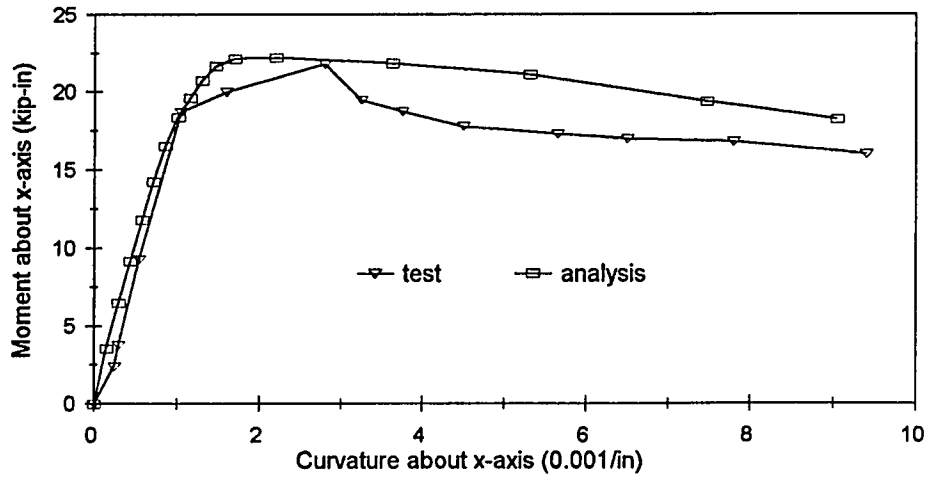


Fig. G-1c Moment-Curvature Curves about X-Axis for Specimen B2

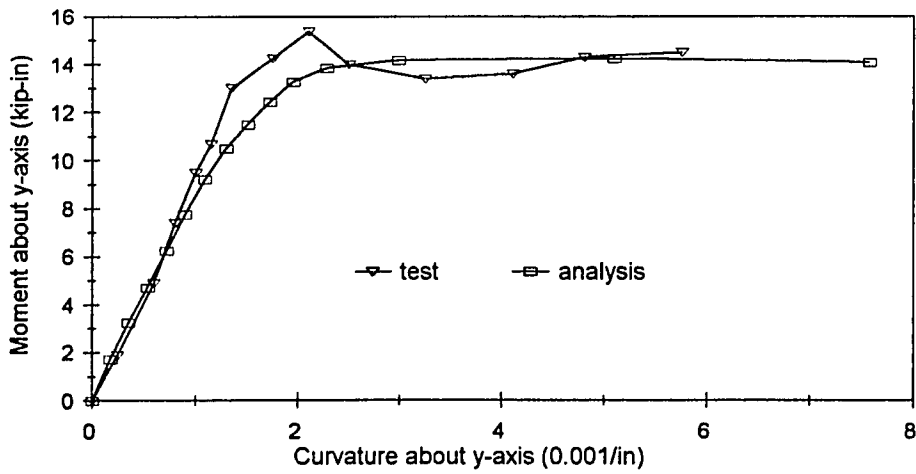


Fig. G-1d Moment-Curvature Curves about Y-Axis for Specimen B2

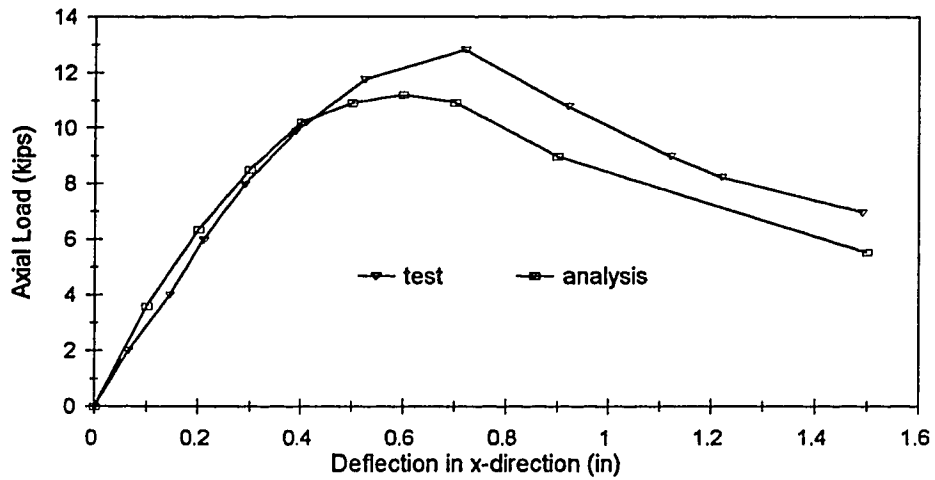


Fig. G-2a Load-Deflection Curves in X-Direction for Specimen B3

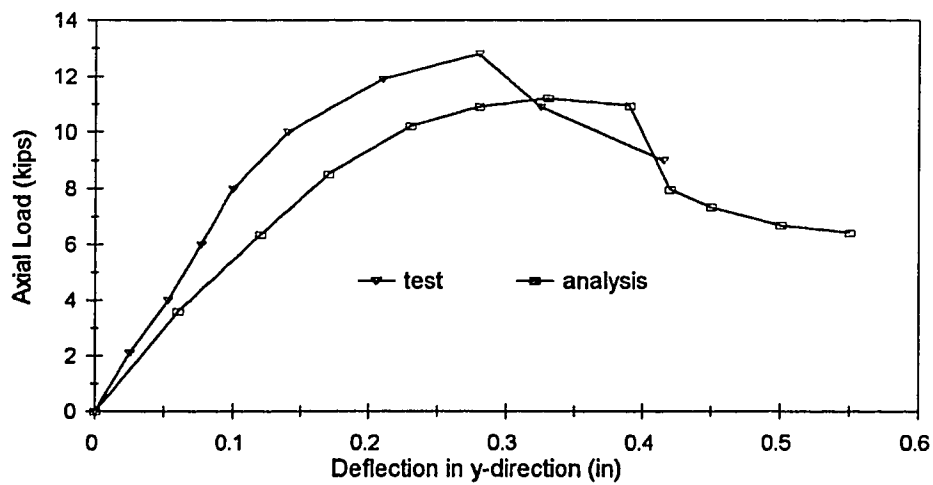


Fig. G-2b Load-Deflection Curves in Y-Direction for Specimen B3

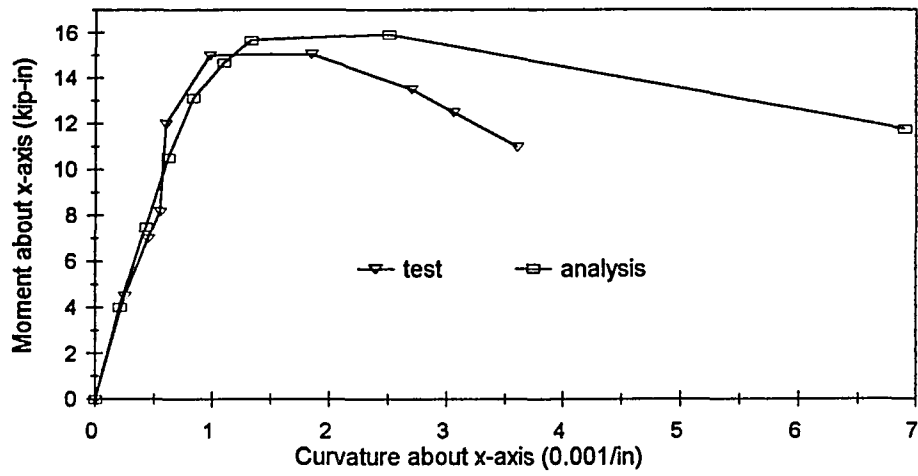


Fig. G-2c Moment-Curvature Curves about X-Axis for Specimen B3

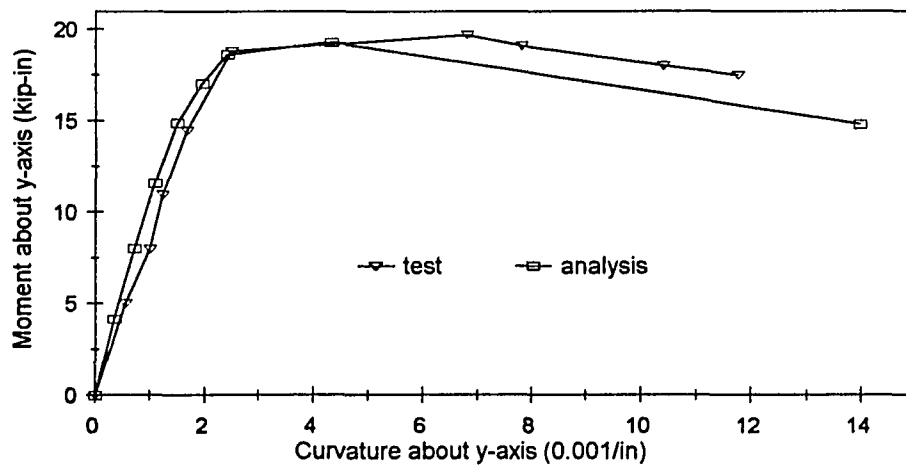


Fig. G-2d Moment-Curvature Curves about Y-Axis for Specimen B3

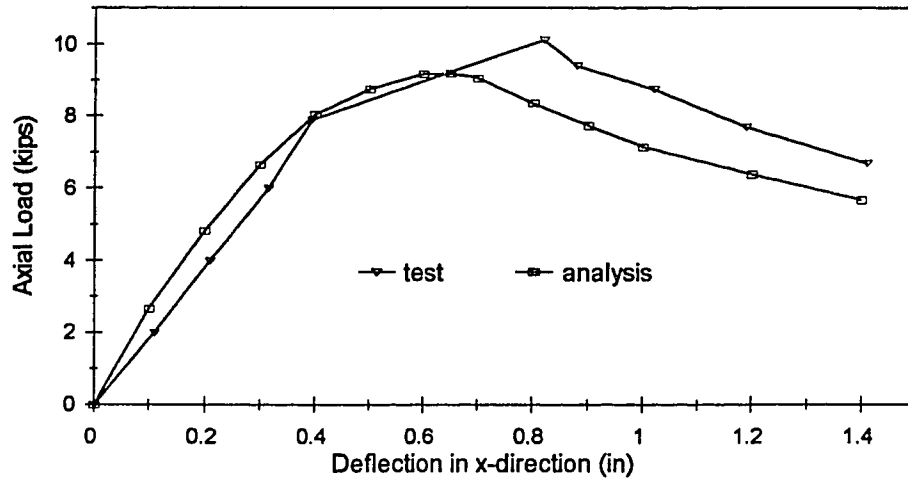


Fig. G-3a Load-Deflection Curves in X-Direction for Specimen B4

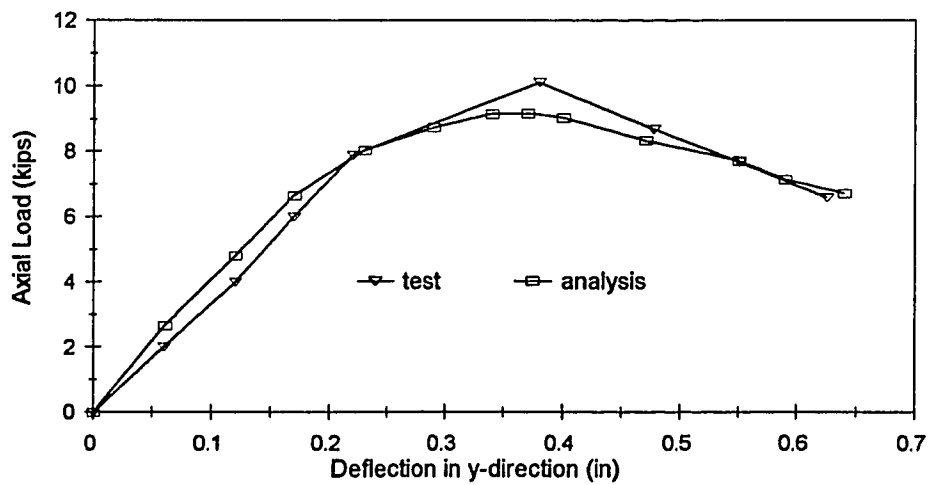


Fig. G-3b Load-Deflection Curves in Y-Direction for Specimen B4

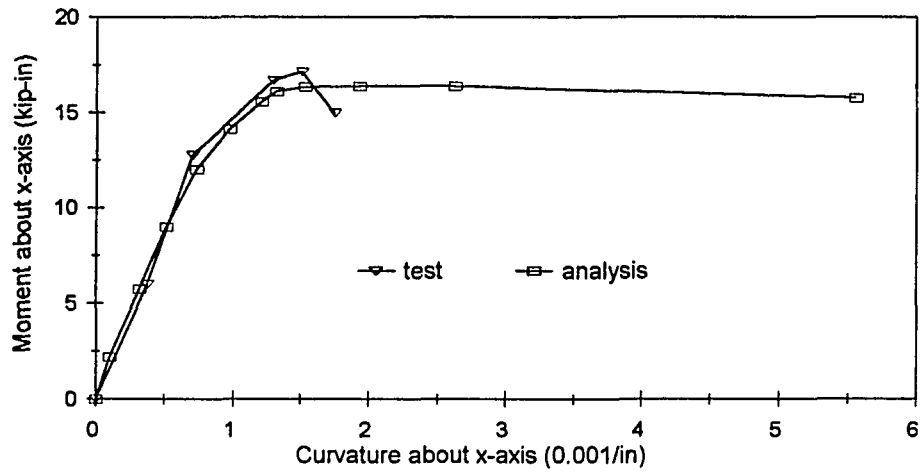


Fig. G-3c Moment-Curvature Curves about X-Axis for Specimen B4

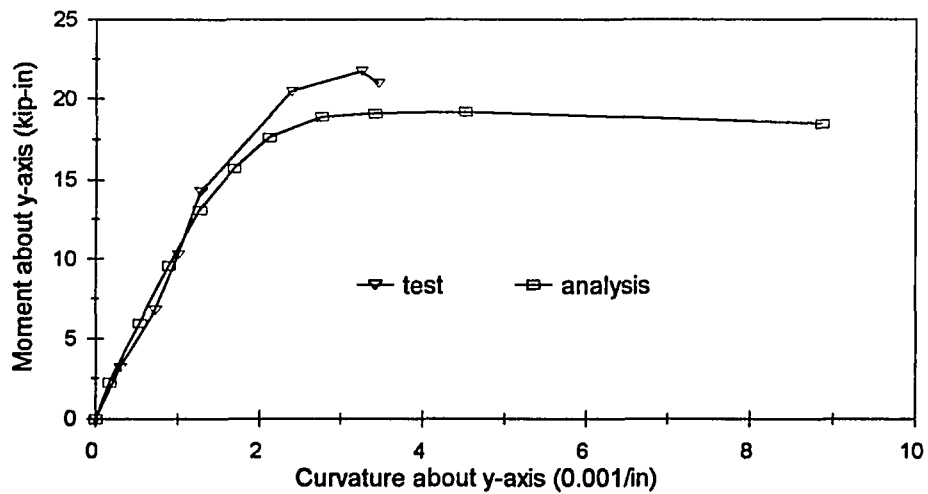


Fig. G-3d Moment-Curvature Curves about Y-Axis for Specimen B4

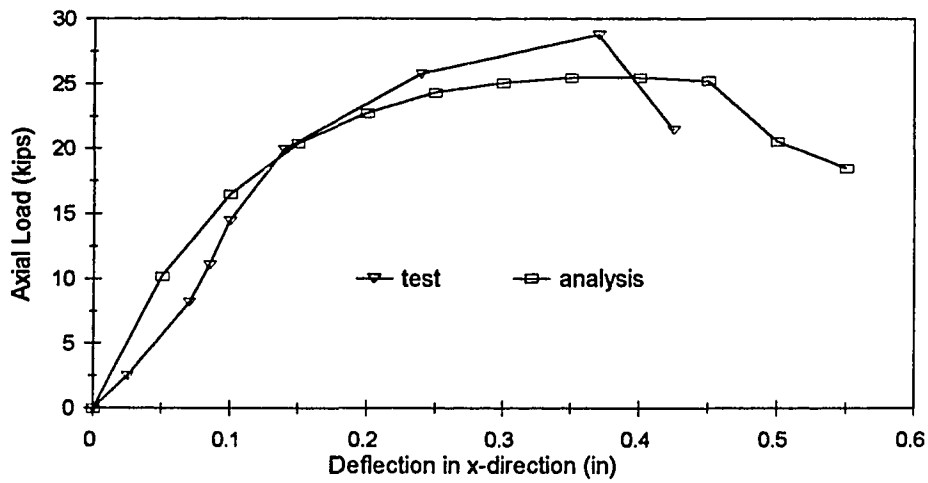


Fig. G-4a Load-Deflection Curves in X-Direction for Specimen B5

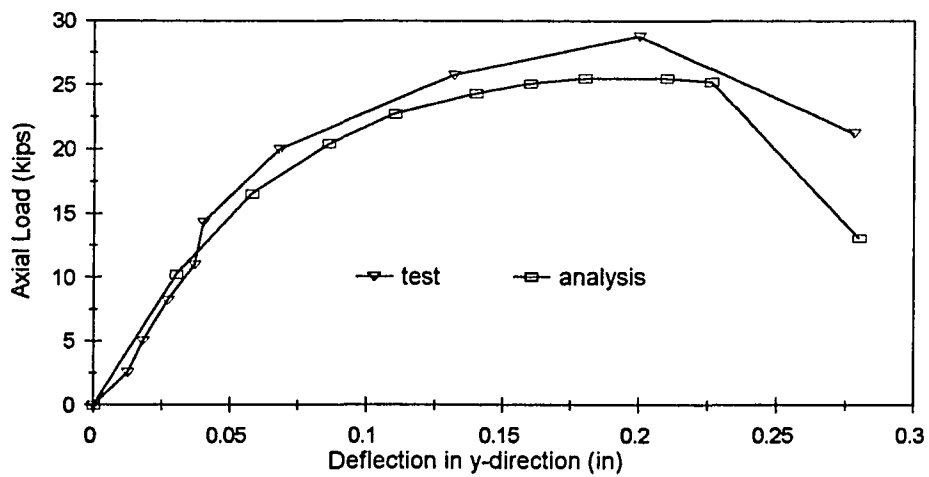


Fig. G-4b Load-Deflection Curves in Y-Direction for Specimen B5

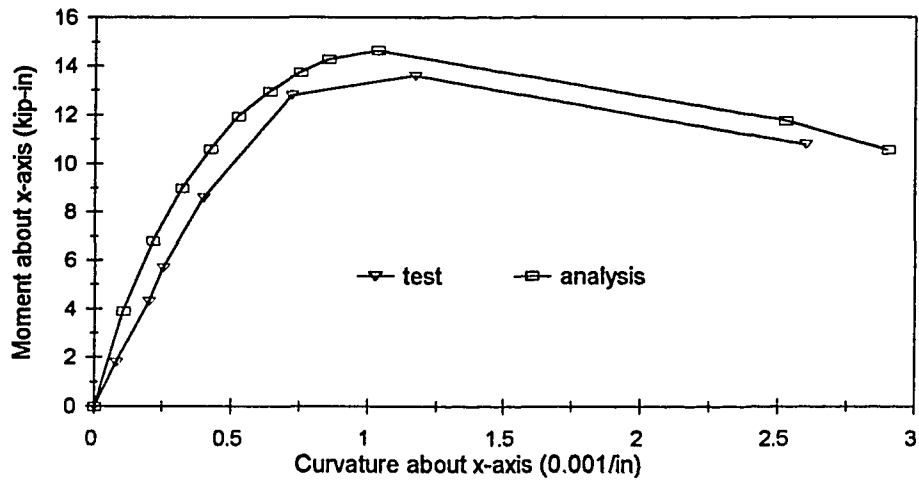


Fig. G-4c Moment-Curvature Curves about X-Axis for Specimen B5

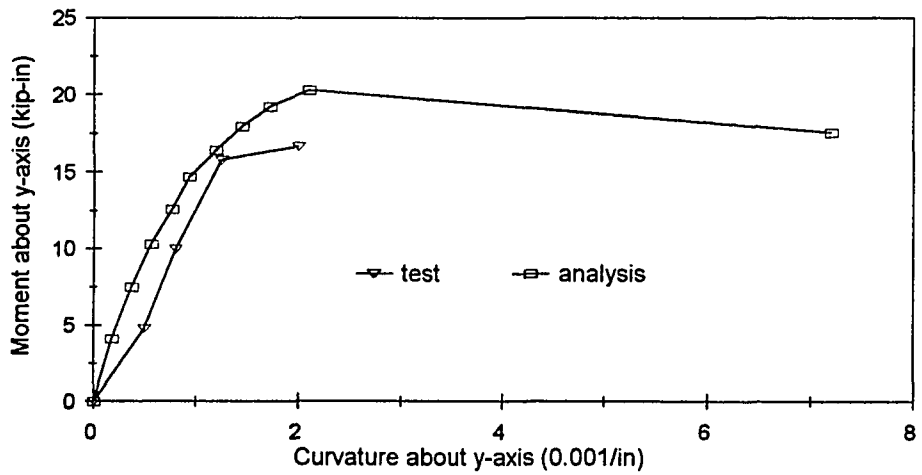


Fig. G-4d Moment-Curvature Curves about Y-Axis for Specimen B5

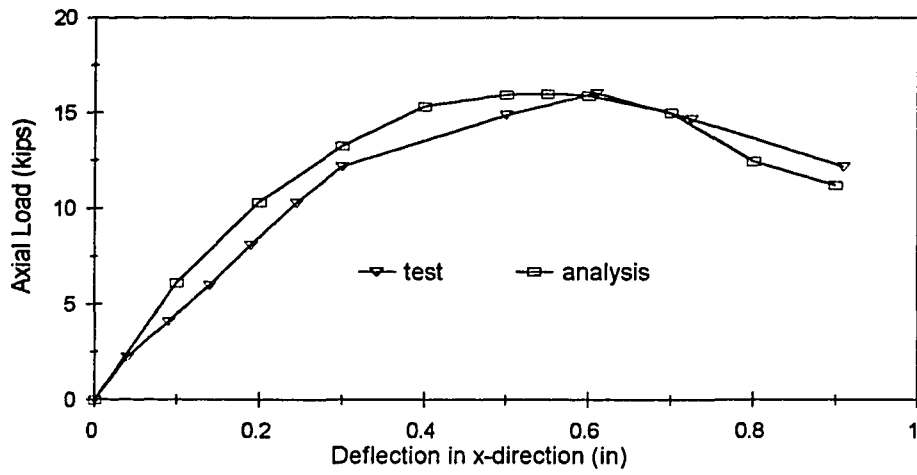


Fig. G-5a Load-Deflection Curves in X-Direction for Specimen B6

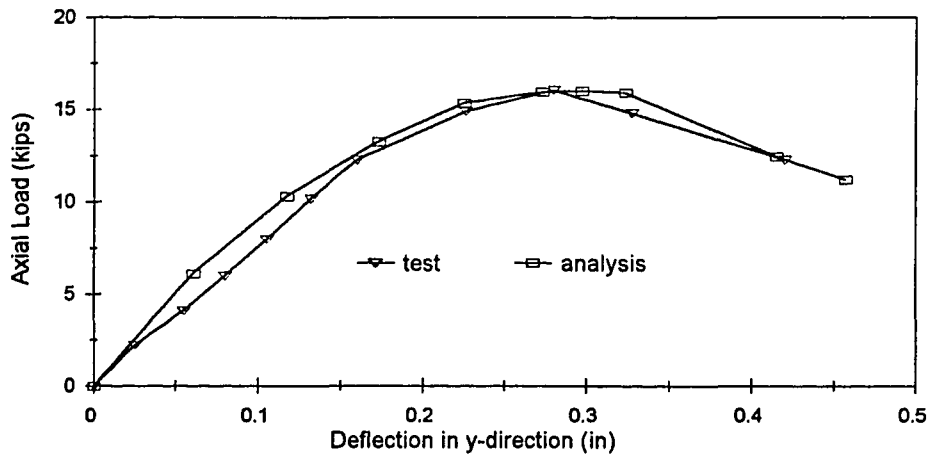


Fig. G-5b Load-Deflection Curves in Y-Direction for Specimen B6

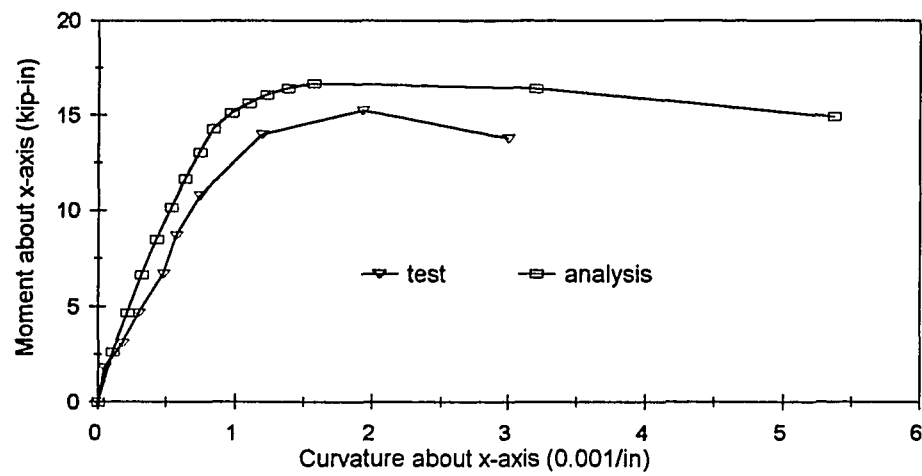


Fig. G-5c Moment-Curvature Curves about X-Axis for Specimen B6

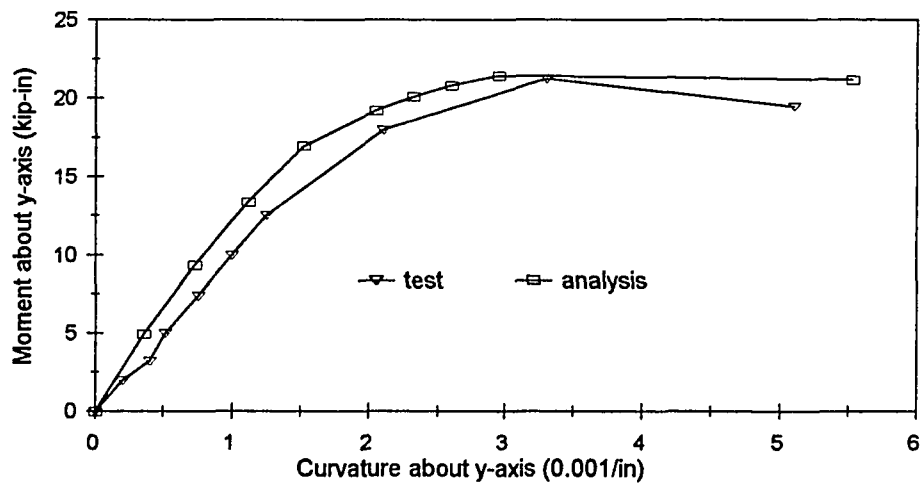


Fig. G-5d Moment-Curvature Curves about Y-Axis for Specimen B6

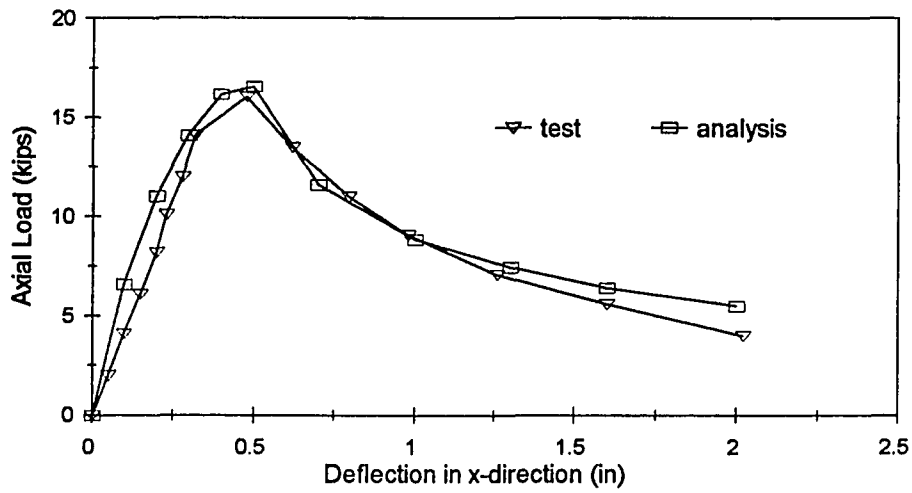


Fig. G-6a Load-Deflection Curves in X-Direction for Specimen B7

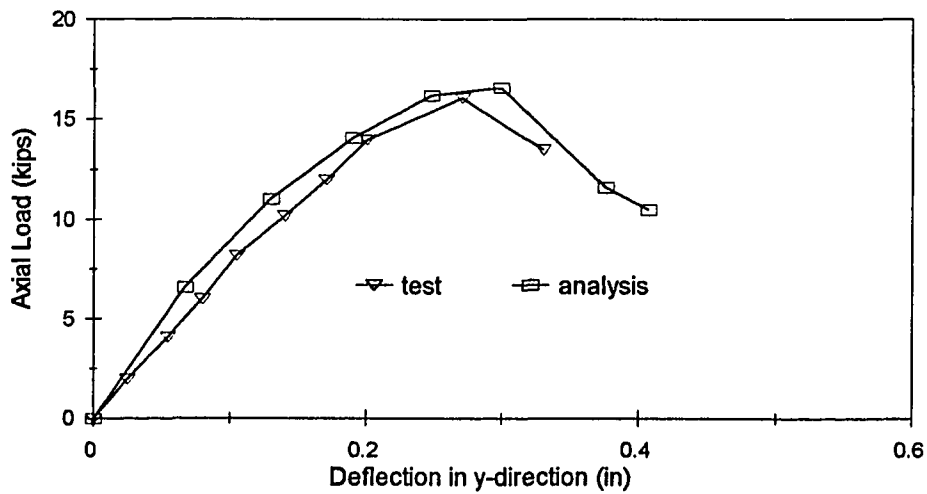


Fig. G-6b Load-Deflection Curves in Y-Direction for Specimen B7

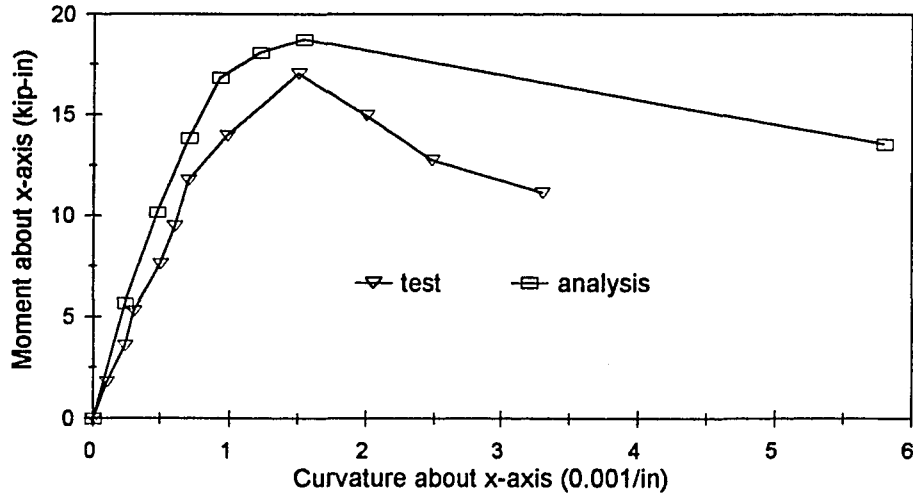


Fig. G-6c Moment-Curvature Curves about X-Axis for Specimen B7

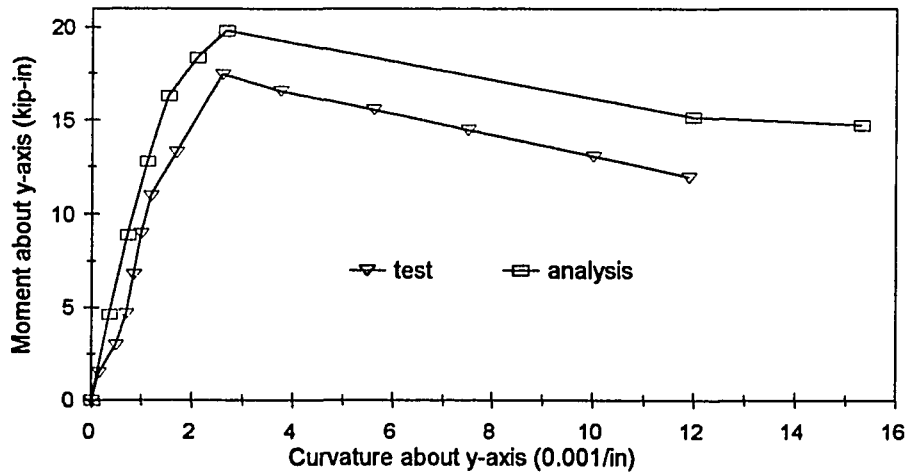


Fig. G-6d Moment-Curvature Curves about Y-Axis for Specimen B7

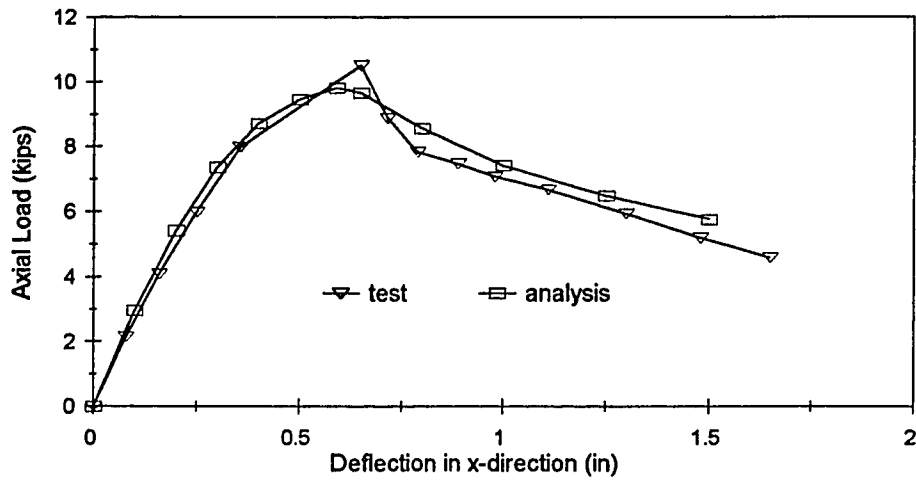


Fig. G-7a Load-Deflection Curves in X-Direction for Specimen B8

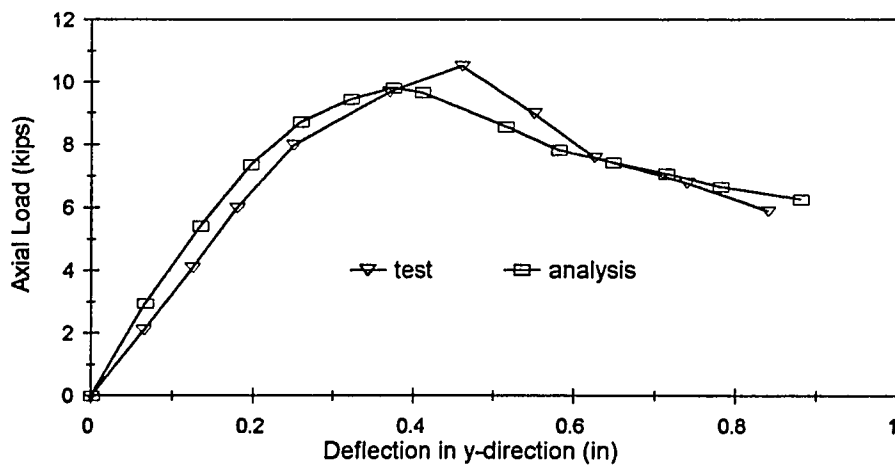


Fig. G-7b Load-Deflection Curves in Y-Direction for Specimen B8

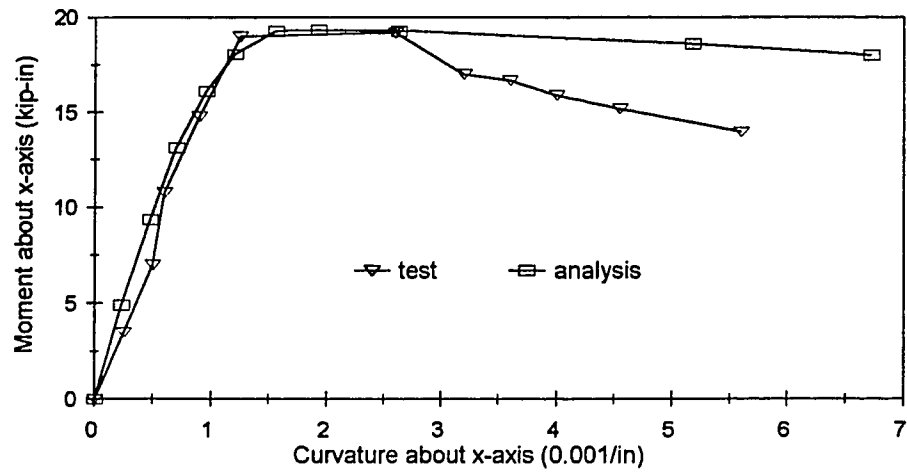


Fig. G-7c Moment-Curvature Curves about X-Axis for Specimen B8

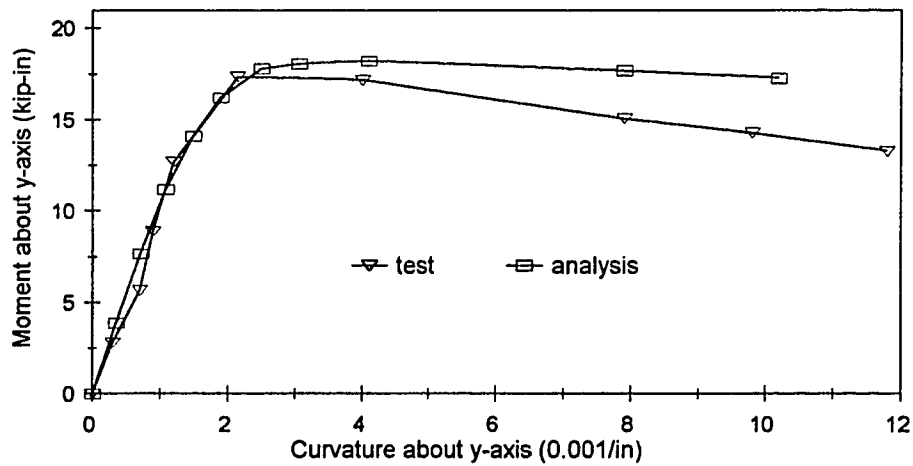


Fig. G-7d Moment-Curvature Curves about Y-Axis for Specimen B8

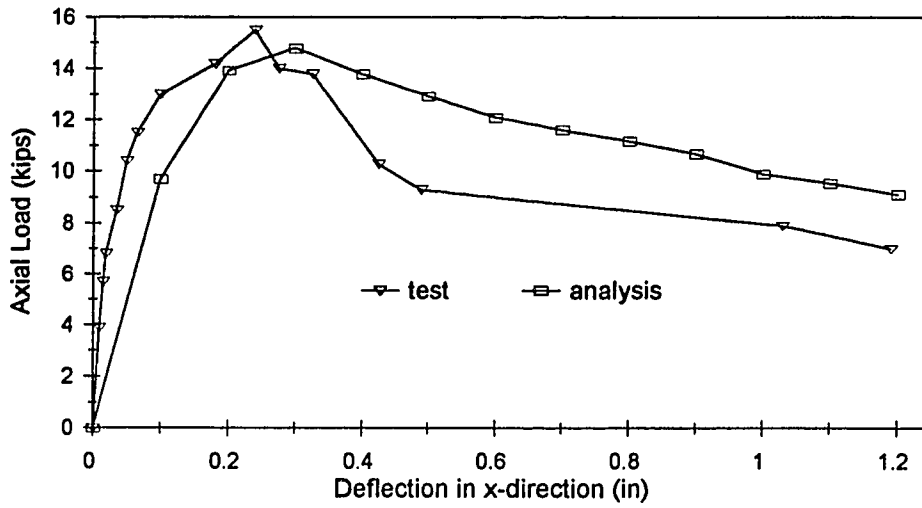


Fig. G-8a Load-Deflection Curves in X-Direction for Specimen C1

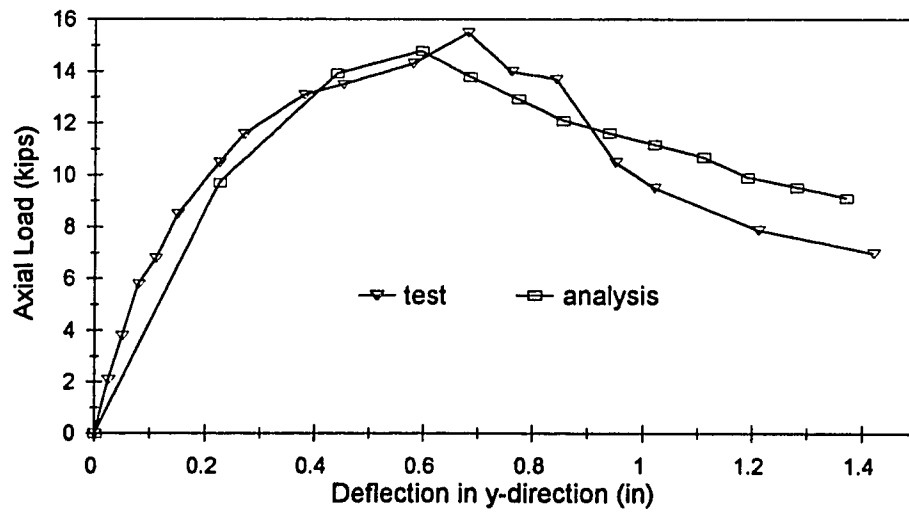


Fig. G-8b Load-Deflection Curves in Y-Direction for Specimen C1

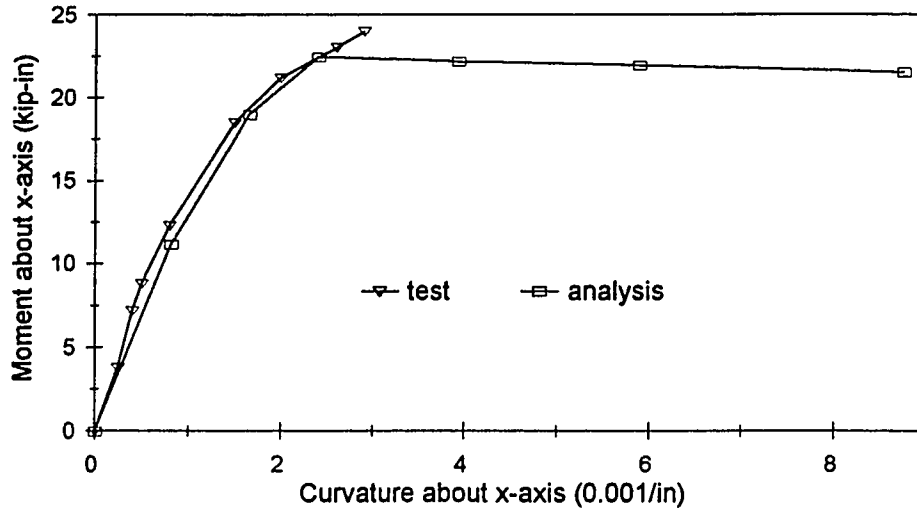


Fig. G-8c Moment-Curvature Curves about X-Axis for Specimen C1

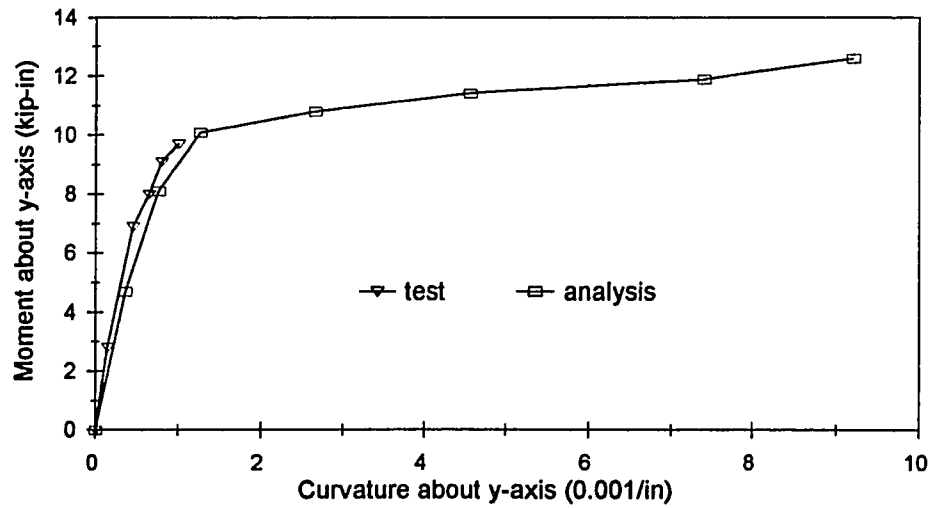


Fig. G-8d Moment-Curvature Curves about Y-Axis for Specimen C1

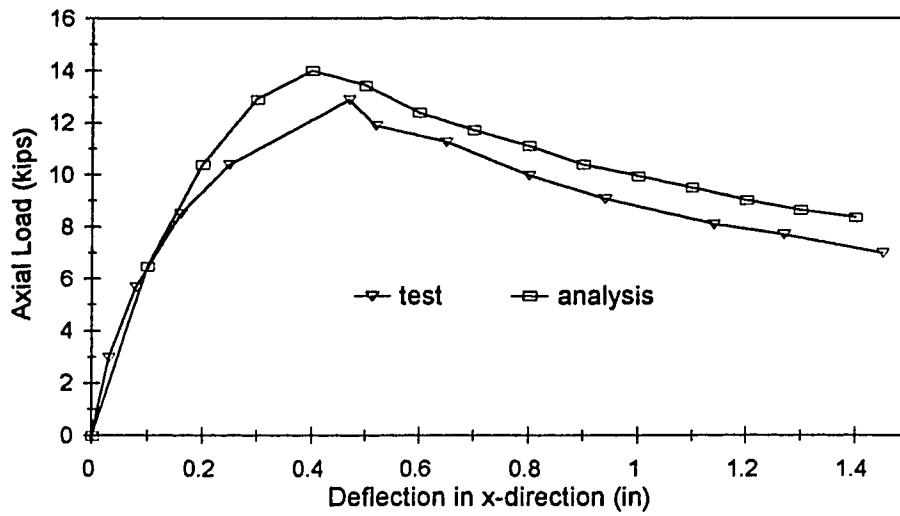


Fig. G-9a Load-Deflection Curves in X-Direction for Specimen C2

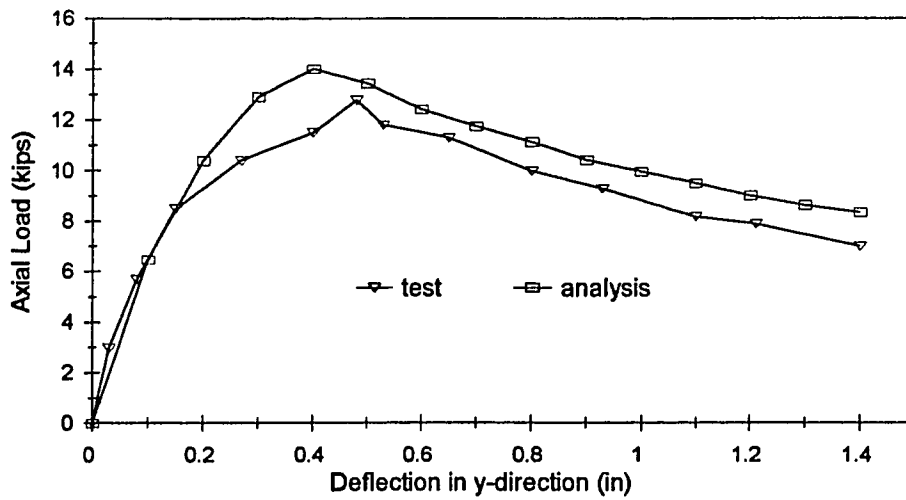


Fig. G-9b Load-Deflection Curves in Y-Direction for Specimen C2

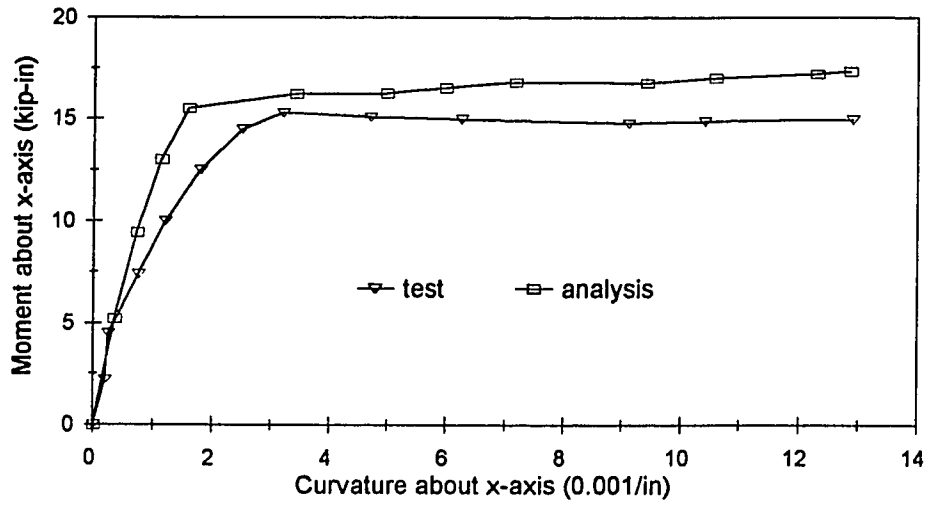


Fig. G-9c Moment-Curvature Curves about X-Axis for Specimen C2

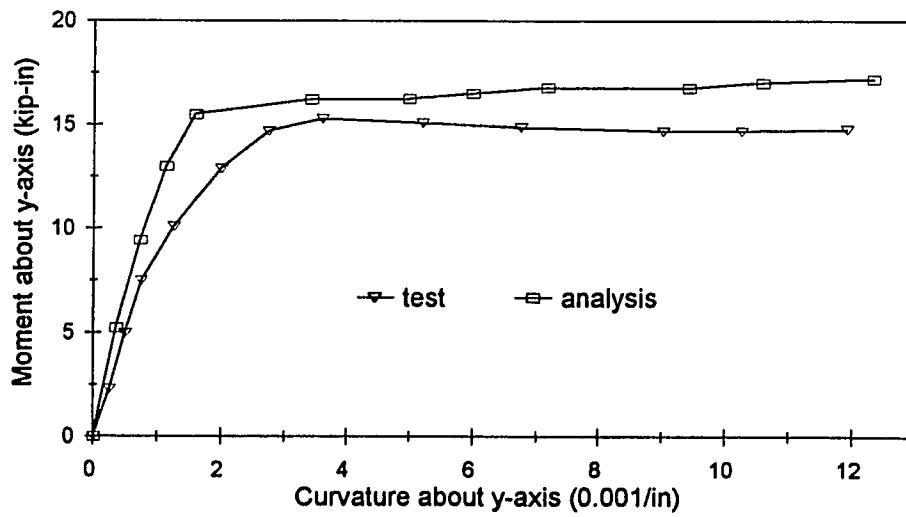


Fig. G-9d Moment-Curvature Curves about Y-Axis for Specimen C2

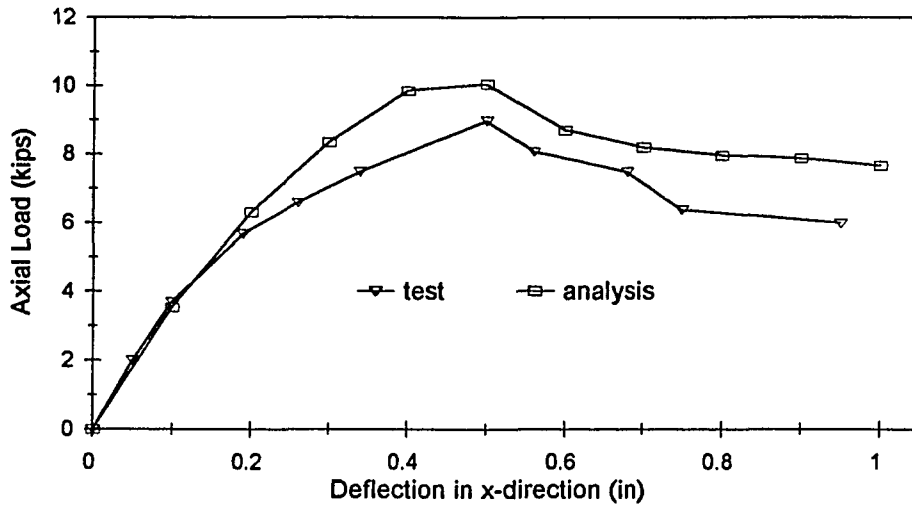


Fig. G-10a Load-Deflection Curves in X-Direction for Specimen C3

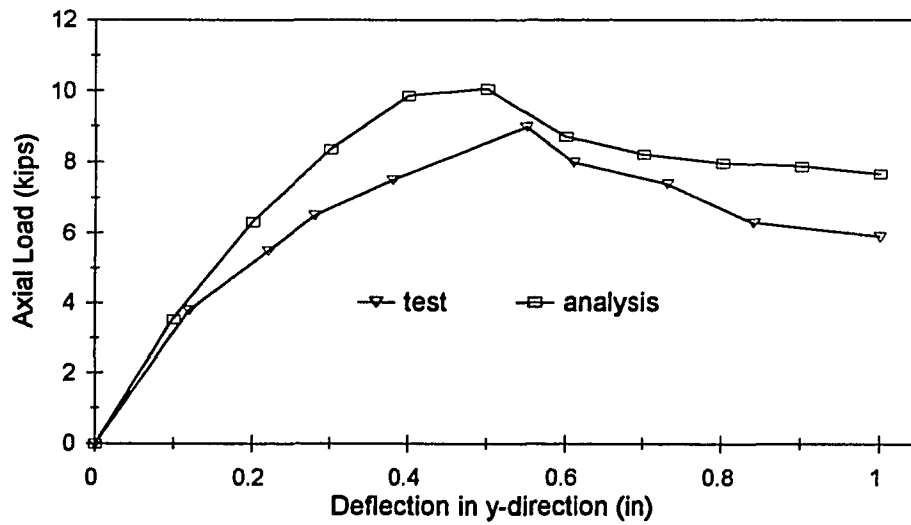


Fig. G-10b Load-Deflection Curves in Y-Direction for Specimen C3

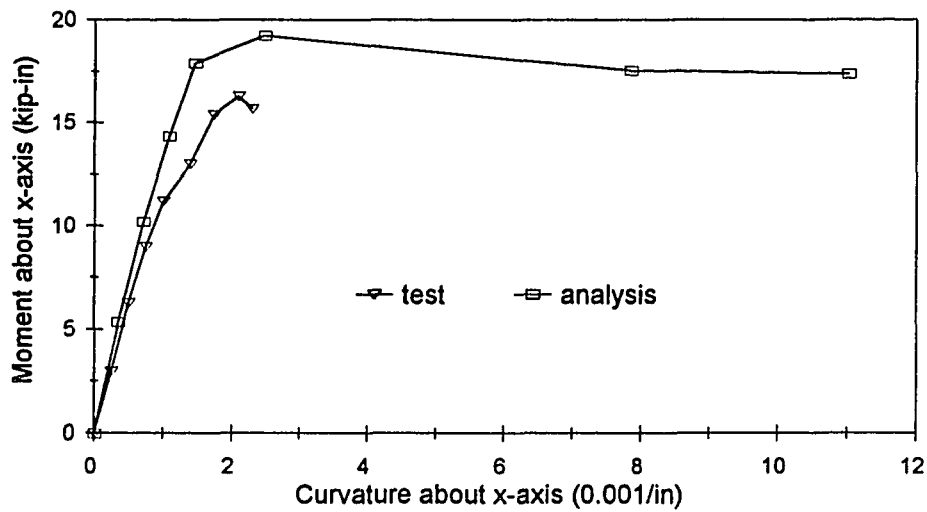


Fig. G-10c Moment-Curvature Curves about X-Axis for Specimen C3

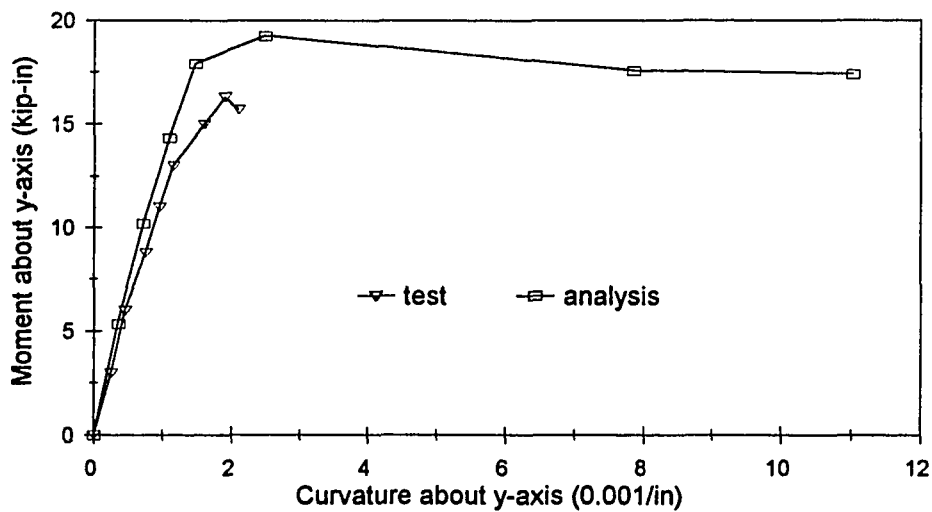


Fig. G-10d Moment-Curvature Curves about Y-Axis for Specimen C3

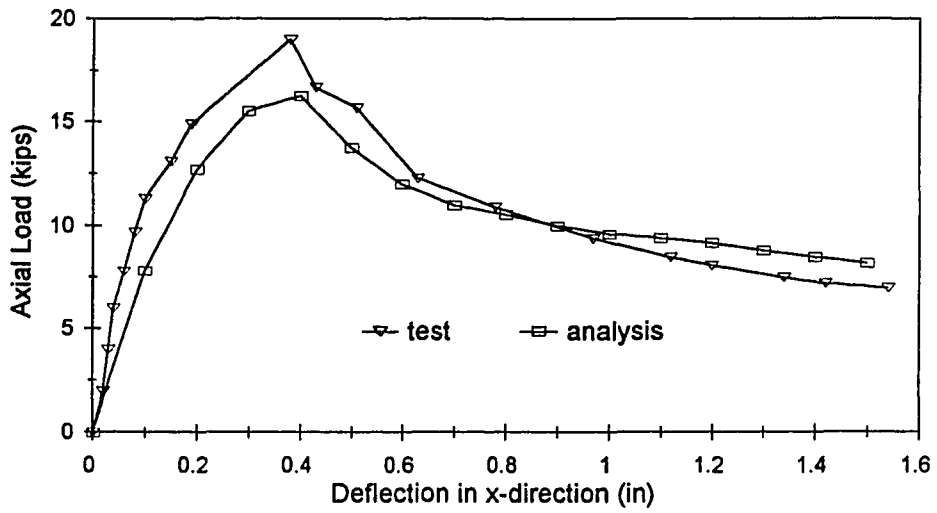


Fig. G-11a Load-Deflection Curves in X-Direction for Specimen C4

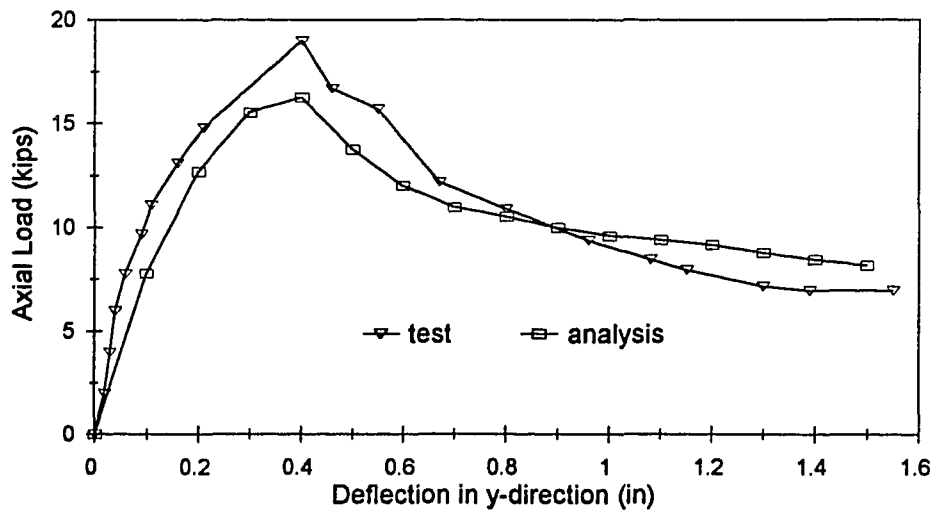


Fig. G-11b Load-Deflection Curves in Y-Direction for Specimen C4

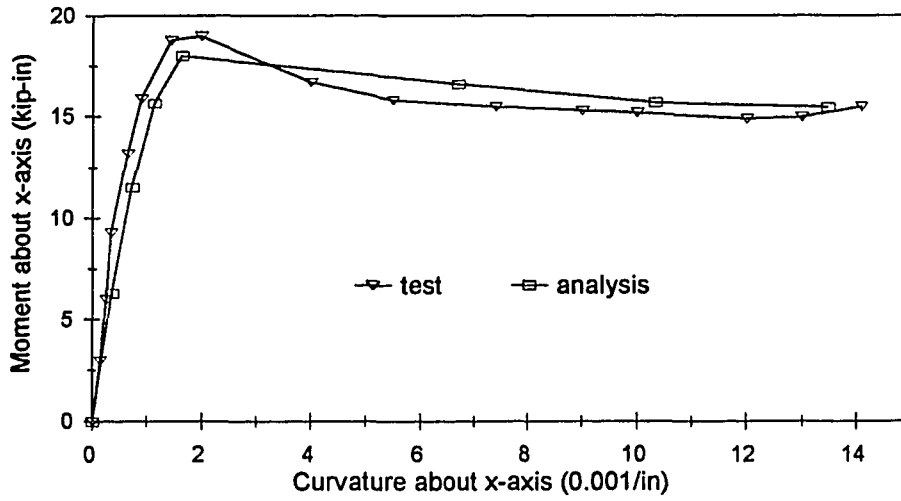


Fig. G-11c Moment-Curvature Curves about X-Axis for Specimen C4

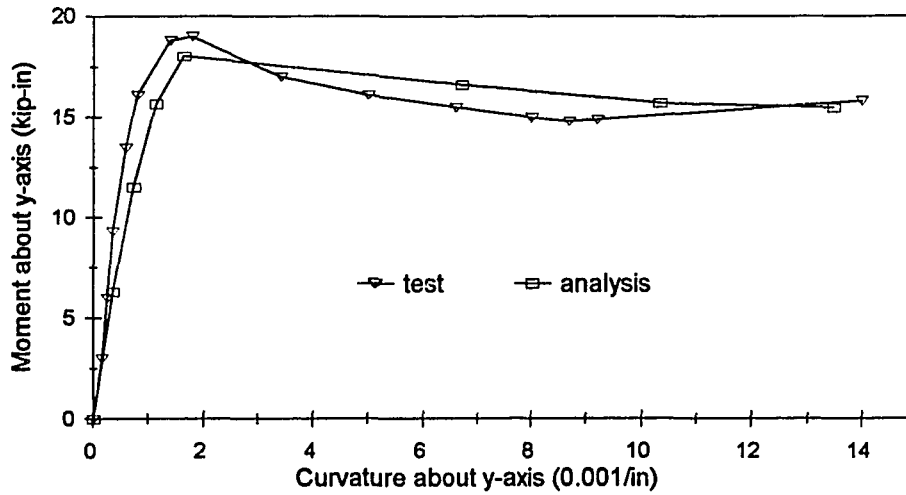


Fig. G-11d Moment-Curvature Curves about Y-Axis for Specimen C4

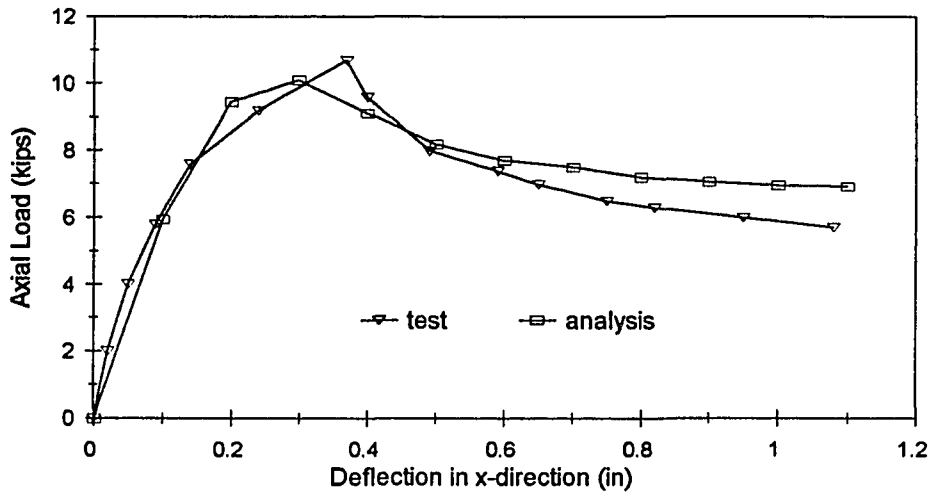


Fig. G-12a Load-Deflection Curves in X-Direction for Specimen C5

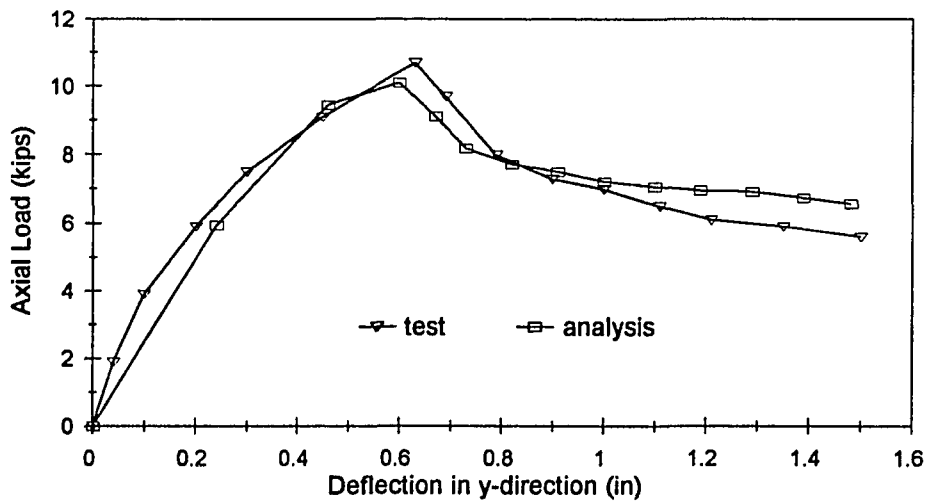


Fig. G-12b Load-Deflection Curves in Y-Direction for Specimen C5

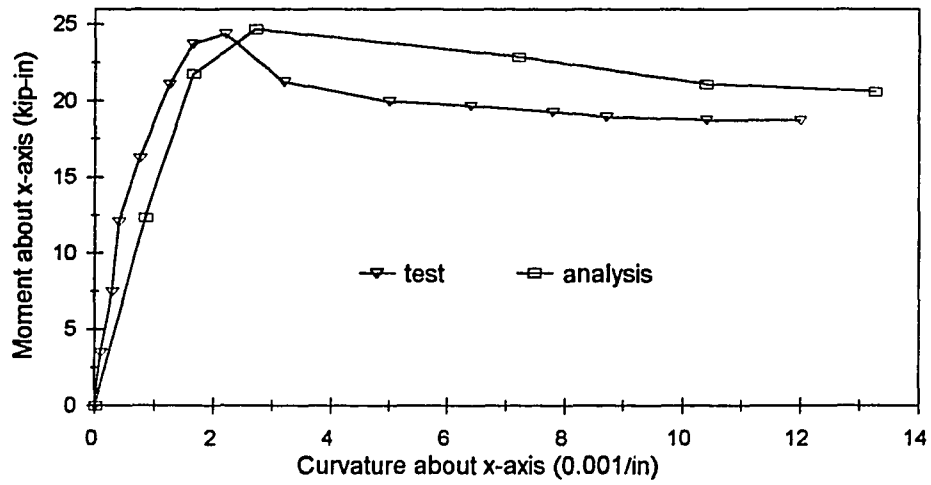


Fig. G-12c Moment-Curvature Curves about X-Axis for Specimen C5

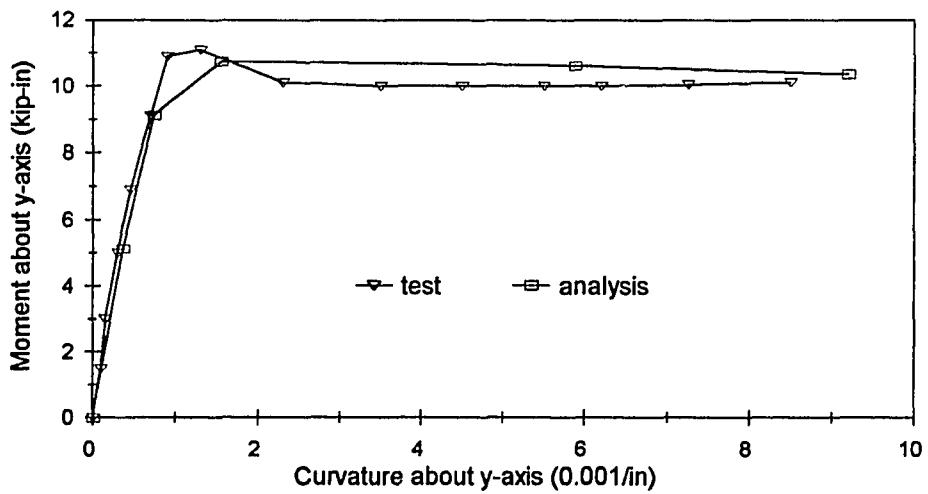


Fig. G-12d Moment-Curvature Curves about Y-Axis for Specimen C5

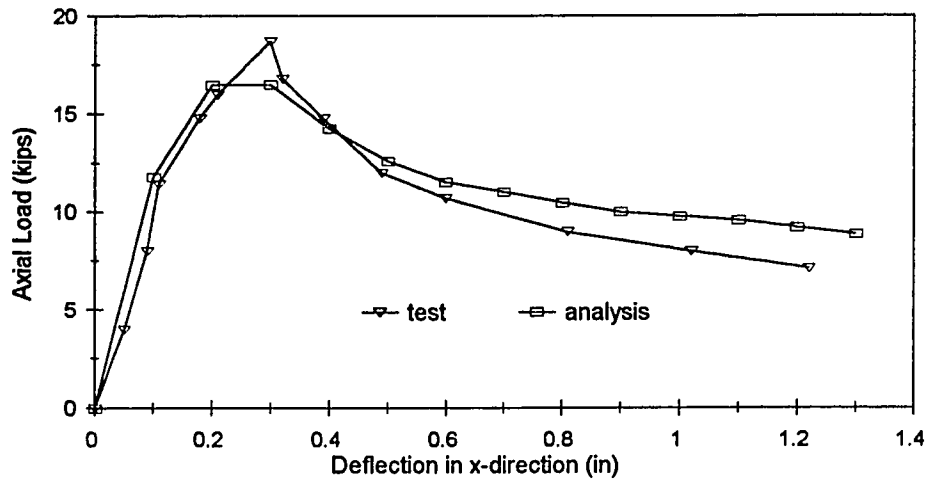


Fig. G-13a Load-Deflection Curves in X-Direction for Specimen C6

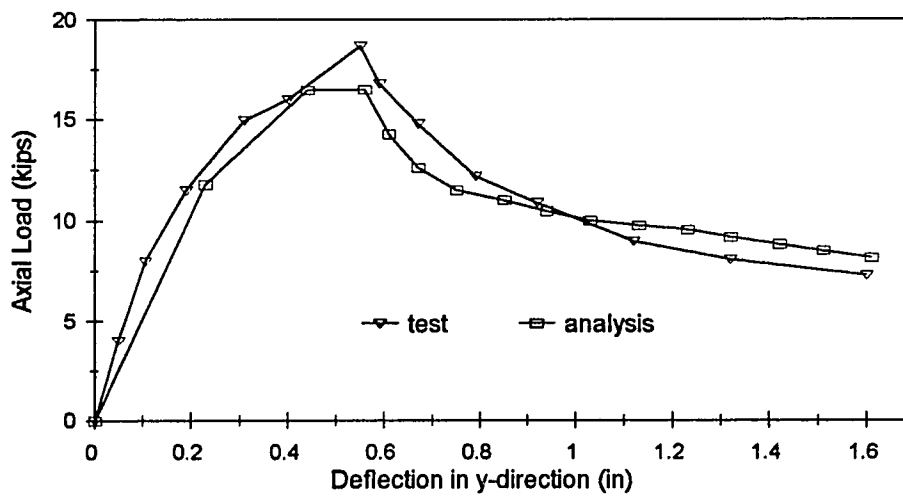


Fig. G-13b Load-Deflection Curves in Y-Direction for Specimen C6

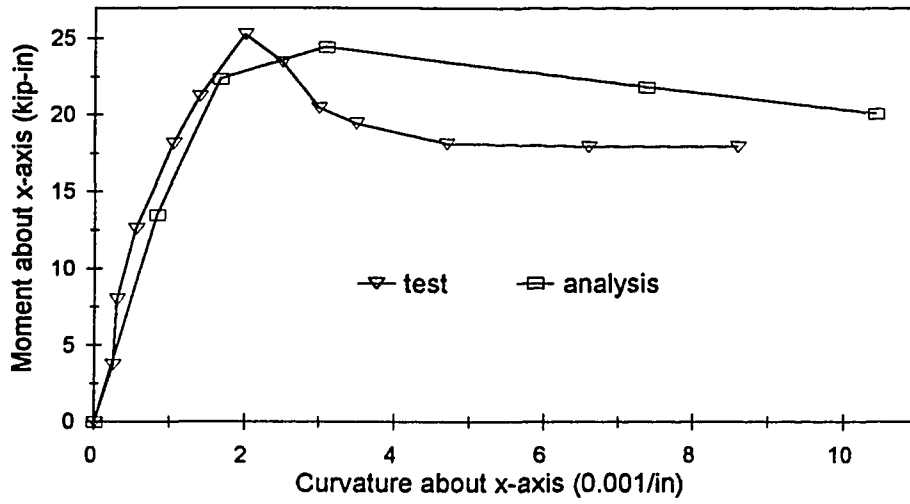


Fig. G-13c Moment-Curvature Curves about X-Axis for Specimen C6

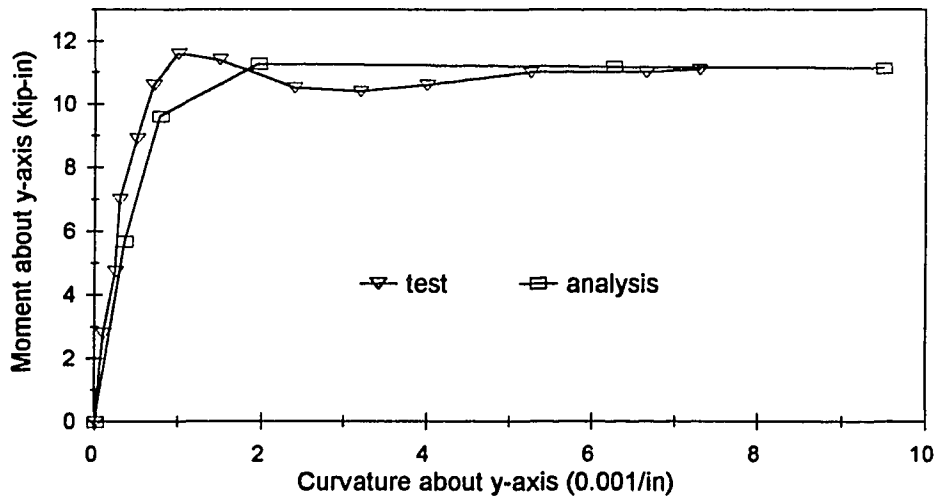


Fig. G-13d Moment-Curvature Curves about Y-Axis for Specimen C6

APPENDIX H

MOMENT-CURVATURE CURVES FOR UNIVERSITY OF TEXAS AT AUSTIN COLUMN SPECIMENS

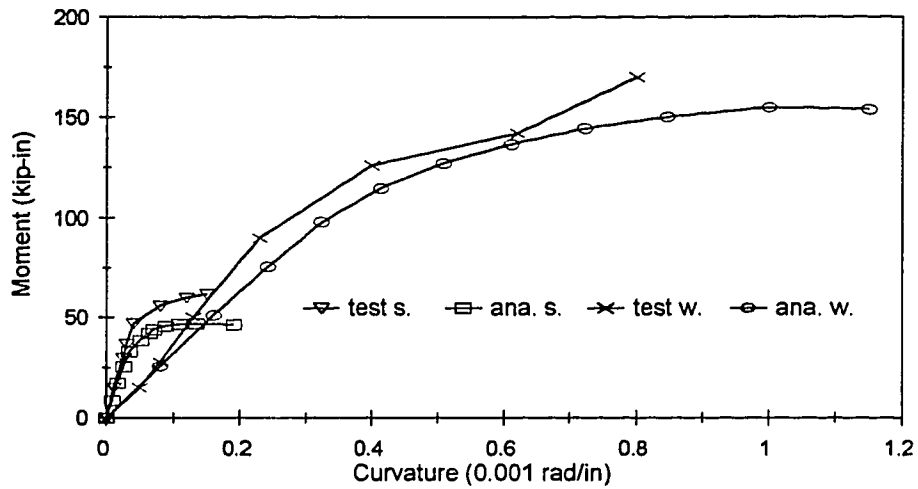


Fig. H-1 Moment-Curvature Curves about Strong and Weak Axes for Specimen RC-1

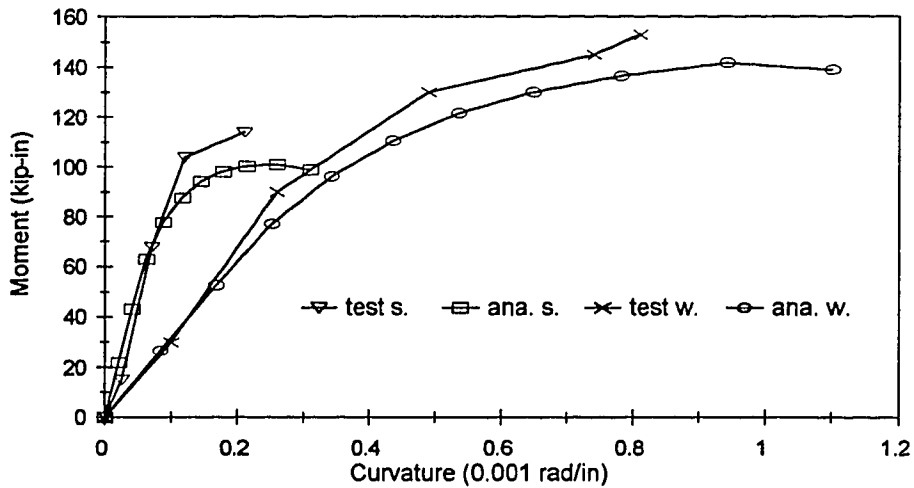


Fig. H-2 Moment-Curvature Curves about Strong and Weak Axes for Specimen RC-2

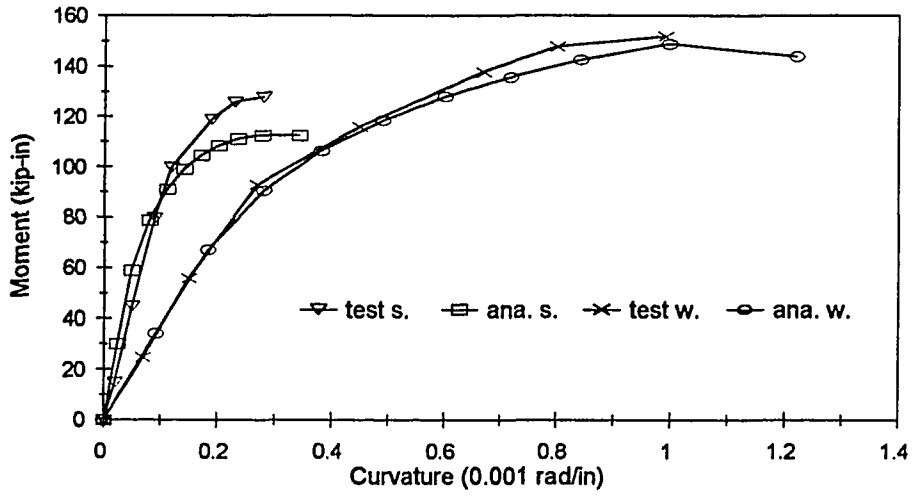


Fig. H-3 Moment-Curvature Curves about Strong and Weak Axes for Specimen RC-3

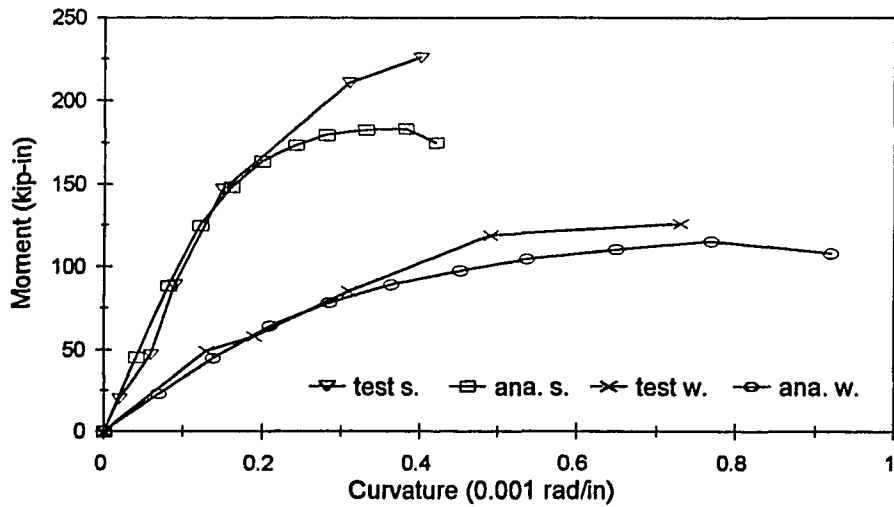


Fig. H-4 Moment-Curvature Curves about Strong and Weak Axes for Specimen RC-4

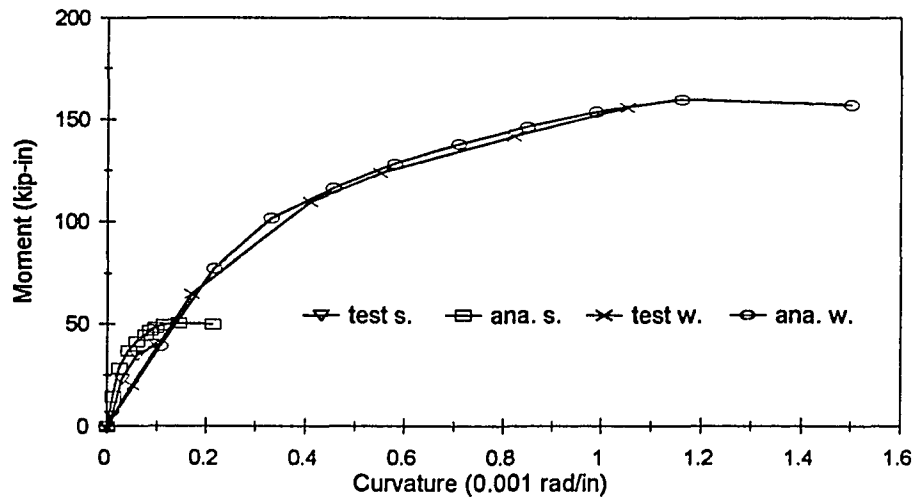


Fig. H-5 Moment-Curvature Curves about Strong and Weak Axes for Specimen RC-5

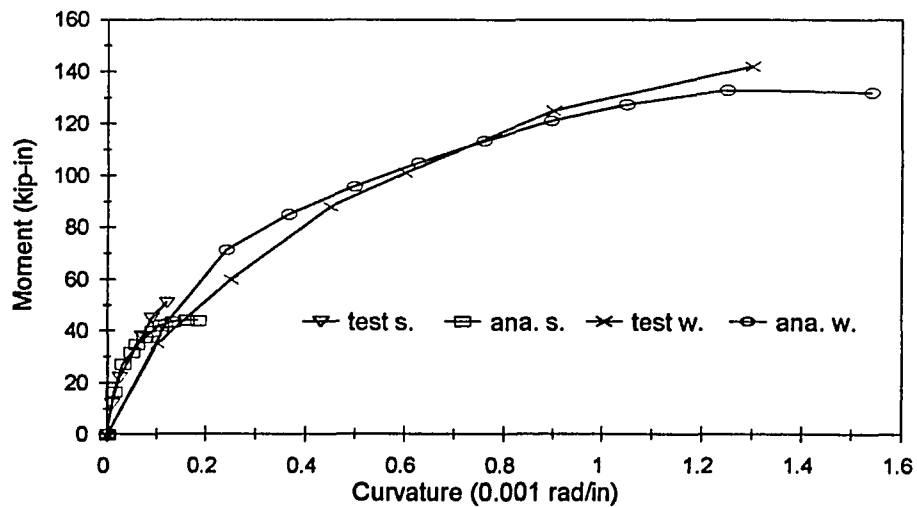


Fig. H-6 Moment-Curvature Curves about Strong and Weak Axes for Specimen RC-6

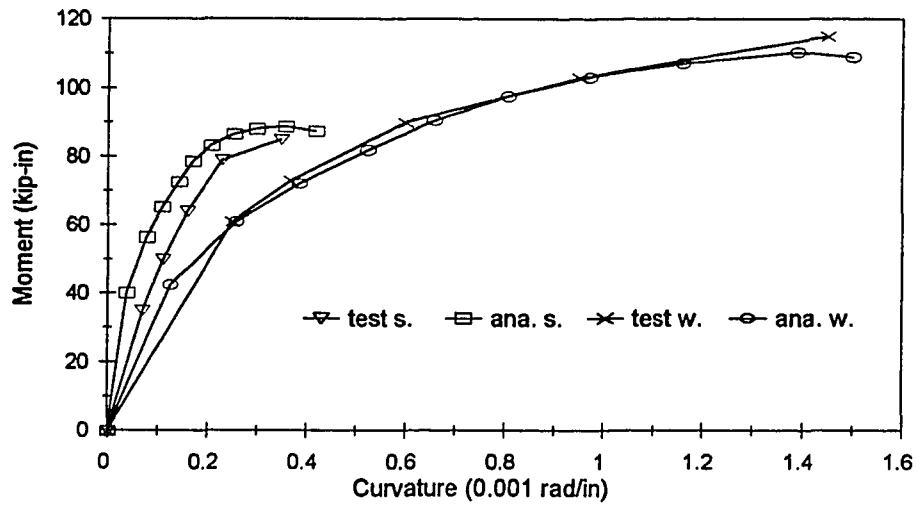


Fig. H-7 Moment-Curvature Curves about Strong and Weak Axes for Specimen RC-7

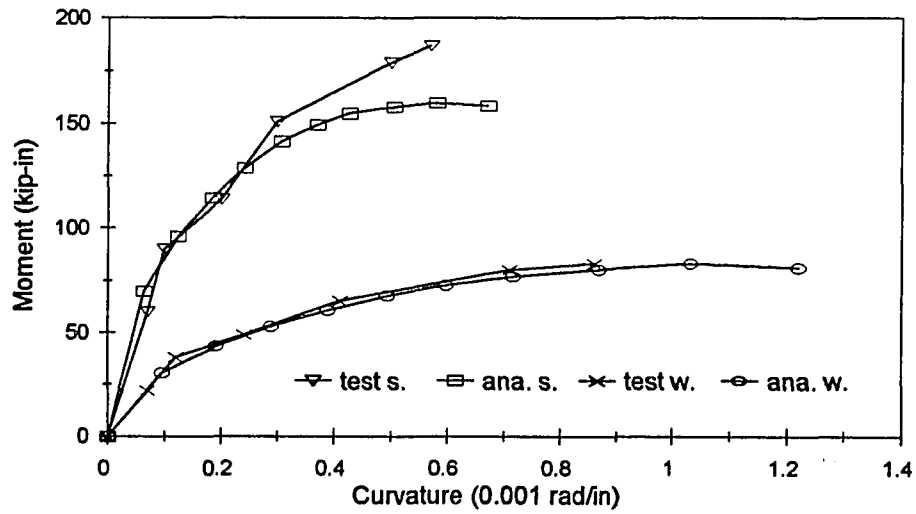


Fig. H-8 Moment-Curvature Curves about Strong and Weak Axes for Specimen RC-8

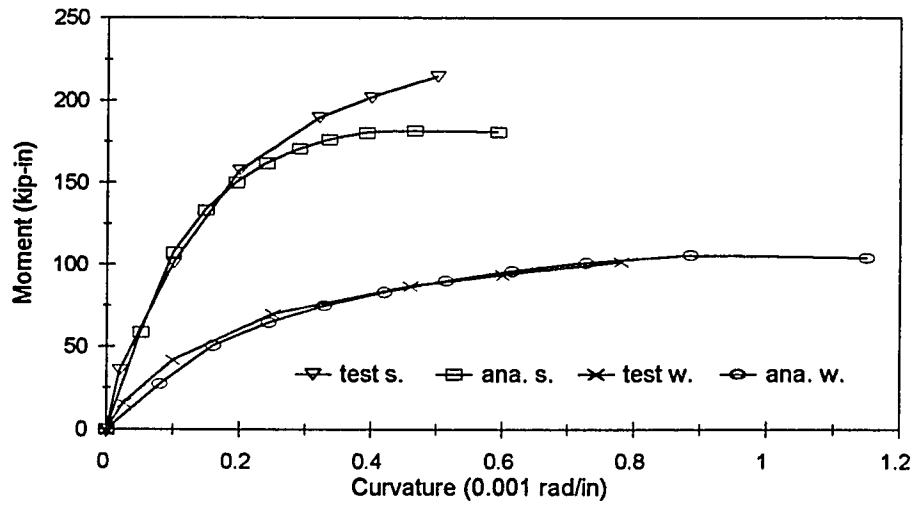


Fig. H-9 Moment-Curvature Curves about Strong and Weak Axes for Specimen RC-9

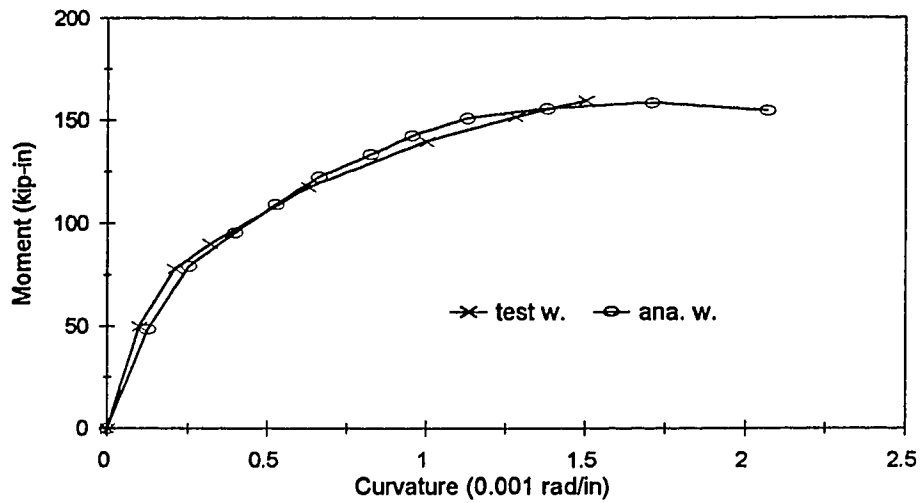


Fig. H-10 Moment-Curvature Curves about Weak Axis for Specimen C-1

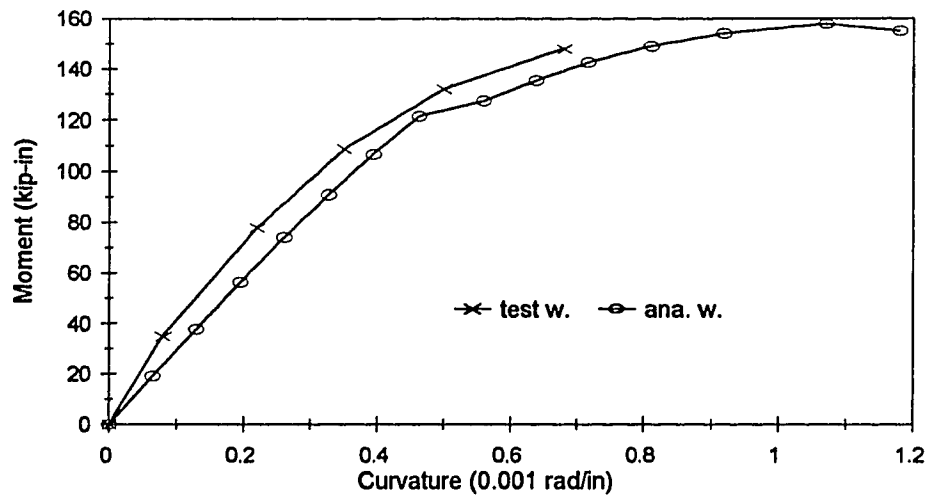


Fig. H-11 Moment-Curvature Curves about Weak Axis for Specimen C-2

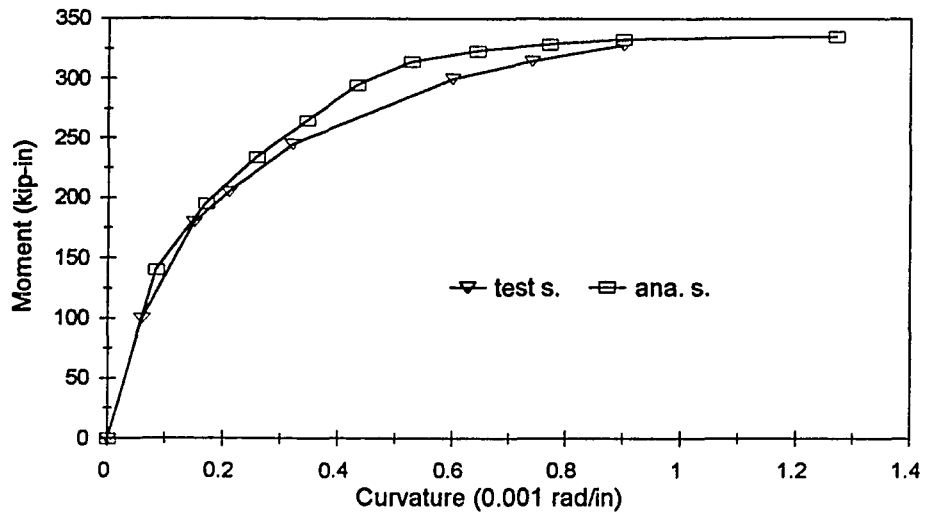


Fig. H-12 Moment-Curvature Curves about Strong Axis for Specimen C-3

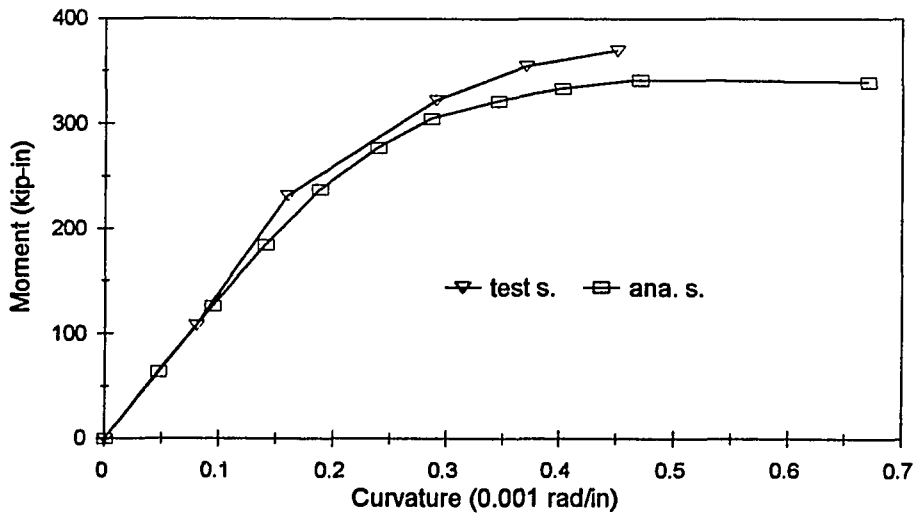


Fig. H-13 Moment-Curvature Curves about Strong Axis for Specimen C-4

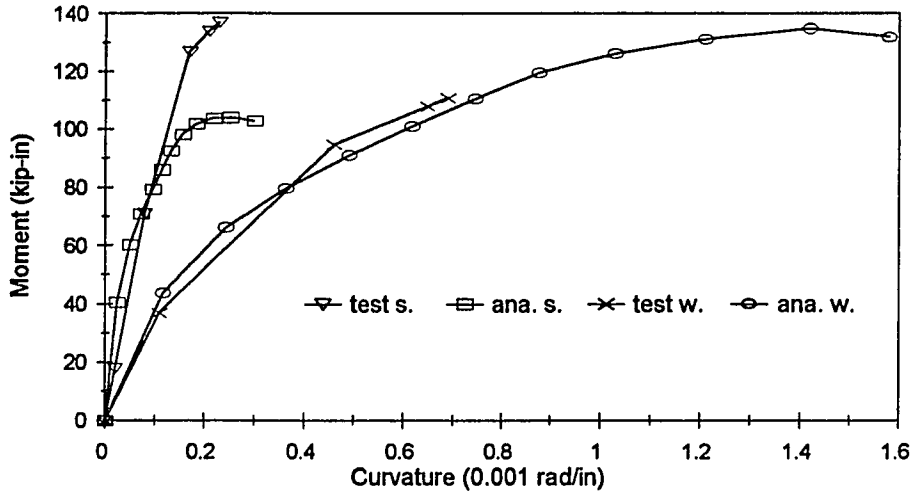


Fig. H-14 Moment-Curvature Curves about Strong and Weak Axes for Specimen C-5

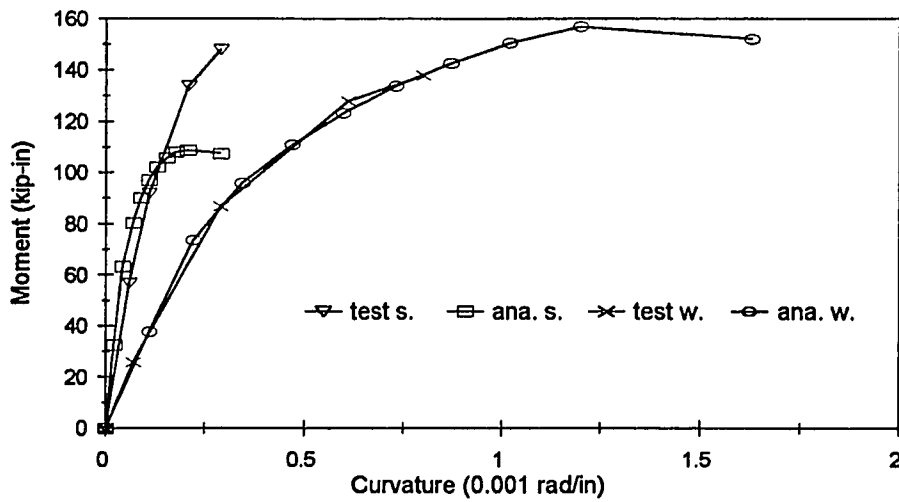


Fig. H-15 Moment-Curvature Curves about Strong and Weak Axes for Specimen C-6

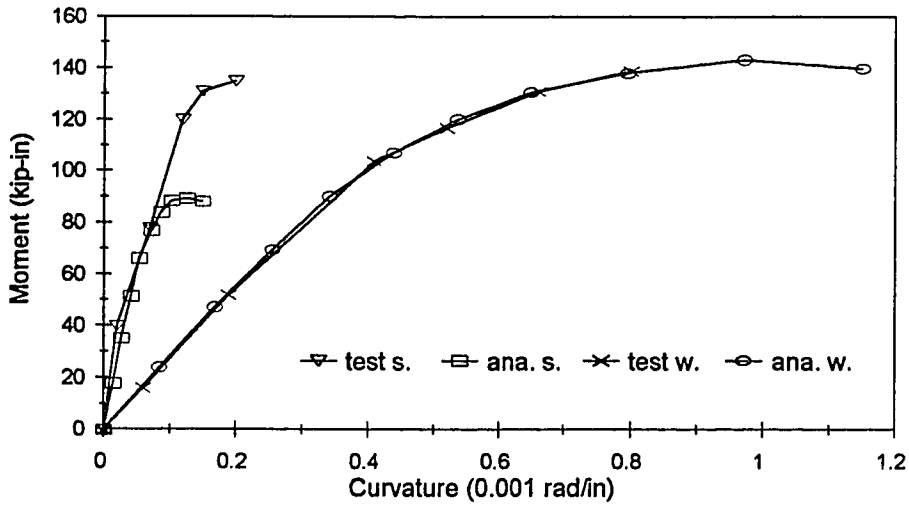


Fig. H-16 Moment-Curvature Curves about Strong and Weak Axes for Specimen C-7

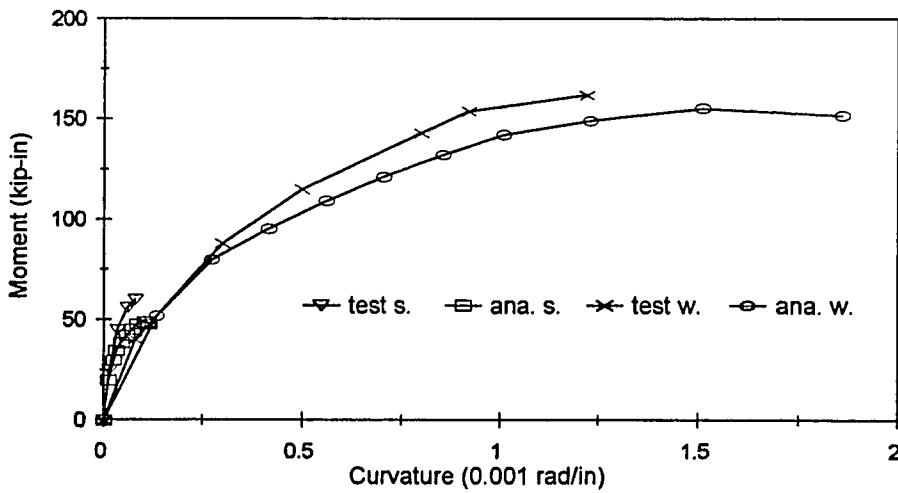


Fig. H-17 Moment-Curvature Curves about Strong and Weak Axes for Specimen C-8

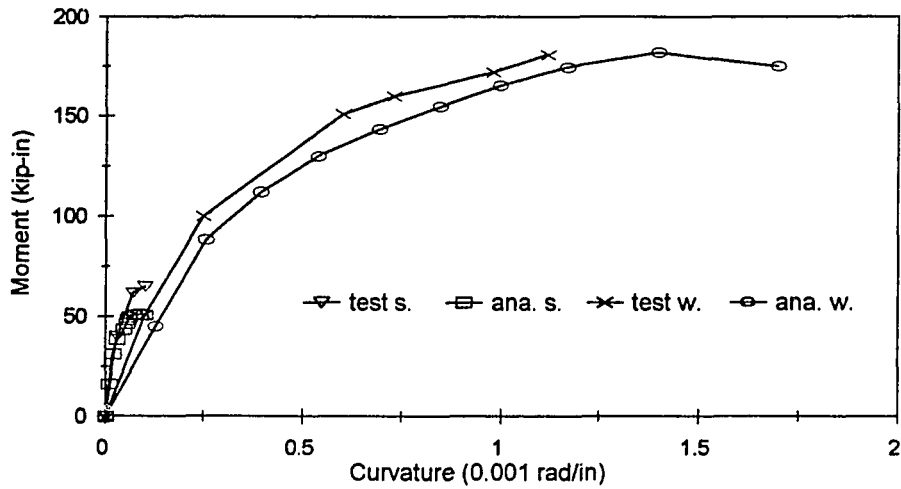


Fig. H-18 Moment-Curvature Curves about Strong and Weak Axes for Specimen C-9

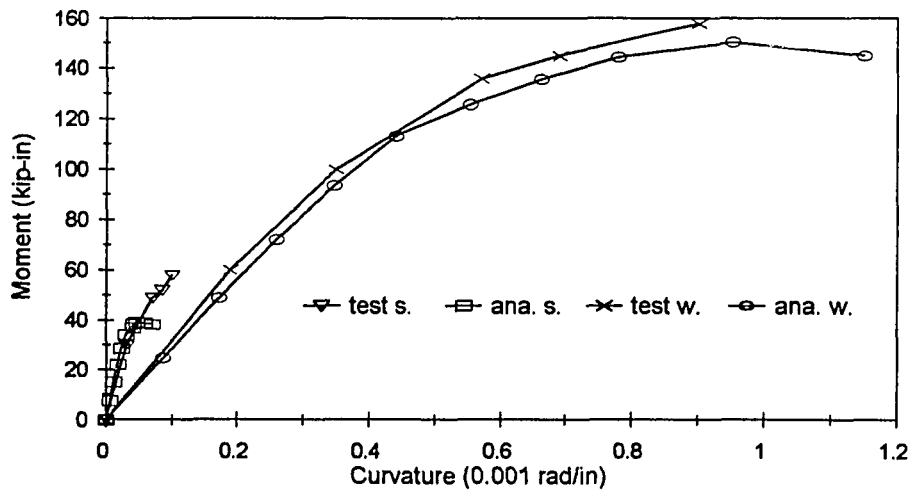


Fig. H-19 Moment-Curvature Curves about Strong and Weak Axes for Specimen C-10

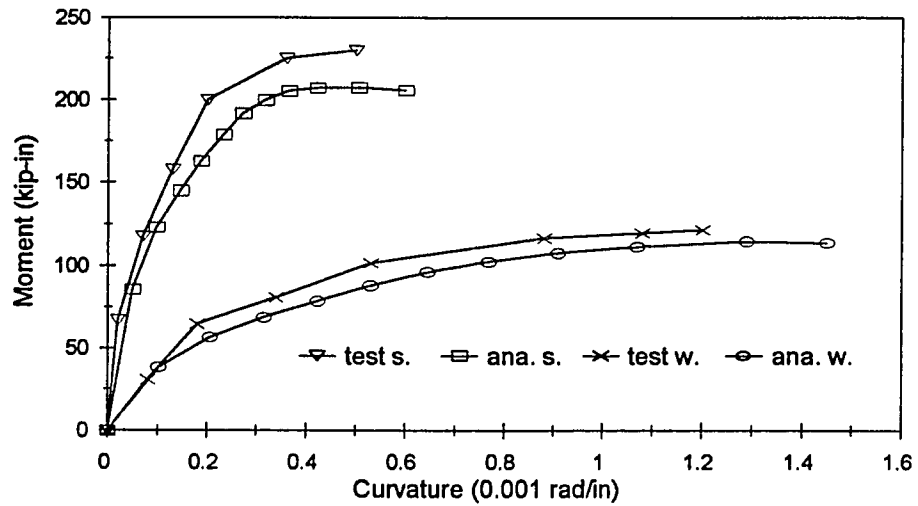


Fig. H-20 Moment-Curvature Curves about Strong and Weak Axes for Specimen C-11

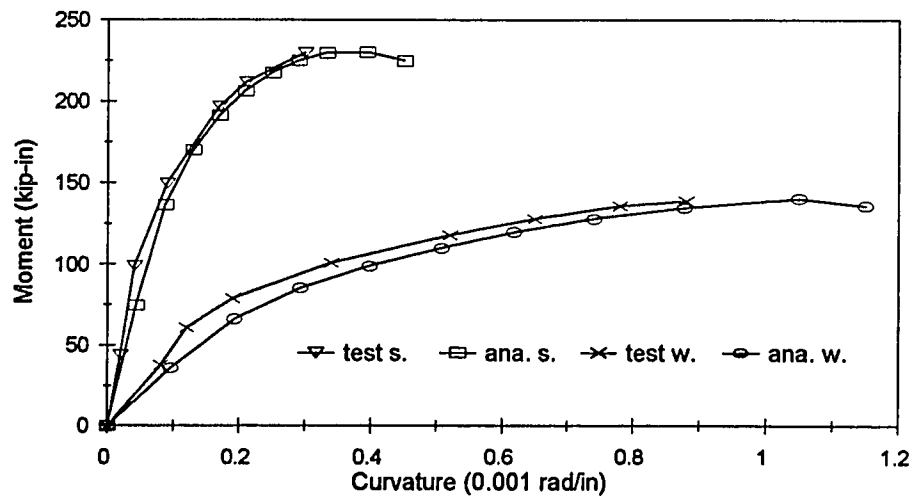


Fig. H-21 Moment-Curvature Curves about Strong and Weak Axes for Specimen C-12

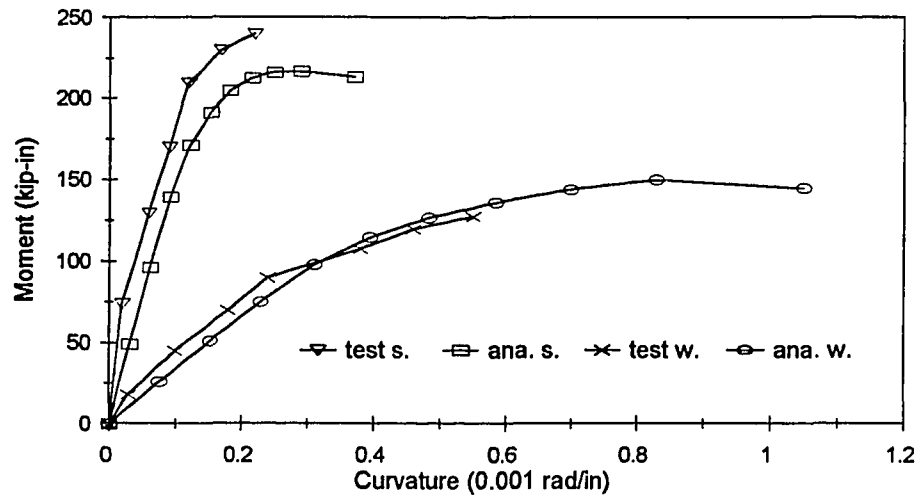


Fig. H-22 Moment-Curvature Curves about Strong and Weak Axes for Specimen C-13

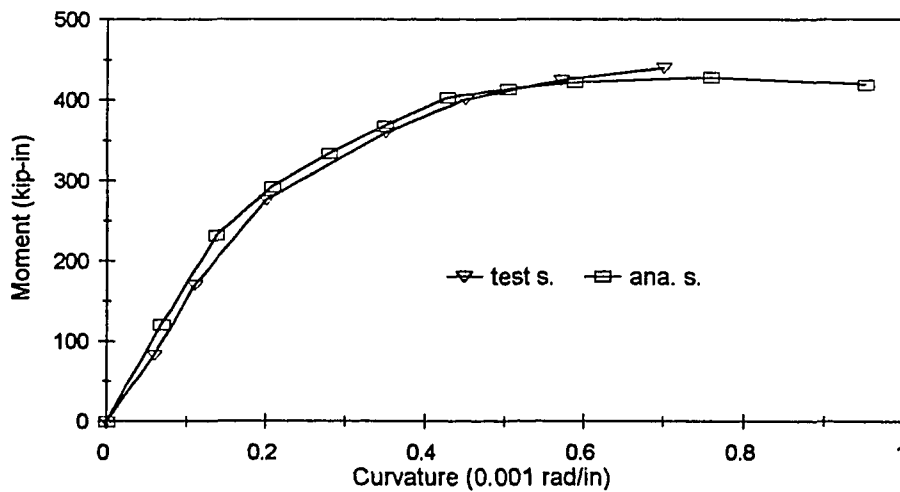


Fig. H-23 Moment-Curvature Curves about Strong Axis for Specimen C-14

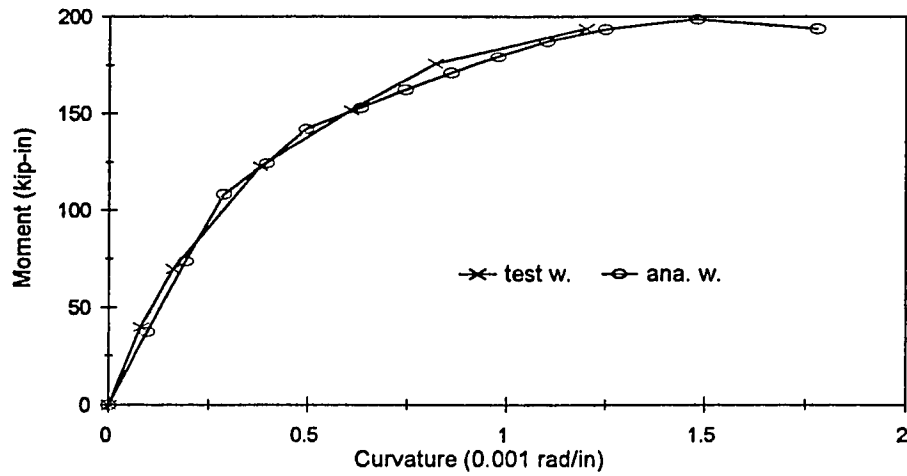


Fig. H-24 Moment-Curvature Curves about Weak Axis for Specimen C-15

BIBLIOGRAPHY

- Al-Noury, S. I. and Chen, W. F. (1982). Finite segment method for biaxially loaded RC columns. *J. Struct. Engrg.* ASCE, **108**(4), 780-799.
- Basu, A. K. and Suryanarayana, P. (1975). Analysis of restrained concrete columns under biaxial bending. *ACI Pub. SP-50, Reinforced Concrete Columns*, ACI, Detroit, Mich. 211-232.
- Carreira, D. J. and Chu, K. H. (1985). Stress-strain relationship for plain concrete in compression. *ACI J.* Nov.-Dec. 1985, 797-804.
- Chen, C. J., Gutkowski, R. M. and Puckett, J. A. (1991). B-spline compound strip analysis of stiffened plates under transverse loading. *Comput. Struct.* **34**(2), 337-347.
- Chen, C. J., Gutkowski, R. M. and Puckett, J. A. (1991). Spline compound strip analysis of folded plate structures with intermediate supports. *Comput. Struct.* **39**(3/4), 369-379.
- Chen, W. F. and Shoraka, M. T. (1975). Tangent stiffness method for biaxial bending of reinforced concrete columns. *Int. Assoc. for Bridge and Struct. Engrg.* **35**-I, 23-44.
- Cheung, Y. K., Fan, S. C. and Wu, C. Q. (1982). Spline finite strip in structural analysis. *Proc. of Int. Conf. of Finite Element Method.* Shanghai, 704-709.
- Chopra, I. and Durvasula, S. (1971). Vibration of simply-supported trapezoidal plates. *J. Sound Vib.* **19**, 379-392.
- Cook, R. D., Malkas, D. S. and Plesha, M. E. (1989). *Concepts and Applications of Finite Element Analysis.* 3rd Edn. John Wiley & Sons, New York.
- Fan, S. C. and Luah, M. H. (1992). New spline finite element for plate bending. *J. Engrg. Mech.* ASCE, **118**(6), 1065-1082.
- Farah, A. and Huggins, M. W. (1969). Analysis of reinforced concrete columns subjected to longitudinal load and biaxial bending. *ACI J.* **66**(7), 569-575.
- Furlong, R. W. (1979). Concrete columns under biaxial eccentric thrust. *ACI J.* **76**(10), 1093-1118.

- Hsu, C. T. (1974). *Behavior of Structural Concrete Subjected to Biaxial Flexure and Axial Compression*. Thesis presented to McGill University at Montreal, Canada, in partial fulfillment of the requirements for the degree of Doctor of Philosophy.
- Hsu, C. T. T. (1985). Biaxially loaded L-shaped reinforced concrete columns. *J. Struct. Engrg. ASCE*, **111**(12), 2576-2595.
- Hsu, C. T. T. (1987). Channel shaped reinforced concrete compression members under biaxial bending. *ACI Struct. J.* **84**(3), 201-211.
- Hsu, C. T. T. (1989). Tee-shaped reinforced concrete members under biaxial bending and axial compression. *ACI Struct. J.* **86**(4), 460-468.
- Hsu, C. T. and Mirza, M. S. (1973). Structural concrete biaxial bending and compression. *J. Struct. Div. ASCE*, **99**(2), 285-290.
- Hsu, C. T. T. and Mirza, M. S. (1980). Non-linear behavior and analysis of reinforced concrete columns under combined loadings. *SM Study No. 14, Non-linear design of concrete structure*, Univ. of Waterloo Press, Waterloo, Ontario, Canada, 109-135.
- Leissa, A. W. (1969). *Vibration of Plates*. National Aeronautics and Space Administration, NASA SP-160.
- Leung, A. Y. T. and Au, F. T. K. (1990). Spline finite elements for beam and plate. *Comput. Struct.* **37**(5), 717-729.
- Li, W. Y., Cheng, Y. K. and Tham, L. G. (1986). Spline finite strip analysis of general plates. *J. Engrg. Mech. ASCE*, **112**(1), 43-54.
- Liew, K. M. (1992). Response of plates of arbitrary shape subject to static loading. *J. Engrg. Mech. ASCE*, **118**(9), 1783-1794.
- Mander, J. B., Priestley, M. J. N. and Park, R. (1988). Theoretical stress-strain model for confined concrete. *J. Struct. Engrg. ASCE*, **114**(8), 1804-1826.
- Mavichak, V. and Furlong, R. W. (1976). Strength and stiffness of reinforced concrete columns under biaxial bending. *Research Report 7-2F, Center for Highway Research*, The University of Texas at Austin, Austin, Texas.
- Mizusawa, T. (1979). Vibration of skew plates by using B-spline functions. *J. Sound Vib.* **62**(2), 301-308.

- Mizusawa, T., Kajita T. and Naruoka, M. (1979). Vibration of stiffened skew plates by using B-spline functions. *Comput. Struct.* **10**(5), 821-826.
- Mizusawa, T., Kajita T. and Naruoka, M. (1980). Buckling of skew plate structures using B-spline functions. *Int. J. Numer. Meth. Engrg.* **15**(1), 87-96.
- Orris, R. M. and Petyt M. (1973). A finite element study of the vibration of trapezoidal plates. *J. Sound Vib.* **27**(3), 325-344.
- Poston, R. W. (1986). Nonlinear analysis of concrete bridge piers. *J. Struct. Engrg.* ASCE, **112**(9), 2057-2065.
- Poston, R. W., Breen, J. E. and Roseset J. M. (1985a). Analysis of nonprismatic of hollow slender concrete bridge piers. *ACI J.* **82**(5), 731-739.
- Poston, R. W., Gilliam, T. E., Yamamoto, Y. and Breen, J. E. (1985b). Hollow concrete bridge pier behavior. *ACI J.* **82**(6), 779-787.
- Prenter, P. M. (1975). *Splines and Variational Methods*. John Wiley & Sons, New York.
- Qin, R. (1982). Fundamentals and applications of spline finite-point method. *Proc. of Int. Conf. of Finite Element Method*. Shanghai, 774-780.
- Qin, R. (1985). *Spline Function Methods of Structural Analysis* (in Chinese). People's Press of Guangxi.
- Raggett, G. F., Stone, J. A. R. and Wilson, P. D. (1974). On the use of cubic splines to solve certain circular plate problems. *Comput. Meth. Appl. Mech. Engrg.* **4**(1), 39-45.
- Rotter, J. M. (1985). Rapid exact inelastic biaxial bending analysis. *J. Struct. Engrg.* ASCE, **111**(12), 2659-2674.
- Santathadaporn, S. and Chen, W. F. (1972). Tangent stiffness method for biaxial bending. *J. Struct. Div.* ASCE, **98**(1), 152-163.
- Schoenberg, I. J. (1946a). Contributions to the problem of approximation of equidistant data by analytic functions. Part A: On the problem of smoothing of graduation. A first class of analytical approximation formulae. *Q. Appl. Math.* **4**(1), 45-99.

- Schoenberg, I. J. (1946b). Contributions to the problem of approximation of equidistant data by analytic functions. Part B: On the problem of osculatory interpolation. A second class of analytical approximation formulae. *Q. Appl. Math.* **4**(2), 112-141.
- Shen, P. C. and Wang, J. G. (1987). Vibration analysis of flat shells by using B spline functions. *Comput. Struct.* **25**(1), 1-10.
- Shen, P. C. and Wang, J. G. (1987). Static analysis of cylindrical shells by using B spline functions. *Comput. Struct.* **25**(6), 809-816.
- Tham, L. G., Li, W. Y., Cheung, Y. K. and Chen, M. J. (1986). Bending of skew plates by spline-finite-strip method. *Comput. Struct.* **22**(1), 31-38.
- Timonshenko, S. P. and Woinowsky-Krieger, S. (1959). *Theory of Plates and Shells*. 2nd Edn. McGraw-Hill Book Co., New York.
- Tsao, W. H. (1991). Square and L-shaped slender reinforced concrete columns under combined biaxial and axial compression. *Ph.D. Dissertation*, New Jersey Institute of Technology, Newark, New Jersey.
- Tsao, W. H. and Hsu, C. T. T. (1993). A nonlinear computer analysis of biaxially loaded L-shaped slender reinforced concrete columns. *Comput. Struct.* **49**(4), 579-588.
- Tsao, W. H. and Hsu, C. T. T. (1994). Behaviour of biaxially loaded square and L-shaped slender reinforced concrete columns. *Magazine of Concrete Research*. **46**(169), December.
- Wang, G. and Hsu, C. T. T. (1990). Complete load-deformation behavior of biaxially loaded RC columns. *Technical Report Structural Series*, No. 90-2, Dept. of Civil and Environmental Engineering, New Jersey Institute of Technology, Newark, New Jersey. pp. 38.
- Wang, G. and Hsu, C. T. T. (1992). Complete biaxial load-deformation behavior of RC columns. *J. Struct. Engrg.* ASCE, **118**(9), 2590-2609.
- Wang, G. and Hsu, C. T. T. (1994). Static and dynamic analysis of arbitrary quadrilateral flexural plates by B₃-spline functions. *Int. J. Solids Struct.* **31**(5), 657-667.
- Zak, M. L. (1993). Computer analysis of reinforced concrete sections under biaxial bending and longitudinal load. *ACI Struct. J.* **90**(2), 163-169.

Zienkiewicz, O. C. (1977). *The Finite Element Method*. 3rd Edn. McGraw-Hill, London.